Aalborg Universitet

AALBORG UNIVERSITY
DENMARK

Satellite Attitude Control Using Only Electromagnetic Actuation

Wisniewski, Rafal

[Link to publication from Aalborg University](#)

Satellite Attitude Control Using
Only Electromagnetic Actuation

Ph.D. Thesis

Rafał Wiśniewski

Department of Control Engineering
Aalborg University
Fredrik Bajers Vej 7, DK-9220 Aalborg Ø, Denmark.

ii

To my wife Dorde and son Viktor

Preface and Acknowledgments

This thesis is submitted in partial fulfillment of the requirements for the Doctor of Philosophy in Automatic Control at Aalborg University. The work has been carried out in the period from November 1992 to December 1996 under supervision of Professor Mogens Blanke.

I am greatly thankful to Professor Mogens Blanke for his guidance during the research program. His assistance in obtaining the financial support during the period of the work is greatly appreciated.

The last three years I shared my office with my colleagues Søren Abildsten Bøgh, Thomas Bak, and Roozbeh Izadi-Zamanabadi. I would like to express my sincere thanks to them for valuable and inspiring discussions, and most of all for their encouragement during my research period.

I am most thankful to the staff at the Department of Control Engineering for all assistance and support.

I am greatly indebted to my parents and my brother who always believed that I would succeed in my doctorate. I would like to express my deepest thanks to my wife Dorde for her patience and support during all those years. I am most gratefull to my mother-in-low for her help in baby-sitting during the most busy periods.

December 1996, Aalborg, Denmark

Rafał Wiśniewski

Summary

The primary purpose of this work was to develop control laws for three axis stabilization of a magnetic actuated satellite. This was achieved by a combination of linear and nonlinear system theory. In order to reach this goal new theoretical results were produced in both fields. The focus of the work was on the class of periodic systems reflecting orbital motion of the satellite. In addition to a theoretical treatment, the thesis contains a large portion of application considerations. The controllers developed were implemented for the Danish Ørsted satellite.

The control concept considered was that interaction between the Earth's magnetic field and a magnetic field generated by a set of coils in the satellite can be used for actuation. Magnetic torquing was found attractive for generation of control torques on small satellites, since magnetic control systems are relatively lightweight, require low power and are inexpensive. However, this principle is inherently nonlinear and difficult to use, because control torques can only be generated perpendicular to the geomagnetic field vector. So far, this has prevented control in all three axes using magnetorquers only.

A fact that the geomagnetic field changed periodically when a satellite is on a near polar low Earth orbit was used throughout this thesis. Confined computer capacity and a limit on electrical power supply were separate obstacles. They demanded computational simplicity and power optimality from the attitude control system. The design of quasi optimal controllers for a real-time implementation was a subject of considerations in the part on linear control methods for a satellite with a gravity gradient boom. Both time varying and constant gain controllers were developed and their performance was tested via simulation.

The nonlinear controller for a satellite without appendages was given in the second part of the thesis. Its design was based on sliding mode control theory. The essence of the sliding control presented in the thesis was to split the controller design into two steps: a sliding manifold design and a sliding condition design. The emphasis was on the sliding condition design, which was stated as a continuous function of the state. A control law for magnetic actuated satellite was proposed.

Complete comprehension of the nature of the satellite control problem required a new ap-

proach merging the nonlinear control theory with physics of the rigid body motion and an extension of earlier results in this field using the theory of periodic systems. The Lyapunov stability theory was employed based on the potential and kinetic energy of the rigid satellite. A velocity controller, that contributes to dissipation of both kinetic and potential energy, was proposed. The velocity control was shown to provide four stable equilibria, one of which was the desired orientation. It was explained how the equilibria depended on the ratio of the satellite's moments of inertia. It was further investigated how to control the attitude, such that the satellite was globally asymptotically stable in the desired orientation, avoiding the undesired equilibria.

The main contribution of this work was to show that three axis control can be achieved with magnetorquers as sole actuators in a low Earth orbit. A rigorous stability analysis was presented, and detailed simulation results showed convincing performance over the entire envelope of operation of the Danish Ørsted satellite. The key results have also been published in international papers.

Synopsis

Det overordnede mål med dette arbejde har været at udvikle kontrolsystemer inden-for treakse-stabilisering af magnetisk styrede satellitter. For at nå dette mål, måtte nye teoretiske resultater udvikles inden for både lineær og ikke-lineær systemteori. De er anvendt på den type af periodiske differentialligninger, som beskriver satellittens bevægelse i en bane. De udviklede regulatorer er implementeret på den Danske Ørsted Satellit.

Magnetisk styring af satellitter fungerer ved interaktion mellem Jordens magnetiske felt og et kunstigt genereret magnetisk moment i satellitten, som frembringes ved hjælp af elektriske spoler. Dette princip kan med fordel anvendes i mindre satellitter på baner tæt på Jorden. Anvendelse af spoler er atraktiv, de indeholder ingen bevægelige dele, deres el-forbrug minimalt sammenlignet med andre aktuatorer, f.eks. momentumhjul, og deres vægt er relativt lille. Det er dog problematisk at designe reguleringsstrategier med traditionelle metoder, da et styringsmoment kun kan generes vinkelret på den geomagnetiske felt-vektor. På grund af de teoretiske vanskeligheder har man ikke tidligere anvendt magnetiske spoler for treakse-stabilisering.

Ved praktiske implementering opstår der yderligere vanskeligheder i form af begrænsede system-ressourcer. Krav om begrænset styreeffekt, lille regnekapacitet og snævre grænser for brug af computerlager skal opfyldes for at en teoretisk løsning kan implementeres. Afhandlingen bidrager med at løse både det teoretiske og implementeringsmæssige problem. Dette er opnået i afsnittet om lineære reguleringsmetoder ved en optimal retningstyring implementeret i realtid. Tidsvarierende kontrol parametre designes udfra den periodiske karakter af det geomagnetiske felt i en polær bane satellit, således at realtids algoritmen simplificeres væsentligt. Designet er evalueret via simulering af en ikke-lineære bevægelsemodel for satellitten. Det vises at en regulator baseret på lineære metoder er velegnet for en satellit med udfoldet bom.

Inden bommen udfoldelse ligger satellittens inertimomenter så tæt på hinanden, at ikke-lineære led bliver dominerende for beskrivelsen af dens bevægelse. I denne tilstand er en ikke-lineær regulator påkrævet. Anvendelsen af ikke-lineære kontrol metoder og teori for periodiske systemer samt en fysisk forståelse af satellittens bevægelse præsenteres

for at give et indblik i de centrale problemer med retningstyring. Lyapunovs stabilitets-analyse anvendes på satellittens potentielle og kinetiske energi. Resultatet er en vinkel-hastighedsregulator, som mindsker den totale energi i systemet. Det vises, at vinkel-hastighedsregulatoren har fire stabile ligevægts-punkter, som er bestemt af satellittens inertimomenter. Et af ligevægtspunkterne svarer til den ønskede retning for satellitten. Der er desuden designet en global stabil regulator, som garanterer, at satellitten ikke ender i et af de uønskede ligevægts-punkter.

Arbejdet bidrager med at vise, at treakse-stabilisering kan opnås alene ved hjælp af mag-netisk styring, og at de udviklede principper velegnet til små satellitter i polære baner tæt på Jorden. Der præsenteres en gennemarbejdet stabilitetsanalyse med design af regula-torer og detaljerede simuleringsresultater giver et overbevisende billede af styresystemet anvendt på den Danske Ørsted Satellit. Udover at være indeholdt i afhandlingen er de vigtigste resultater publiceret internationalt som separate papers.

Contents

List of Figures

List of Tables

Nomenclature

Glossary

Space Terminology

- **Apogee** is the point at which a satellite in orbit around the Earth reaches its farthest distance from the Earth.
- **Attitude** of a spacecraft is its orientation in a certain coordinate system.
- **Altitude** is the distance from a reference **geoid** to the satellite.
- **Boom is upright** boom tip is above horizon.
- **Boom is upside-down** boom tip is below horizon.
- **Ecliptic** is the mean plane of the Earth's orbit around the Sun.
- **Eclipse** is a transit of the Earth in front of the Sun, blocking blocking all or a significant part of the Sun's radiation.
- **Geoid** is an equipotential surface that coincides with mean sea level in the open ocean.
- **Latitude** is the angular distance on the Earth measured north or south of the equator along the meridian of a satellite location.
- **Longitude** is the angular distance measured along the Earth's equator from the Greenwich meridian to the meridian of a satellite location.
- **Mean Anomaly** is the angle from the **perigee** to the satellite moving with a constant angular speed (**orbital rate** ω_o) required for a body to complete one revolution in an orbit. Mean anomaly, M, is $\omega_o \Delta t$, where Δt is the time since last perigee passage.
- **Orbital rate** is the mean angular velocity of the satellite rotation about the Earth.
- **Pitch, Roll, Yaw** are the angle describing satellite attitude. Pitch is referred to the rotation about the x-axis of a reference coordinate system, roll to the y-axis, and yaw to the z-axis.
- **Perigee** is the point at which a satellite in orbit around the Earth most closely approaches the Earth.
- **Vernal Equinox** is the point where the **ecliptic** crosses the Earth equator going from south to north.
- **Zenith** is a unit vector in the Control Coordinate System along the line connecting the satellite centre of gravity and the Earth centre pointing away from the Earth.

Mathematics and Control Theory

- **Autonomous system** a system which is time invariant.

- **Class K** a function $f : \mathbb{R}_+ \to \mathbb{R}_+$ is of class K if it is continuous, strictly increasing, and $f(0) = 0$.

- **Class L** a function $f : \mathbb{R}_+ \to \mathbb{R}_+$ is of class L if it is continuous, strictly decreasing, $f(0) < \infty$, and $\lim_{r \to \infty} f(r) = 0$ and $f(0) = 0$.

- **Connected set** a set is connected if it is not disconnected. A set S is called disconnected if $S = A \cup B$, where A and B are are disjoint sets in S, for every subsets $A, B \subseteq S$.

- **Decrescent function** a function $f : \mathbb{R}_+ \times \mathbb{R}^n \to \mathbb{R}$ is said to be decrescent in a neighbourhood B_r if there exist a constant $r > 0$ and a function β of **class K** such that for each $t > 0$ and for each $\mathbf{x} \in B_r$

$$f(t, \mathbf{x}) \leq \beta(\| \mathbf{x} \|).$$

- **Locally positive definite function** a function $f : \mathbb{R}_+ \times \mathbb{R}^n \to \mathbb{R}$ is said to be locally positive definite in a neighbourhood B_r if it is continuous, furthermore for all $t \geq 0$ the function $f(t, \mathbf{0}) = 0$, and there exist a constant $r > 0$ and a function α of **class K** such that for each $t > 0$ and for each $\mathbf{x} \in B_r$

$$\alpha(\| \mathbf{x} \|) \leq f(t, \mathbf{x}).$$

- **Negative definite function** a function $f : \mathbb{R}_+ \times \mathbb{R}^n \to \mathbb{R}$ is said to be negative definite if $-f$ is **positive definite function**.

- **Non autonomous system** a system which is time dependent.

- **Positive definite function** a function $f : \mathbb{R}_+ \times \mathbb{R}^n \to \mathbb{R}$ is said to be positive definite if it is **locally positive definite** for all $\mathbf{x} \in \mathbb{R}^n$

- **Radially unbounded** a **positive definite function** $f : \mathbb{R}_+ \times \mathbb{R}^n \to \mathbb{R}$ is said to be radially unbounded if there exists a continuous function γ such that $\gamma(r) \to \infty$ as $r \to \infty$.

Acronyms and Abbreviations

ACS	Attitude Control Subsystem,
CS	Coordinate System,
CSC	Compact Spherical Coil, Magnetometer,
GPS	Global Positioning System,
LEO	Low Earth Orbit,
r.h.s.	right hand side,
l.h.s.	left hand side,
rpm	revolutions per minute,
w.r.t	with respect to.

Notation

Vectors and Matrices

$\mathbf{A}, \mathbf{v}$	matrices and vectors are written in bold type,
$^c\mathbf{v}, {}^o\mathbf{v}, {}^w\mathbf{v}$	vector $\mathbf{v}$ resolved in Control CS, Orbit CS or World CS respectively,
v_{ox}, v_{oy}, v_{oz}	x, y, and z components of vector $\mathbf{v}_o$,
$\mathbf{P} >= 0$	a matrix $\mathbf{P}$ is positive semidefinite,
$\mathbf{P} > 0$	a matrix $\mathbf{P}$ is positive definite,
$\mathbf{P}_1 > \mathbf{P}_2$	the difference of matrices $(\mathbf{P}_1 - \mathbf{P}_2)$ is positive definite,
$diag([a_1 \ a_2 \ \ldots \ a_n]^T)$	diagonal matrix with components on diagonal corresponding to $[a_1 \ a_2 \ \ldots \ a_n]^T$ and zero off-diagonal components.

List of Symbols

$\mathbf{\Omega}_{cw}$	angular velocity of Control CS w.r.t. World CS,
$\mathbf{\Omega}_{co}$	angular velocity of Control CS w.r.t. Orbit CS,
$\mathbf{\Omega}_{ow}$	angular velocity of Orbit CS w.r.t. World CS,
$_o^c\mathbf{q}$	attitude quaternion representing rotation of Control CS w.r.t. Orbit CS,
$\mathbf{q}, q_4$	vector part and scalar part of $_o^c\mathbf{q}$,
$\mathbf{A}(_o^c\mathbf{q})$	attitude matrix based on $_o^c\mathbf{q}$,
$\mathbf{i}_o, \mathbf{j}_o, \mathbf{k}_o$	unit vector along x-, y-, z-axis of Orbit CS,
$\delta\mathbf{q}$	small perturbation of vector part of attitude quaternion, $_o^c\mathbf{q}$,
$\delta\mathbf{\Omega}$	small perturbation of angular velocity $^c\mathbf{\Omega}_{co}$,
ω_o	orbital rate,
T	period of orbit,
$\mathbf{h}_o$	angular momentum due to satellite revolution about the Earth,
M	mean anomaly,
$\mathbf{I}$	inertia tensor of the satellite,
I_x, I_y, I_z	moments of inertia about x-,y- and z-principal axes,
$\mathbf{N}_{ctrl}$	control torque,
$\mathbf{N}_{gg}$	gravity gradient torque,
$\mathbf{N}_{dist}$	disturbance torques,
$\mathbf{N}_{aero}$	aerodynamic drag torque,
E_{kin}	kinetic energy,
E_{gg}	energy due to gravity gradient,
E_{gyro}	energy due to satellite revolution about Earth,
$\mathbf{m}$	magnetic moment generated by set of coils,
$\mathbf{B}$	magnetic field of Earth,
$\tilde{\mathbf{B}}$	matrix representation of product $\mathbf{B}\times$,
$\hat{\mathbf{B}}$	control matrix averaged within one orbit,
n_{coil}	number of coil windings,
A_{coil}	coil area,

i_{coil}	current in coil,
$\mathbf{x}(t, t_0, \mathbf{x}_0)$	solution of non autonomous differential equation $\dot{\mathbf{x}}(t) = \mathbf{f}(t, \mathbf{x}(t))$ at time t for initial conditions $\mathbf{x}(t_0) = \mathbf{x}_0$,
$\mathbf{x}(t, \mathbf{x}_0)$	solution of autonomous differential equation $\dot{\mathbf{x}}(t) = \mathbf{f}(\mathbf{x}(t))$ at time t for initial conditions $\mathbf{x}_0$,
$\| \mathbf{x} \|$	Euclidean norm of vector $\mathbf{x}$,
$\| \mathbf{x} \|_2$	L_2 norm of vector $\mathbf{x}$,
$\mathbb{R}_+$	set of all positive real numbers together with 0,
C^1	$f \in C^1$ means that function f is continuously differentiable (f has continuous partial derivatives),
B_r	open ball of radius r and a certain centre specified in the text,
$\Phi_A(t_f, t_0)$	transition matrix of linear non autonomous system $\dot{\mathbf{x}} = \mathbf{A}(t)\mathbf{x}$ evaluated from time t_0 to time t_f,
$\Psi_A(t_0)$	monodromy matrix of periodic system $\dot{\mathbf{x}} = \mathbf{A}(t)\mathbf{x}$ evaluated at time t_0,
$\mathbf{s}$	Sliding variable,
$\mathbf{S}$	Sliding manifold,
$\hat{\epsilon}$	quaternion gain in operational mission phase algorithm,
$\tilde{\epsilon}$	limit of stability of quaternion gain,
$\bar{\epsilon}$	quaternion gain in boom upside-down algorithm,
$\mathbf{E}_{n \times n}$	$n \times n$ identity matrix.

Chapter 1

Introduction

1.1 Background

The aim of this Ph.D. thesis is to develop control algorithms for a magnetic actuated satellite. The work has been motivated and supported by the Ørsted Satellite Project and the Faculty of Technology and Science at Aalborg University. The Ørsted satellite is a 60 kg auxiliary payload scheduled to be launched by a MD-Delta II launch vehicle in the late 1997 into a 450 x 850 km orbit with a 96 degree inclination. The satellite is developed by a consortium of Danish research organizations and space industries. Details of the orbit parameters and the satellite system are listed in Table 1.1.

The purpose of the Ørsted satellite is to conduct a research program in the discipline of the magnetic field of the Earth. The scientific payload fulfills two major objectives. The primary is to measure and collect data of the Earth's magnetic field. The secondary is to provide measurements of radiation from the high energy particles. The Ørsted satellite will carry five science experiments in order to meet these objectives: a CSC magnetometer (providing 3-axis measurements of the local geomagnetic field), an Overhauser magnetometer (a scalar magnetometer providing the amplitude of the magnetic field of the Earth), particle detectors (detecting electrons, protons and alpha particles), two GPS receivers (used for position determination), a star imager (measuring the satellite attitude relative to an inertial coordinate system). Furthermore, a set of wide angle sun sensors measuring the Sun incident angle has been added to the instrument set solely for the purpose of Attitude Control Subsystem (ACS). Table 1.2 gives an overview of the sensors and actuators used by the ACS.

The Ørsted satellite's main body is box shaped, $680\,mm$ high x $450\,mm$ wide x $340\,mm$ deep. The solar arrays cover all sides except the bottom. The satellite separation mechanism, which is the interface with the launch vehicle, is mounted on the bottom side of

Table 1.1: The Ørsted satellite mission

Item	Description
Body size	H 680 x W 450 x D 340 mm
Boom	8 m Deployable
Mass	61.8 kg
Moments of inertia about principal axes:	
boom deployed	X 181.78, Y 181.25, Z 1.28 kgm^2
boom stowed	X 3.428, Y 2.904, Z 1.275 kgm^2
Apogee	850 km
Perigee	450 km
Inclination	96.4 deg
Nodal drift	0.77 deg/day

Table 1.2: Sensors and actuators used for the Ørsted satellite attitude control

Item	Description
Star Imager	Provides attitude estimates with the angular resolution of 10 $arc\ sec$ w.r.t. the Word CS,
Set of Sun Sensors	Provides the x,y, and z components of the sun vector within 4π steradian coverage,
CSC Magnetometer	Measures the x, y and z components of the magnetic field with an accuracy of 1.5 nT (RMS).
GPS Receiver	Provides time, local position and velocity estimates with accuracy 100 m (2RMS), 0.2 m/s respectively,
Magnetorquers	3 electromagnetic coils mounted on the x, y and z facets of the satellite main body providing maximum magnetic moment of 20 Am^2.

the satellite body.

After separation from the launch vehicle the ACS shall acquire the satellite from a random tumbling. This mission phase is called the detumbling phase. When the satellite is firmly stabilized and the ground contact is established, an 8 m long boom is deployed by ground command. The boom carries the scientific instruments that must be displaced from the electro-magnetic disturbances present in the main body of the satellite. The part of the mission after boom deployment is referred to as the normal operation or the science observation phase. The Ørsted satellite configuration after boom deployment is depicted in Fig. 1.1.
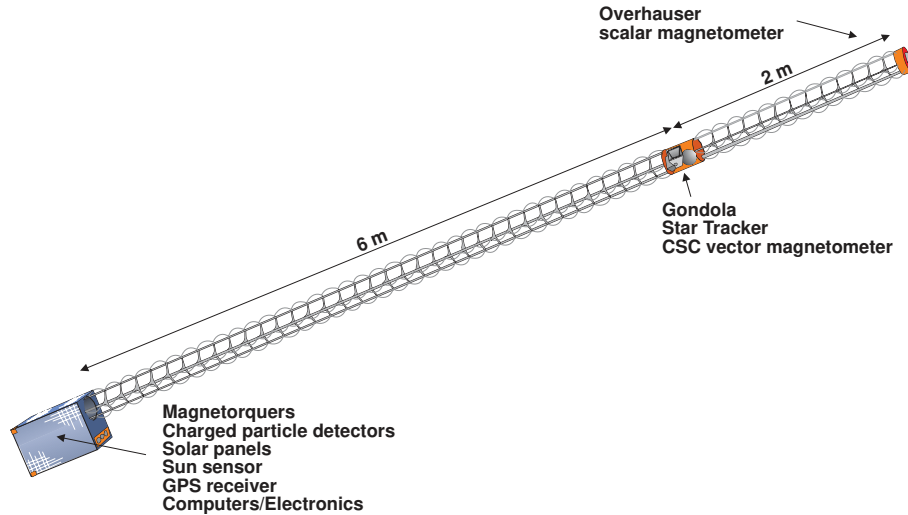
Figure 1.1: The Ørsted satellite consists of a main body and an 8 m long scientific boom.

Stabilization of the Ørsted satellite is accomplished by active use of a set of mutually perpendicular coils called magnetorquers. Magnetic control systems are relatively lightweight, require low power and they are inexpensive. The coils are mounted in the x, y, and z facets of the satellite main body. A maximum producible magnetic moment is 20 Am^2. The interaction between external magnetic field of the Earth and the magnetic field generated in the coils produces a mechanical torque, which is used to correct the attitude, i.e. the rotation of the satellite relative to a reference coordinate system. The maximum mechanical torque produced by the coils is approximately $0.6 \cdot 10^{-3} \ Nm$ above the equator, and $1.2 \cdot 10^{-3} \ Nm$ above the Poles. The current sent into the magnetorquer coils by the controller is dependent on the attitude and angular velocity information obtained from the attitude determination system Bak *et al.* (1996). The attitude determination system uses measurements from the star imager, or alternatively magnetometer and sun sensor data in an extended Kalman filter.

The control objectives vary dependent on the mission phase. Following separation from the launch vehicle, the satellite will rotate with a comparatively large angular velocity (up to 2 rpm). The attitude determination system is inactive in detumbling phase due to lack of position information. The only attitude information is the local geomagnetic field. A rate detumbling control is activated in this mission phase Wisniewski (1994*a*). The rate detumbling controller is required to despin the satellite from an arbitrary initial tumbling and turns the satellite in the direction opposite to the geomagnetic field vector, making boom deployment over Denmark viable. After boom deployment the normal operation phase controller is activated. The satellite shall be three axis stabilized with its boom

pointing outwards. Referring to Fig. 2.1, a certain coordinate system fixed in the satellite structure shall coincide with a reference coordinate system fixed in orbit. The pointing accuracy is required to be within 10 degrees in pitch, roll, and 20 degrees in yaw.

During science observation the satellite attitude is influenced by a gravity gradient torque which causes an oscillatory motion around either of two equilibria, boom upright or boom upside-down. This is called libration. A sum of potential and kinetic energy for librating satellite is maintained, and the system is only marginally stable.

If the boom should be upside-down, control action is required to turn the satellite. This is considered as a contingency mission phase.

Therefore, investigation of both linear and nonlinear methods is necessary. A linear model of the satellite can be successfully applied in the science observation phase, because nominally the satellite motion is about the reference, but nonlinear control is required for large angle recovery of the satellite. Development of attitude control methods for three axis stabilization of a low Earth orbit satellite is the subject of this thesis. A key challenge in this work is the fact that the mechanical torque can only be produced in a plane perpendicular to the local geomagnetic field vector.

1.2   Previous Work

Several control methods have been developed over the past years since the first satellite was launched in 1957. Generally speaking those techniques may be classified as active or passive. The most common passive techniques are spin stabilization, in which a bias angular momentum is producible, such that the satellite spin axis is approximately fixed in inertial space; and gravity gradient stabilization, in which the satellite is fixed relative to the zenith. Active techniques are needed for missions where high pointing accuracy is required, and typical actuators are: reaction or momentum wheels for precision control combined with gas jets and/or electromagnetic coils for wheel despin by angular momentum dumping.

Magnetic torquing is attractive for generation of control torque on small, cheap satellites in low Earth orbits where sub degree pointing accuracy is not required. This is the main reasons to suggest this actuation principle for the Danish Ørsted satellite mission in an early phase when a spin stabilized mission, i.e. two-axis control, was foreseen. Later redefinition of the scientific objectives demanded an alteration of the control requirements to three axis stabilization. The challenge was that three axis control was not possible with an actuation principle that leaves the system controllable in only two degrees of freedom since the control torque can only be generated perpendicular to the local magnetic field of the Earth.

There is extensive literature covering satellite attitude control design. Most of the algorithms assume application of reaction wheels and/or thrusters for three axis stabilization,

though. Attitude control with sole use of magnetorquers has the significant challenge that the system is only controllable in two axes at any point in time with the axes being perpendicular to the local geomagnetic field vector.

The number of internationally published papers on magnetic attitude control is still rather small. The available literature on nonlinear control for 3-axis stabilization of satellites includes Yon-Pin and Shih-Che (1993), and Cavallo *et al.* (1993). Both of these papers consider application of the sliding mode control. In the first paper the use of gas jets was investigated. A configuration with two magnetic coils and a reaction wheel were analysed in the latter. A geometric control approach to a satellite actuated by a set of two thruster jets was addressed in Byrnes and Isidori (1991). A general framework for the analysis of the attitude tracking control problem using Lyapunov theory for a rigid body was presented in Wen and Kreutz-Delgado (1991). Time invariant systems were considered, and magnetic torquing was outside the scope of this paper. However, salient features of proportional-derivative controllers for attitude control were found. The problem of three axis magnetic control was addressed in Martel *et al.* (1988), where a linearized time varying satellite motion model was approximated by a linear time invariant counterpart. Another linear approach was given by Musser and Ward (1989). The local stabilization of the satellite was achieved via implementation of the infinite time horizon linear quadratic regulator.

1.3   Structure of Thesis

The thesis deals with linear and nonlinear methods for magnetic attitude control.The work is divided into four main parts. The first part, Chapter 2, cope with the development of a mathematical model of a low Earth orbit satellite. The second part, Chapters 3 and 4, considers the satellite as a linear periodic system, and provides variety of locally stable attitude controllers. Chapter 3 deals with theoretical aspects of a class of periodic linear systems. Findings from this investigations are applied in Chapter 4. In the third part, Chapters 5, 6, and 7, local and global stability analysis of the satellite is made from the point of view of the nonlinear control theory and a family of proportional-derivative feedback cross product with the local geomagnetic field is presented. Chapter 5 gives general theoretical foundations, and Chapters 6 and 7 treats the problem of the attitude control. The fourth and the last part, Chapter 8 carries out simulation tests of those controllers, which are implemented for the Ørsted satellite. This chapter constitutes a summary of the Ørsted Attitude Control System. Advantages and disadvantages of the Ørsted controllers are discussed.

In Chapters 4, 6 and 7 general theoretical results are examined via simulation tests in ideal conditions, i.e. the orbit is circular, atmospheric density is zero. The Ørsted satellite's moments of inertia about the x and y axes are roughly equal. In order to evaluate theoretical findings the moment of inertia about the y principal axis is made 25 per cent

smaller in simulation studies in Chapter 7. A detailed simulation test is performed for realistic disturbances of the Ørsted satellite in elliptic orbit in Chapter 8.

- **Chapter 2, Satellite Motion Model**

  This chapter provides definitions of coordinate systems used throughout the thesis. Detailed description of the satellite motion is given, and linearization of the satellite dynamics/kinematics using multiplicative nature of the quaternion calculus is presented. Environment models are briefly reviewed in the last part of the chapter.

- **Chapter 3, Periodic Linear Systems**

  This chapter gives introductory information about periodic systems. Floquet theory is introduced. The infinite quadratic cost problem is investigated, and it is shown that the steady state solution to the periodic Riccati equation is periodic. The finite quadratic cost problem is then presented. The major part of this chapter is concerned with an investigation of the influence of the final condition of the periodic Riccati equation on stability of the receding horizon controller. Application of Picard's method of successive approximation to periodic systems is investigated in the last section of this chapter.

- **Chapter 4, Three Axis Attitude Control: Linear Approach**

  This chapter is devoted to the design issues of the linear attitude control. It is shown that a low Earth orbit satellite actuated by a set of perpendicular magnetorquers may indeed be considered as a periodic system. An infinite horizon periodic controller is implemented, which gain is parameterized by the mean anomaly. Eventually, final horizon and constant gain controllers are proposed.

- **Chapter 5, Periodic Nonlinear Systems**

  Important definitions and concepts of stability are given in this chapter. The Lyapunov direct method and Krasovskii-LaSalle theory of nonlinear periodic systems are reviewed.

- **Chapter 6, Three Axis Attitude Control: Sliding Mode Control**

  The essence of the sliding controller design for magnetic actuated satellite is given in this chapter. A three dimensional sliding manifold is proposed, and it is shown that the satellite motion on the sliding manifold is asymptotically stable. An ideal case of the sliding condition development is when the control torque is producible in x, y, and z directions independently. Firstly, a solution to this control problem is proposed, then a sliding condition for the magnetic generated control torque is addressed.

- **Chapter 7, Three Axis Attitude Control: Energy Approach**

This chapter plays a fundamental role for this thesis. Attitude stabilization at large is considered, and an angular velocity controller is introduced. This control principle is proved to be asymptotically stable around four equilibria. This results are extended to a locally stabilizing controller with velocity and attitude information. A velocity/attitude feedback cross product with the local geomagnetic field vector makes the desired reference attitude the only stable equilibrium. This analysis is extended to a globally stable controller in the last section.

- **Chapter 8, Ørsted Attitude Control**

  The attitude controllers implemented for the Ørsted satellite are simulated in a realistic space environment. The major part of this chapter deals with an investigation of the influence of an inertia error, ellipticity of the Ørsted orbit and aerodynamic drag torque on the performance of the attitude control. Pros and cones of the Ørsted satellite controllers are given.

- **Chapter 9, Conclusions and Recommendations**

  This chapter contains the concluding remarks and the recommendations for future work.

- **Appendix A: Orbit and Atmospheric Density Models**

  High fidelity models of the aerodynamic drag, orbit propagator, and the geomagnetic field are outlined in this appendix.

- **Appendix B: Rate Detumbling Controller**

  The theory behind the rate detumbling controller for the Ørsted satellite is given in this appendix.

1.4 Contributions of This Thesis

A number of new solutions to the attitude control problem are provided in this work. A list of the main contributions is given below.

- In Section 2.6 the multiplicative linearization of the unit quaternion for the attitude control purpose is proposed. Similar technique has been used earlier but for an extended Kalman filter Psiaki *et al.* (1990).

- In Chapters 4 and 5 the magnetic actuated satellite is considered periodic, and methods for linear and nonlinear periodic systems are applied. Floquet stability analysis is used in Chapter 4, and Krasovski-LaSalle theory of periodic systems is used in the proofs of theorems in the parts dealing with nonlinear attitude control methods, Section 7.1.

- It is proved in Chapter 3 that the steady state solution to the periodic Riccati equation is periodic. Furthermore, it is shown that the choice of a final condition of the periodic Riccati equation in a receding horizon controller has an influence on stability of the systems with time-varying and bounded parameters. Attitude controllers based on these findings are designed in Chapter 4 and published Wisniewski (1995*b*).

- It is demonstrated in Section 3.5 that the ad-hock method presented in Martel *et al.* (1988), proposing substitution of a non autonomous system by its time invariant counterpart, has a theoretical basis.

- It is shown in Section 4.2 that the time varying coefficients of the optimal attitude controller can be parameterized by the mean anomaly (orbital position). The findings are published in Wisniewski (1997).

- A sliding mode controller for the magnetic actuated satellite is designed in Section 6.1. A sliding manifold is proposed in the state space of the attitude quaternion and satellite angular velocity. A modified sliding condition incorporating time variation of the geomagnetic field. This is published in Wisniewski (1994*b*) and Wisniewski and Blanke (1996*a*).

- It was demonstrated in Section 7.1 that a low Earth orbit satellite actuated by the velocity feedback cross product with the geomagnetic field has four locally asymptotically stable equilibria. This is published in Wisniewski and Blanke (1996*c*).

- A method consisting of a plot of the root locus of the characteristic multipliers parameterized by the quaternion gain was proposed in Sections 4.4 and 7.2. This is published in Wisniewski and Blanke (1996*c*).

- The potential/kinetic energy dissipation control for three axis magnetic attitude control is developed in Section 7.3. This results are published in Wisniewski and Blanke (1996*b*)

- A globally stable control law was proposed in Section 7.4. The controller is not only asymptotically stable for attitudes such that the boom is upright, but it rescues the satellite when the the boom is upside-down. This is also part of the publication Wisniewski and Blanke (1996*b*).

Chapter 2

Satellite Motion Model

This chapter presents definitions of coordinate systems used throughout the thesis. A thorough description of the satellite motion is provided in Sections 2.2 and 2.3. A description of kinetic and potential energy of a low Earth satellite (LEO) is given in Section 2.4. Controllability issues of a magnetic actuated satellite are outlined in Section 2.5. Finally, in the last Section 2.6 the linearized equations of motion are given, where the hybrid of the additive and multiplicative linearization of the dynamics and kinematics is considered.

2.1   Coordinate Systems

The coordinate systems used in the thesis are a Control Coordinate System (CS), built on the satellite principal axes, a Body CS corresponding to the satellite structure, an Orbit CS referring to the current position of the satellite in orbit, and a World CS, which is an inertial coordinate system. The formal definitions of these coordinate systems are

- **The Control CS** is a right orthogonal coordinate system built on the principal axes of the satellite with the origin placed in the centre of mass. The x axis is the axis of the maximum moment of inertia, and the z axis is the minimum, Fig. 2.1.

- **The Body CS** is a right orthogonal coordinate system with the origin in the centre of gravity. The z axis is parallel to the boom direction and points towards boom tip. The x axis is perpendicular to the shortest edge of the bottom of the satellite body, and points away from the boom canister. The y axis is perpendicular to the longest edge of the bottom satellite body, Fig. 2.2. It is the reference coordinate system for attitude measurements and the magnetorquers.
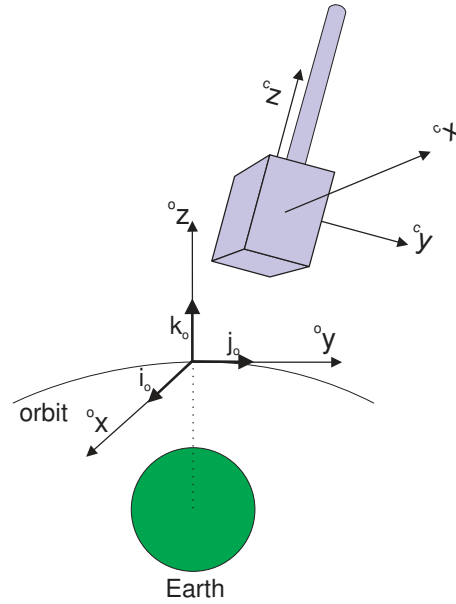
Figure 2.1: Definition of the Control CS in the Orbit CS. The Control CS is built on the principal axes of the satellite, whereas the Orbit CS is fixed in orbit.
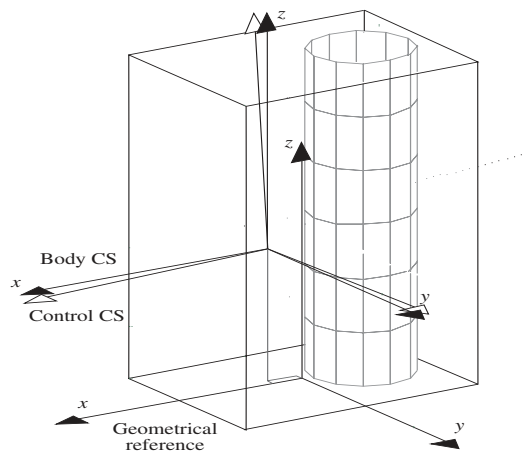
Figure 2.2: Definition of the Body CS. The Body CS refers to geometry of the satellite main body, its axes are perpendicular to the satellite facets.

- **The Orbit CS** is a right orthogonal coordinate system fixed in the centre of mass of the satellite. The z axis points at the zenith (is aligned with the centre of the Earth and points away from the Earth), the x axis points in the orbital plane normal direction and its sense coincides with the sense of the orbital angular velocity vector. The Orbit CS is the reference for the attitude control system.

- **The World CS** is an inertial right orthogonal coordinate system with origin in the centre of mass of the satellite. The z axis is parallel to the rotation axis of the Earth and points towards the North Pole. The x axis is parallel to the line connecting the centre of the Earth with Vernal Equinox and points towards Vernal Equinox (Vernal Equinox is the point where the ecliptic crosses the Earth equator going from South to North on the first day of spring).

2.2 Quaternions

This section gives an introduction to a unit quaternion, providing a singularity-free representation of kinematics. Information included in this section is based primarily on Wertz (1990).

Rotation of coordinate systems can be described by means of a quaternion. A salient feature of quaternions is that they provide a convenient product rule for successive rotations and a simple form of kinematics.

The four parameters $[q_1 \ q_2 \ q_3 \ q_4]^T$ form the components of the quaternion, $\tilde{\mathbf{q}}$, defined as follows

$$\tilde{\mathbf{q}} \equiv i \, q_1 + j \, q_2 + k \, q_3 + q_4, \tag{2.1}$$

where i, j, and k are hyper imaginary numbers satisfying the condition

$$
\begin{aligned}
i^2 = j^2 = k^2 &= \Leftrightarrow 1 \\
ij = \Leftrightarrow ji &= k \\
jk = \Leftrightarrow kj &= i \\
ki = \Leftrightarrow ik &= j.
\end{aligned}
\tag{2.2}
$$

The first three components, $\mathbf{q} = [q_1 \ q_2 \ q_3]^T$, form a vector part of the quaternion and the quantity, q_4 is a scalar part. Thus the quaternion $\tilde{\mathbf{q}} = [q_1 \ q_2 \ q_3 \ q_4]^T$ may be written as $[\mathbf{q}^T \ q_4]^T$.

The inverse of $\tilde{\mathbf{q}}$ is defined as

$$\tilde{\mathbf{q}}^* \equiv \Leftrightarrow i \, q_1 \Leftrightarrow j \, q_2 \Leftrightarrow k \, q_3 + q_4. \tag{2.3}$$

The norm of quaternion $\tilde{\mathbf{q}}$ is given by

$$|\tilde{\mathbf{q}}| \equiv \sqrt{\tilde{\mathbf{q}}^* \tilde{\mathbf{q}}} = \sqrt{q_1^2 + q_2^2 + q_3^2 + q_4^2}. \tag{2.4}$$

The construction of the unit quaternion arises from an observation by Euler and Hamilton that the rotation of coordinate systems can be uniquely described by a unit vector, $\mathbf{e} = [e_1 \; e_2 \; e_3]^T$ giving an axis of rotation as well as its sense, and an angle of rotation ϕ. The quaternion, $\tilde{\mathbf{q}}$, has four parameters:

$$
\begin{aligned}
q_1 &\equiv e_1 sin\frac{\phi}{2} \\
q_2 &\equiv e_2 sin\frac{\phi}{2} \\
q_3 &\equiv e_3 sin\frac{\phi}{2} \\
q_4 &\equiv cos\frac{\phi}{2}.
\end{aligned}
\tag{2.5}
$$

The norm of the quaternion defined according to Eq. (2.6) is 1. Furthermore, the same attitude can be described by two quaternions $\mathbf{q}$ and $\Leftrightarrow\mathbf{q}$, the first is given when the angle of rotation is ϕ, and the latter for the angle $2\pi + \phi$.

Quaternions provide simple methods for calculation of successive rotations. Let the quaternion reflecting the rotation of the Control CS in the Orbit CS and the quaternion describing transformation from the World CS to the Orbit CS be given. Then the product quaternion in Eqs. (2.6) provides an elegant method for calculation of the total transformation from the World CS to the Control CS.

$$
{}^{c}_{w}\mathbf{q} = \mathbf{R}({}^{o}_{w}\mathbf{q}){}^{c}_{o}\mathbf{q},
\tag{2.6}
$$

where

$$
\mathbf{R}(\tilde{\mathbf{q}}) =
\begin{bmatrix}
q_4 & q_3 & \Leftrightarrow q_2 & q_1 \\
\Leftrightarrow q_3 & q_4 & q_1 & q_2 \\
\Leftrightarrow q_2 & \Leftrightarrow q_1 & q_4 & q_3 \\
\Leftrightarrow q_1 & \Leftrightarrow q_2 & \Leftrightarrow q_3 & q_4
\end{bmatrix}
\tag{2.7}
$$

Moreover, the following equalities are true

$$
\mathbf{R}(\tilde{\mathbf{q}})\mathbf{R}^T(\tilde{\mathbf{q}}) = \mathbf{R}^T(\tilde{\mathbf{q}})\mathbf{R}(\tilde{\mathbf{q}}) = \tilde{\mathbf{q}}^T\tilde{\mathbf{q}}\mathbf{E}_{4\times 4}.
\tag{2.8}
$$

The relation between the attitude quaternion and the direction cosine matrix is also useful. The direct cosine matrix from the Orbit CS to the Control CS is given as

$$
{}^{c}_{o}\mathbf{A} = \begin{bmatrix} {}^{c}\mathbf{i}_o & {}^{c}\mathbf{j}_o & {}^{c}\mathbf{k}_o \end{bmatrix},
\tag{2.9}
$$

where ${}^{c}\mathbf{i}_o$, ${}^{c}\mathbf{j}_o$, ${}^{c}\mathbf{k}_o$, see Fig. 2.1, are the unit vectors of the x, y, and z axes of the Orbit CS, respectively, projected on the coordinates of the Control CS.

The unit vectors ${}^{c}\mathbf{i}_o$, ${}^{c}\mathbf{j}_o$, ${}^{c}\mathbf{k}_o$ may be parameterized by the attitude quaternion, ${}^{c}_{o}\mathbf{q}$

$$
\begin{aligned}
{}^{c}\mathbf{i}_{o} &= \begin{bmatrix} q_1^2 \Leftrightarrow q_2^2 \Leftrightarrow q_3^2 + q_4^2 & 2(q_1 q_2 \Leftrightarrow q_3 q_4) & 2(q_1 q_3 + q_2 q_4) \end{bmatrix}^T, \\
{}^{c}\mathbf{j}_{o} &= \begin{bmatrix} 2(q_1 q_2 + q_3 q_4) & \Leftrightarrow q_1^2 + q_2^2 \Leftrightarrow q_3^2 + q_4^2 & 2(q_2 q_3 \Leftrightarrow q_1 q_4) \end{bmatrix}^T, \quad (2.10) \\
{}^{c}\mathbf{k}_{o} &= \begin{bmatrix} 2(q_1 q_3 \Leftrightarrow q_2 q_4) & 2(q_2 q_3 + q_1 q_4) & \Leftrightarrow q_1^2 \Leftrightarrow q_2^2 + q_3^2 + q_4^2 \end{bmatrix}^T.
\end{aligned}
$$

Now, the transformation of a vector $\mathbf{v}$ observed in Orbit CS (${}^{o}\mathbf{v}$) to the vector $\mathbf{v}$ observed in the Control CS (${}^{c}\mathbf{v}$) is simply given by ${}^{c}\mathbf{v} = {}^{c}_{o}\mathbf{A}\,{}^{o}\mathbf{v}$.

Frequently, it is necessary to obtain the inverse transformation, i.e. from the Control CS to the Orbit CS. The inverse transformation is given by the conjugate of the attitude quaternion

$$
{}^{o}_{c}\mathbf{q} = {}^{c}_{o}\mathbf{q}^{*}. \tag{2.11}
$$

2.3 Equations of Motion

The mathematical model of a satellite is described by dynamic and kinematic equations of motion, see Wertz (1990). The dynamics relates torques acting on the satellite to the satellite's angular velocity in the World CS. The kinematics provides integration of the angular velocity. In the thesis the attitude is parameterized by four components of a quaternion describing rotation of the Control CS in the Orbit CS.

2.3.1 Dynamics

The dynamic equation of motion of a rigid satellite in low Earth orbit is

$$
\mathbf{I}\,{}^{c}\dot{\boldsymbol{\Omega}}_{cw}(t) = \Leftrightarrow {}^{c}\boldsymbol{\Omega}_{cw}(t) \times \mathbf{I}\,{}^{c}\boldsymbol{\Omega}_{cw}(t) + {}^{c}\mathbf{N}_{ctrl}(t) + {}^{c}\mathbf{N}_{gg}(t) + {}^{c}\mathbf{N}_{dis}(t). \tag{2.12}
$$

The summand ${}^{c}\boldsymbol{\Omega}_{cw}(t) \times \mathbf{I}\,{}^{c}\boldsymbol{\Omega}_{cw}(t)$ represents a cross coupling between the components of the angular velocity vector, ${}^{c}\boldsymbol{\Omega}_{cw}(t)$. It arises due to the fact that the dynamics is described in a rotating coordinate system (the Control CS), in an inertial coordinate system this summand disappears.

Control torque is generated by an interaction of the geomagnetic field with the magnetorquer current $i(t)$ which gives rise to a magnetic moment $m(t)$

$$
m(t) = n_{coil}\, i_{coil}(t)\, A_{coil}. \tag{2.13}
$$

The electromagnetic coils are placed perpendicular to the x, y and z axes of the Body CS, thus the vector representing entire magnetic moment producible by all three coils is given

in the Body CS. The transformation from the Body CS to the Control CS (the coordinate system in which the dynamics is described) is necessary

$$^c\mathbf{m} = {}^c_b\mathbf{A}\,{}^b\mathbf{m}. \tag{2.14}$$

The control torque acting on the satellite is then

$$^c\mathbf{N}_{ctrl}(t) = {}^c\mathbf{m}(t) \times {}^c\mathbf{B}(t). \tag{2.15}$$

The magnetic moment given in the Control CS, $^c\mathbf{m}$, will be considered as the control signal throughout the thesis.

According to Wertz (1990) the gravity gradient torque is given as

$$^c\mathbf{N}_{gg} = \frac{3\mu}{R_{cm}^3}({}^c\hat{\mathbf{R}}_{cm} \times \mathbf{I}{}^c\hat{\mathbf{R}}_{cm}), \tag{2.16}$$

where μ is the Earth gravitational constant, R_{cm} is the distance from the centre of the Earth to the satellite's centre of gravity (R_{cm} is a subject of variation, when an elliptic orbit is considered), $^c\hat{\mathbf{R}}_{cm}$ is the zenith[1].

Observe that the zenith is equivalent to the unit vector $^c\mathbf{k}_o$ and the constant $\frac{\mu}{R_{cm}^3} = \omega_o^2$, where ω_o is the orbital rate. Now, the gravity gradient torque is

$$^c\mathbf{N}_{gg} = 3\omega_o^2({}^c\mathbf{k}_o \times \mathbf{I}{}^c\mathbf{k}_o). \tag{2.17}$$

The disturbance torque is mainly due to the aerodynamic drag, see Section 2.7.

2.3.2 Kinematics

The kinematics describes the body's orientation in space and is obtained through integration of the angular velocity. The kinematic equations are expressed by separate integrations of the vector and the scalar part of the attitude quaternion

$$
\begin{aligned}
\dot{\mathbf{q}} &= \frac{1}{2}{}^c\mathbf{\Omega}_{co}q_4 \Leftrightarrow \frac{1}{2}{}^c\mathbf{\Omega}_{co} \times \mathbf{q}, \\
\dot{q}_4 &= \Leftrightarrow\frac{1}{2}{}^c\mathbf{\Omega}_{co} \cdot \mathbf{q}.
\end{aligned}
\tag{2.18}
$$

It is convenient to represent Eq. (2.18) by an equivalent bilinear form as stated in Morton (1993)

$$^c_o\dot{\mathbf{q}} = \frac{1}{2}\mathbf{R}({}^c\tilde{\mathbf{\Omega}}_{co}){}^c_o\mathbf{q}, \tag{2.19}$$

---

[1] See Space Terminology in Nomenclature.

where $^c\tilde{\boldsymbol{\Omega}}_{co} = [^c\boldsymbol{\Omega}_{co}^T \ 0]^T$, and $\mathbf{R}(\cdot)$ is given in Eq. (2.7).

A relation between the satellite angular velocity w.r.t. to the Word CS and the angular velocity w.r.t. the Orbit CS is given by

$$^c\boldsymbol{\Omega}_{co} = {}^c\boldsymbol{\Omega}_{cw} \Leftrightarrow \omega_o{}^c\mathbf{i}_o. \tag{2.20}$$

The orbital rate, ω_o is constant for a circular orbit, but time varying for an elliptic orbit. The eccentricity of the Ørsted orbit is comparatively small and the variation of ω_o can be disregarded.

Remark 2.3.1 *In summary a satellite motion is characterized by the 7th order nonlinear differential equation (Eqs. (2.12), (2.15), (2.17), (2.18), and (2.20)). The quaternion representation of the attitude provides one redundant equation in kinematics. The advantage is that the description of the kinematics is free from any singularity. Note that a singularity is observed in the attitude parameterization if the Euler angles are used, see Wertz (1990).*

2.4   Kinetic and Potential Energy

The objective of the present section is to derive the kinetic and potential energy, which will be extensively used in the chapter on nonlinear control methods.

2.4.1   Kinetic Energy

The standard kinetic energy of the satellite is a quadratic form relating the satellite velocity in the World CS. In this study we focus only on the rotation of the satellite w.r.t the reference coordinate system, i.e. the Orbit CS.

The total angular velocity of the satellite relative to the Word CS is a sum of the satellite angular velocity w.r.t the Orbit CS and the angular velocity of the satellite's revolution about the Earth (the orbital rate). It is assumed that the orbit is circular and thus the orbital rate, ω_o is constant. The kinetic energy of the rotary motion is then

$$E_{kin} = \frac{1}{2}{}^c\boldsymbol{\Omega}_{co}^T \mathbf{I}^c\boldsymbol{\Omega}_{co}. \tag{2.21}$$

Note that the eccentricity of the Ørsted orbit is $e = 0.025$, thus ω_o is constant within 3 percent.

2.4.2   Potential Energy

The potential energy due to the gravity gradient is minimum ($E_{gg} = 0$) when the scientific boom is ideally aligned with the z axis of the Orbit CS, since there is no gravity

gradient acting on the satellite. Its maximum value is reached when the satellite attitude is such that the z axis of the Orbit CS coincides with the x axis of the Control CS.

The potential energy associated with the gravity gradient is represented as

$$E_{gg} = \frac{3}{2}\omega_o^2({}^c\mathbf{k}_o^T\mathbf{I}^c\mathbf{k}_o \Leftrightarrow I_z), \tag{2.22}$$

where the vector ${}^c\mathbf{k}_o$ is a unit vector along the z axis of the Orbit CS projected on the axes of the Control CS. The unit vector ${}^c\mathbf{k}_o$ is parameterized by the attitude quaternion as in Eq. (2.11).

The potential energy has also a component originating from the revolution of the satellite about the Earth. Consider the summand ${}^c\mathbf{\Omega}_{cw}(t)\times\mathbf{I}\,{}^c\mathbf{\Omega}_{cw}(t)$ in the equation of dynamics (2.12). Using Eq. (2.20) this can be rewritten as

$$\begin{aligned}{}^c\mathbf{\Omega}_{cw}(t) \times \mathbf{I}\,{}^c\mathbf{\Omega}_{cw}(t) &= {}^c\mathbf{\Omega}_{co}(t) \times \mathbf{I}\,{}^c\mathbf{\Omega}_{co}(t) + \omega_o\,{}^c\mathbf{i}_o \times \mathbf{I}\,{}^c\mathbf{\Omega}_{co}(t) \\ &+ \omega_o\,{}^c\mathbf{\Omega}_{co}(t) \times \mathbf{I}\,{}^c\mathbf{i}_o + \omega_o^2\,{}^c\mathbf{i}_o \times \mathbf{I}\,{}^c\mathbf{i}_o, \end{aligned} \tag{2.23}$$

where ${}^c\mathbf{i}_o$ is a unit vector on the x axis of the Orbit CS resolved in the Control CS, see Eq. (2.11).

The summand $\omega_o^2\,{}^c\mathbf{i}_o \times \mathbf{I}\,{}^c\mathbf{i}_o$ is not dependent on the satellite's angular velocity, and hence gives a contribution only to the potential energy. The potential energy due to the revolution of the satellite about the Earth is

$$E_{gyro} = \frac{1}{2}\omega_o^2(I_x \Leftrightarrow {}^c\mathbf{i}_o^T\mathbf{I}^c\mathbf{i}_o). \tag{2.24}$$

The minimum of this energy is obtained when the x axis of the Control CS is aligned with the x axis of the Orbit CS, and maximum when the x axis of the Orbit CS coincides with the z axis of the Control CS.

2.5 Controllability

The satellite actuated by a set of magnetorquers has a serious limitation. The mechanical torque, produced by the interaction of the geomagnetic field and the magnetic field generated by the magnetorquers, is always perpendicular to the geomagnetic field vector. Thus the direction parallel to the geomagnetic field vector is not controllable. The geomagnetic field changes its orientation in the Orbit CS when the satellite moves in orbit. This implies that e.g. yaw is not controllable over the poles but only a quarter of orbit later, i.e. over the equator, it reaches controllability, see Fig. 2.3.
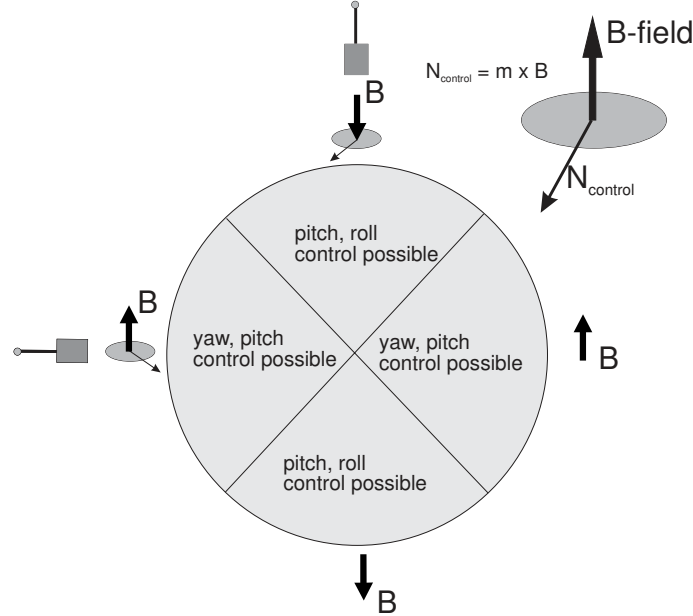
Figure 2.3: Control torque is always perpendicular to the geomagnetic field vector. This implies that yaw is not controllable over poles, and roll is not controllable over equator.

2.6   Linearized Equation of Motion

A linearized time-varying model of the satellite motion will be used in the chapter on application of the linear periodic systems to the attitude control, Chapter 4.

The satellite motion is considered in a neighbourhood of the following reference: the angular velocity of the satellite rotation w.r.t. the Orbit CS is zero ($^c\mathbf{\Omega}_{co} = \mathbf{0}$), and the attitude is such that the Control CS coincides with the Orbit CS ($^c_o\mathbf{q} = [0\ 0\ 0\ 1]^T$).

Linearization of the angular velocity is commonplace and based on the first order extension of the Taylor series. The angular velocity $^c\mathbf{\Omega}_{cw}$ from Eq. (2.20) is

$$^c\mathbf{\Omega}_{cw} = {}^c_o\mathbf{A}\,[\omega_0\ 0\ 0]^T + \delta\mathbf{\Omega}, \tag{2.25}$$

where $\delta\mathbf{\Omega}$ is a small perturbation of the angular velocity $^c\mathbf{\Omega}_{cw}$ from the reference.

Linearization of the attitude quaternion is different due to the multiplicative transformation in Eq. (2.6) is needed to describe a rotation. Two successive rotations are used, the first one is a transformation from the Orbit CS to a reference coordinate system, the second from the reference coordinate system to the Control CS. The reference coordinate system is the Orbit CS in the thesis, thus the rotation from the Orbit CS to the reference

coordinate system is trivially given by the identity operation.

$$
{}_o^c\mathbf{q} = \mathbf{Q}([0\ 0\ 0\ 1]^T)\delta\tilde{\mathbf{q}} = \delta\tilde{\mathbf{q}}, \tag{2.26}
$$

where $\delta\tilde{\mathbf{q}}$ is a small perturbation of the attitude quaternion, ${}_o^c\mathbf{q}$, from the reference, and according to Eq. (2.6) is

$$
\delta\tilde{\mathbf{q}} = \begin{bmatrix} e_1 sin\frac{\delta\phi}{2} \\ e_2 sin\frac{\delta\phi}{2} \\ e_3 sin\frac{\delta\phi}{2} \\ cos\frac{\delta\phi}{2} \end{bmatrix} \approx \begin{bmatrix} \delta q_1 \\ \delta q_2 \\ \delta q_3 \\ 1 \end{bmatrix} \equiv \begin{bmatrix} \delta\mathbf{q} \\ 1 \end{bmatrix}. \tag{2.27}
$$

Remark 2.6.1 *Consider a certain reference coordinate system the Reference CS , such that the quaternion ${}_o^r\mathbf{q}$ of the transformation from the Orbit CS to the Reference CS is constant. The linearization of the angular velocity w.r.t. the Reference CS is then*

$$
{}^c\mathbf{\Omega}_{cw} = {}_r^c\mathbf{A}\,{}_o^r\mathbf{A}[\omega_0\ 0\ 0]^T + \delta\mathbf{\Omega}, \tag{2.28}
$$

and the linerization of the attitude quaternion is as follows

$$
{}_o^c\mathbf{q} = \mathbf{Q}({}_o^r\mathbf{q})\delta\tilde{\mathbf{q}}. \tag{2.29}
$$

The linearized dynamics and kinematics based on the hybrid approach of the multiplicative and additive linearization will be derived in the next two subsections.

2.6.1 Linearized Dynamics

The equation of dynamics is divided into the cross coupling, the contribution of the gravity gradient torque and the part due to control torque. The disturbance torque $\mathbf{N}_{dis}$ is primarily dependent on the satellite position w.r.t the Sun and the Earth, therefore it is not included in the linear model of the satellite.

$$
\frac{d}{dt}\delta\mathbf{\Omega} = \delta(\text{Cross Coupling}) + \mathbf{I}^{-1}\delta(\text{Gravity Gradient Torque}) + \mathbf{I}^{-1}\delta(\text{Control Torque}). \tag{2.30}
$$

2.6.1.1 Linearization of Cross Coupling

$$
\text{Cross Coupling} = \begin{bmatrix} \sigma_x{}^c\omega_{cwy}{}^c\omega_{cwz} \\ \sigma_y{}^c\omega_{cwz}{}^c\omega_{cwx} \\ \sigma_z{}^c\omega_{cwx}{}^c\omega_{cwy} \end{bmatrix} \approx \begin{bmatrix} 0 \\ \sigma_y\omega_o\delta\omega_z \\ \sigma_z\omega_o\delta\omega_y \end{bmatrix}, \tag{2.31}
$$

where

$$\sigma_x = \frac{I_y \Leftrightarrow I_z}{I_x}, \ \sigma_y = \frac{I_z \Leftrightarrow I_x}{I_y}, \ \sigma_z = \frac{I_x \Leftrightarrow I_y}{I_z}, \tag{2.32}$$

and

$$\boldsymbol{\delta\Omega} = \begin{bmatrix} \delta\omega_x & \delta\omega_y & \delta\omega_z \end{bmatrix}^T. $$

2.6.1.2 Linearization of Gravity Gradient Torque

$$
\begin{aligned}
\text{Gravity Gradient Torque} \quad &\approx \quad 3\omega_o^2 \begin{bmatrix} \Leftrightarrow 2\delta q_2 \\ 2\delta q_1 \\ 1 \end{bmatrix} \times \begin{bmatrix} \Leftrightarrow 2I_x \delta q_2 \\ 2I_y \delta q_1 \\ I_z \end{bmatrix} \\
&\approx \quad 6\omega_o^2 \begin{bmatrix} (I_z \Leftrightarrow I_y)\delta q_1 \\ (I_z \Leftrightarrow I_x)\delta q_2 \\ 0 \end{bmatrix},
\end{aligned}
\tag{2.33}
$$

where

$$\boldsymbol{\delta q} = \begin{bmatrix} \delta q_1 & \delta q_2 & \delta q_3 \end{bmatrix}^T. $$

2.6.1.3 Linearization of Control Torque

$$\text{Control Torque} = {}^c\mathbf{m} \times {}^c_o\mathbf{A}^o\mathbf{B} \approx {}^c\mathbf{m} \times {}^o\mathbf{B} \Leftrightarrow 2{}^c\mathbf{m} \times (\boldsymbol{\delta q} \times {}^o\mathbf{B}),$$
$$\tag{2.34}$$

but the summand $2{}^c\mathbf{m} \times (\delta\mathbf{q} \times {}^o\mathbf{B})$ diminishes when a linear feedback is implemented as it is a term of second order approximation[2], and finally

$$\text{Control Torque} \approx {}^c\mathbf{m} \times {}^o\mathbf{B}. \tag{2.35}$$

2.6.2 Linearized Kinematics

2.6.2.1 Linearized Kinematic Equation

$$\frac{d}{dt}\mathbf{q} = \frac{1}{2}{}^c\boldsymbol{\Omega}_{co}q_4 \Leftrightarrow \frac{1}{2}{}^c\boldsymbol{\Omega}_{co} \times \mathbf{q} \approx \frac{1}{2}{}^c\boldsymbol{\Omega}_{co}. \tag{2.36}$$

Now, according to Eqs. 2.20 and 2.25 the linearized kinematics is

$$\frac{d}{dt}\boldsymbol{\delta q} = \frac{1}{2}\boldsymbol{\delta\Omega} \Leftrightarrow \frac{1}{2}[\omega_o \ 0 \ 0]^T \Leftrightarrow \boldsymbol{\delta q} \times [\omega_o \ 0 \ 0]^T = \frac{1}{2}\begin{bmatrix} \delta\omega_x \Leftrightarrow \omega_o \\ \delta\omega_y + 2\delta q_3\omega_o \\ \delta\omega_z \Leftrightarrow 2\delta q_2\omega_o \end{bmatrix}. \tag{2.37}$$

---

[2]The summand $2{}^c\mathbf{m} \times (\delta\mathbf{q} \times {}^o\mathbf{B})$ becomes $2\left(\mathbf{K}(t)\begin{bmatrix} \boldsymbol{\delta\Omega} & \boldsymbol{\delta q} \end{bmatrix}^T\right) \times (\boldsymbol{\delta q} \times {}^o\mathbf{B})$.

2.6.3 Linearized Equation of Satellite Motion

The matrix form of the linearized satellite motion about ${}^c\boldsymbol{\Omega}_{co} = \mathbf{0}$, and ${}^c_o\mathbf{q} = [0\ 0\ 0\ 1]^T$ is

$$\frac{d}{dt}\left[\begin{array}{c} \delta\boldsymbol{\Omega} \\ \delta q \end{array}\right] = \mathbf{A}\left[\begin{array}{c} \delta\boldsymbol{\Omega} \\ \delta\mathbf{q} \end{array}\right] + \mathbf{B}(t)\,{}^c\tilde{\mathbf{m}}, \qquad (2.38)$$

where

$$\mathbf{A} = \left[\begin{array}{cccccc} 0 & 0 & 0 & \Leftrightarrow 2k\sigma_x & 0 & 0 \\ 0 & 0 & \omega_o\sigma_y & 0 & 2k\sigma_y & 0 \\ 0 & \omega_o\sigma_z & 0 & 0 & 0 & 0 \\ \frac{1}{2} & 0 & 0 & 0 & 0 & 0 \\ 0 & \frac{1}{2} & 0 & 0 & 0 & \omega_o \\ 0 & 0 & \frac{1}{2} & 0 & \Leftrightarrow\omega_o & 0 \end{array}\right],$$

$$\mathbf{B}(t) = \left[\begin{array}{c} \mathbf{I}^{-1}\left[\begin{array}{ccc} 0 & \Leftrightarrow^o B_z(t) & {}^o B_y(t) \\ {}^o B_z(t) & 0 & \Leftrightarrow^o B_x(t) \\ \Leftrightarrow^o B_y(t) & {}^o B_x(t) & 0 \end{array}\right] \\ \left[\begin{array}{ccc} 0 & 0 & 0 \\ 0 & 0 & 0 \\ 0 & 0 & 0 \end{array}\right] \end{array}\right].$$

2.7 Environmental Models

A concise description of environmental models is addressed in this section. Our emphasis is on the geomagnetic field, and the primary disturbance torque for LEO satellites, which is the aerodynamic torque. The periodic properties of the geomagnetic field will be used in Chapter 4, treating the linear controller design. An aerodynamic torque is modeled in a simulation program. The performance test of the attitude controllers in Section 8 is executed with the aerodynamic torque present. Further details on modeling of the space environment is provided in Appendix A.

2.7.1 Aerodynamic Drag

The interaction of the upper atmosphere molecules with satellite's surface introduces an aerodynamic torque. Assuming that the energy of the molecules is totally absorbed on impact with the spacecraft, the force $\mathbf{df}_{aero}$ on a surface element dA is described by

$$\mathbf{df}_{aero} = \Leftrightarrow\frac{1}{2}C_D\rho v^2(\hat{\mathbf{n}}\cdot\hat{\mathbf{v}})\hat{\mathbf{v}}dA, \qquad (2.39)$$

where $\hat{\mathbf{n}}$ is an outward normal to the surface, $\hat{\mathbf{v}}$ is the unit vector in the direction of the translational velocity of the surface element relative to the incident stream of the
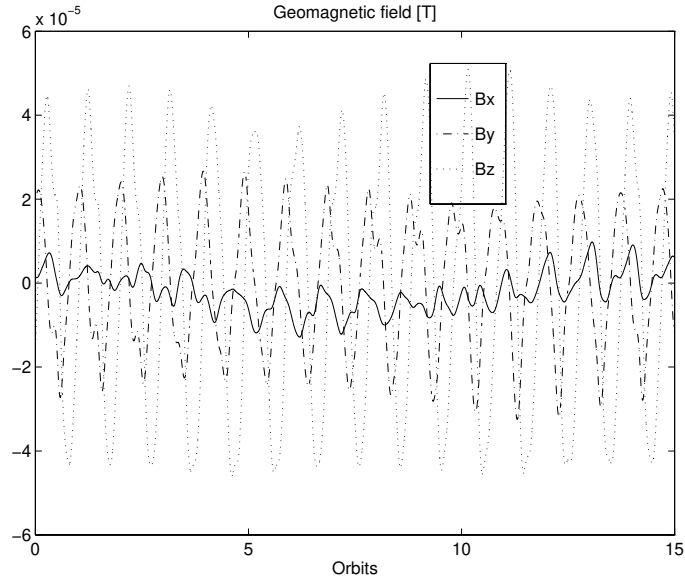
Figure 2.4: The geomagnetic field vector in the Ørsted Orbit CS propagated by a 10th order spherical harmonic model during a period of 24 h in April 1997.

molecules. The atmospheric density is denoted by ρ, and the drag coefficient by C_D. The total aerodynamic torque is determined by integration over the total spacecraft surface. A detailed description of the modeling of the aerodynamic drag for the Ørsted satellite can be found in Wisniewski (1995a).

The Jacchia-Roberts atmospheric model described in Cappellari (1976), was adopted in the simulation programs. The atmospheric density is determined as a function of the satellite altitude and the exospheric temperature. The exospheric temperature is parameterized by the daily average 10.7-centimetre solar flux, $F_{10.7}$, as observed in the solar observatory at Ottawa, Canada, and a geomagnetic activity index: the geomagnetic planetary index, K_p.

2.7.2 Geomagnetic Field

The geomagnetic field is essentially that of a magnetic dipole. The south pole is in the northern hemisphere at about $79°N$ latitude and $290°E$ longitude. There are certain deviations from the dipole model called anomalies. The largest anomalies are encountered over Brazil and Siberia, see Fig. 2.5 from Wertz (1990).

Let a near polar orbit be considered. The geomagnetic field observed in this orbit, i.e.
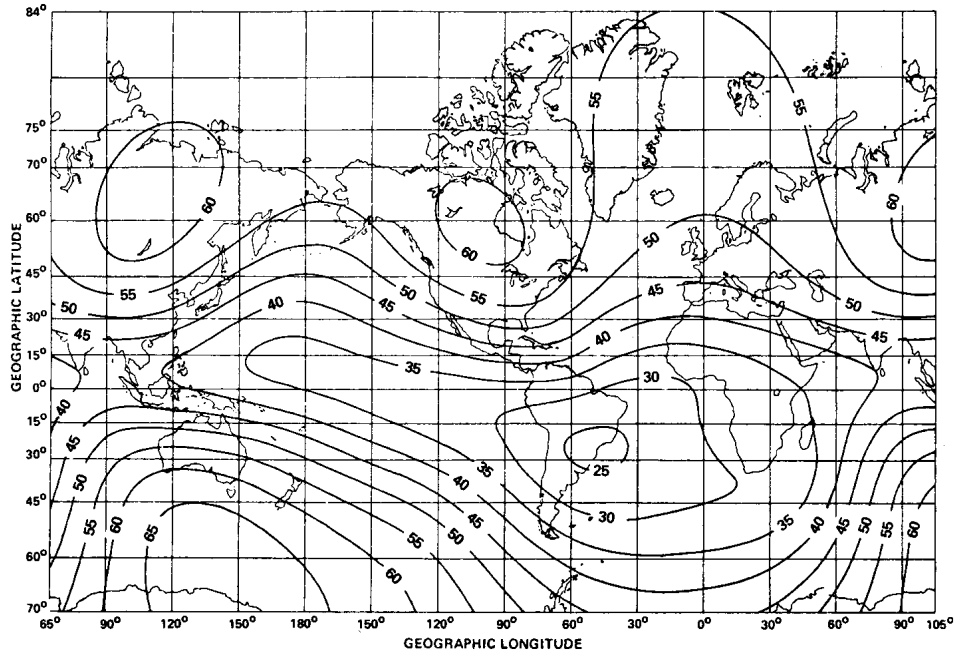
Figure 2.5: Total magnetic field intensity at the Earth's surface in nT

seen in the Orbit CS, has large y and z components, while the x component is comparatively small. The orbit position is fixed in the World CS, thus the rotation of the Earth is visible via fluctuations of the geomagnetic field vector's x component with frequency $1/24$ 1/hour. An example of geomagnetic field variation on orbit is given in Fig. 2.4. The geomagnetic field has been computed using 10th order spherical harmonic model, see Wertz (1990).

The observation that the geomagnetic field on near polar orbit is approximately periodic with period $T = 2\pi/\omega_0$ is used in the design of a constant gain and a time varying linear controller.

Chapter 3

Periodic Linear Systems

Both linear and nonlinear methods can be implemented for the attitude controller design. The adequacy of a particular technique is highly dependent on the satellite mission phase. During scientific observation, the satellite motion can be regarded as in the vicinity of the reference. Thus an application of a linear model of the satellite equations of motion is reasonable. In contrast, a nonlinear control method is required for the inverted boom mission phase. The next two chapters cope only with the linear control methods. This chapter deals with theory development, the next with implementation issues.

It was already mentioned that due to the actuation principle, the satellite is only controllable in two degrees of freedom at any given position in orbit. The geomagnetic field varies along the orbit and this time variation can be utilized for controller design. Incorporating time variation of system parameters into the structure of the attitude controller requires some background of methods for time varying linear systems. The class of all time varying systems can be furthermore limited to periodic systems from the observation, that the geomagnetic field seen from the Orbit CS is periodic.

Stability theory for periodic systems is not widely known in the engineering community, therefore a few necessary results in this field are first presented, where Floquet theory described in Section 3.1 plays the fundamental role. An objective is to design a controller with a time varying gain. Consequently, the problems of the optimal and quasi optimal controllers are formulated. Both finite and infinite cost problems are investigated in Sections 3.3 and 3.4. The properties of a steady state equilibrium and a transient solution to the periodic Riccati equation are examined. A novel method for periodic controller design is elaborated. Further work presented in this chapter is inspired by Martel *et al.* (1988), who proposed a PD attitude controller with parameters based on an average value of the geomagnetic field along the orbit. An issue of application of Picard's method of successive approximations for the design of a constant gain control law is considered in Section 3.5. The result is a time invariant approximation to the satellite linear periodic

model, appearing to be similar to the one proposed by Martel *et al.* (1988).

The references used for preparation of this chapter are mentioned in the beginning of each sections dealing with a particular theory. Most of theorems are given without proofs, only results , which are contributions of this thesis are provided with proofs.

The following linear T-periodic system is considered in this chapter

$$
\begin{aligned}
\dot{\mathbf{x}}(t) &= \mathbf{A}(t)\mathbf{x}(t) + \mathbf{B}(t)\mathbf{u}(t), \\
\mathbf{y}(t) &= \mathbf{C}(t)\mathbf{x}(t).
\end{aligned}
\tag{3.1}
$$

where $\mathbf{x}(t) \in \mathbb{R}^n$, $\mathbf{u}(t) \in \mathbb{R}^m$ are state and input vector respectively, $\mathbf{A}(t)$, $\mathbf{B}(t)$ are periodic matrices of period T

$$
\mathbf{A}(t+T) = \mathbf{A}(t), \ \mathbf{B}(t+T) = \mathbf{B}(t).
\tag{3.2}
$$

3.1 Floquet Theory

This section highlights key results from the theory of Floquet on linear differential equations with periodic coefficients. The stability of a periodic system is to be considered over time, therefore the transition matrix calculated within one period, from t_0 to $t_0 + T$, plays a significant role in the stability analysis. Namely, placement of its eigenvalues in the open unit disk determines whether the system is stable. The material in this section is based on Mohler (1991).

Consider the system in Eq. (3.1) with zero input vector

$$
\dot{\mathbf{x}}(t) = \mathbf{A}(t)\mathbf{x}(t).
\tag{3.3}
$$

The transition matrix of the system in Eq. (3.3) is denoted by $\boldsymbol{\Phi}_A(t, t_0)$, where t_0 is the time when the initial state is applied and t is the time when the state is observed. The following holds

$$
\boldsymbol{\Phi}_A(t+T, t_0) = \boldsymbol{\Phi}_A(t, t_0)\mathbf{C},
\tag{3.4}
$$

where $\mathbf{C}$ is a constant matrix.

To check this equality, it is enough to calculate the time derivative of $\boldsymbol{\Phi}_A(t+T, t_0)$

$$
\dot{\boldsymbol{\Phi}}_A(t+T, t_0) = \dot{\boldsymbol{\Phi}}_A(t, t_0)\mathbf{C} = \mathbf{A}(t)\boldsymbol{\Phi}_A(t, t_0)\mathbf{C} = \mathbf{A}(t+T)\boldsymbol{\Phi}_A(t+T, t_0),
\tag{3.5}
$$

since

$$
\dot{\boldsymbol{\Phi}}_A = \mathbf{A}(t)\boldsymbol{\Phi}_A.
$$

There exists a constant matrix $\mathbf{R}$ such that

$$
\mathbf{C} \equiv e^{\mathbf{R}T}.
\tag{3.6}
$$

From the equality $\mathbf{\Phi}_A(t_0, t_0) = \mathbf{I}$ and Eq. (3.4) it follows that

$$\mathbf{\Phi}_A(t_0 + T, t_0) = e^{\mathbf{R}T}. \tag{3.7}$$

Thus the state transition matrix consists of a periodically modulated exponential matrix function. The matrix $\mathbf{\Phi}_A(t_0 + T, t_0)$ is named the monodromy matrix at t_0 and is denoted by $\mathbf{\Psi}_A(t_0)$. It is concluded from Eq. (3.7) that the eigenvalues of the monodromy matrix are independent of t_0.

The system (3.3) is asymptotically stable if, and only if the eigenvalues of the matrix $\mathbf{R}$ all have negative real parts. The eigenvalues of $\mathbf{R}$ are defined as characteristic exponents of $\mathbf{A}(t)$. One can alternatively examine, whether the eigenvalues of the monodromy matrix belong to the open unit disk. The eigenvalues of the monodromy matrix are called characteristic multipliers of $\mathbf{A}(t)$.

3.2 Structural Properties of Periodic Systems

Once the concept of characteristic multipliers has been established, it is important to clarify the definitions of the structural properties of a periodic system as reachability, observability, stabilizability and detectability. The following definitions of unreachable and unobservable characteristic multipliers are available in Bittanti (1991).

Definition 3.2.1 *A characteristic multiplier λ of $\mathbf{A}(t)$ in Eq. (3.1) is said to be $(\mathbf{A}(t), \mathbf{B}(t))$ unreachable if*

$$\mathbf{\Psi}_A(t_0)^T \mathbf{x} = \lambda \mathbf{x}, \ \mathbf{x} \neq \mathbf{0} \ \Rightarrow \ \mathbf{B}(t)^T \mathbf{\Phi}_A(t, t_0)^T \mathbf{x} = \mathbf{0}, \ \text{for all } t \in [t_0, t_0 + T]. \tag{3.8}$$

A characteristic multiplier of $\mathbf{A}(t)$ is said to be $(\mathbf{A}(t), \mathbf{B}(t))$ reachable if it is not $(\mathbf{A}(t), \mathbf{B}(t))$ unreachable. The pair $(\mathbf{A}(t), \mathbf{B}(t))$ is said to be reachable if all the characteristic multipliers of $\mathbf{A}(t)$ are $(\mathbf{A}(t), \mathbf{B}(t))$ reachable.

Definition 3.2.2 *A characteristic multiplier λ of $\mathbf{A}(t)$ in Eq. (3.1) is said to be $(\mathbf{A}(t), \mathbf{C}(t))$ unobservable if*

$$\mathbf{\Psi}_A(t_0)\mathbf{x} = \lambda \mathbf{x}, \ \mathbf{x} \neq \mathbf{0} \ \Rightarrow \ \mathbf{C}(t)\mathbf{\Phi}_A(t_0, t)\mathbf{x} = \mathbf{0}, \ \text{for all } t \in [t_0, t_0 + T]. \tag{3.9}$$

A characteristic multiplier of $\mathbf{A}(t)$ is said to be $(\mathbf{A}(t), \mathbf{C}(t))$ observable if it is not $(\mathbf{A}(t), \mathbf{C}(t))$ unobservable. The pair $(\mathbf{A}(t), \mathbf{C}(t))$ is said to be observable if all the characteristic multipliers of $\mathbf{A}(t)$ are $(\mathbf{A}(t), \mathbf{C}(t))$ observable.

Definition 3.2.1 can be explained in the following way. A characteristic multiplier is unreachable if the eigenvector corresponding to this characteristic multiplier determines a direction which is not controllable in the whole envelope of time from t_0 to $t_0 + T$.

A test for reachability of the pair $(\mathbf{A}(t), \mathbf{B}(t))$ can by derived from Eq. (3.8). The following reasoning is used.

If the controllability gramian matrix $\mathbf{G}_c(t_0 + T, t_0)$

$$\mathbf{G}_c(t, \tau) \equiv \int_\tau^t \mathbf{\Phi}(t, s) \mathbf{B}(s) \mathbf{B}^T(s) \mathbf{\Phi}^T(t, s) ds \tag{3.10}$$

is not singular, then the statement

$$\mathbf{B}(t)^T \mathbf{\Phi}_A^T(t, t_0) \mathbf{x} = \mathbf{0}, \quad \text{for all } t \in [t_0, t_0 + T]. \tag{3.11}$$

is false for any nonzero vector $\mathbf{x}$, and the pair $(\mathbf{A}(t), \mathbf{B}(t))$ is reachable. Therefore, it is concluded that the pair $(\mathbf{A}(t), \mathbf{B}(t))$ is reachable, if $\mathbf{G}_c(\tau, \tau + T)$ is nonsingular.

Reachability is a property of a periodic system evaluated within one period. The system is reachable if the controllability gramian, $\mathbf{G}_c$ is not singular. If a non autonomous system is considered at a fixed time t_c,

$$\dot{\mathbf{x}}(t) = \mathbf{A}(t_c)\mathbf{x} + \mathbf{B}(t_c)\mathbf{u}, \tag{3.12}$$

controllability rank condition may not be fulfilled. The system (3.12) is then partitioned into a uncontrollable part and a part which is completely controllable. According to Kwakernaak and Sivan (1972), there exists a transformation matrix $\mathbf{T}$

$$\tilde{\mathbf{x}}(t) \equiv \mathbf{T}^{-1}\mathbf{x}(t), \tag{3.13}$$

such that the state differential equation (3.12) is transformed into the controllability canonical form

$$\dot{\tilde{\mathbf{x}}}(t) = \begin{bmatrix} \tilde{\mathbf{A}}_{11}(t_c) & \tilde{\mathbf{A}}_{12}(t_c) \\ \mathbf{0} & \tilde{\mathbf{A}}_{22}(t_c) \end{bmatrix} \tilde{\mathbf{x}}(t) + \begin{bmatrix} \tilde{\mathbf{B}}_1(t_c) \\ \mathbf{0} \end{bmatrix} \mathbf{u}(t), \tag{3.14}$$

here $\tilde{\mathbf{A}}_{11}(t_c)$ is a $k \times k$ matrix, and the pair $(\tilde{\mathbf{A}}_{11}(t_c), \mathbf{B}_1(t_c))$ is completely controllable.

Remark 3.2.1 *A necessary condition for controllablity at fixed time of a LEO satellite is that the control torque can be independently generated in x, y, and z directions of the Control CS. However, the magnetic actuated satellite produces the control torque, which is perpendicular to the local geomagnetic field, see Fig. 2.3. Thus, there exists an eigenvalue which is completely uncontrollable at any fixed position in orbit i.e. any single instant.*

In the next sections both a constant gain and a time varying gain control are investigated. Stability issues are in the focus. If a constant gain controller is applied, the characteristic multipliers of the closed loop system

$$\dot{\mathbf{x}}(t) = \mathbf{A}_c(t)\mathbf{x}(t), \tag{3.15}$$

where $\mathbf{A}_c(t) = \mathbf{A}(t) + \mathbf{B}(t)\mathbf{K}$, shall lie in the open unit disk. Picard's method of successive approximations will be used for the synthesis of a constant gain controller in Section 3.5.

Stability of the system (3.1) with a time varying control gain, $\mathbf{K}(t)$ is determined by Lypunov direct method, Chapter 5.

Consider the following Lyapunov function

$$v(t) = \frac{1}{2}\mathbf{x}^T(t)\mathbf{P}(t)\mathbf{x}(t), \tag{3.16}$$

where $\mathbf{P}(t)$ is a positive definite, symmetric $n \times n$ matrix.

The time derivative of the Lyapunov function is

$$\dot{v}(t) = \mathbf{x}^T(t)\mathbf{P}(t)\dot{\mathbf{x}}(t) + \frac{1}{2}\mathbf{x}^T(t)\dot{\mathbf{P}}(t)\mathbf{x}(t). \tag{3.17}$$

If the matrix $\mathbf{P}(t)$ is a solution to the following differential equation

$$\Leftrightarrow \dot{\mathbf{P}}(t) = \mathbf{A}_c^T(t)\mathbf{P}(t) + \mathbf{P}(t)\mathbf{A}_c(t) + \mathbf{Q}(t), \tag{3.18}$$

where $\mathbf{Q}(t)$ is a positive definite $n \times n$ matrix, then $\dot{v}(t)$ is

$$\dot{v}(t) = \Leftrightarrow \frac{1}{2}\mathbf{x}^T(t)\mathbf{Q}(t)\mathbf{x}(t). \tag{3.19}$$

From Eq. (3.19) $\dot{v}(t)$ is negative definite, thus the closed-loop system is stable. Eq. (3.18) is called the Lyapunov equation and will be discussed in more detail in Subsection 3.3.2. Time varying optimal controllers are investigated in Sections 3.3 and 3.4.

Remark 3.2.2 *Consider an attitude controller for magnetic actuated satellite that stabilizes the controllable part at fixed time, t_c. This is equivalent to a projection of the desired control torque, which stabilizes the entire state of the satellite on the plane perpendicular to the local geomagnetic field. The stability of such a controller cannot be satisfied since only the first summand of r.h.s. of Eq. (3.17)*

$$\mathbf{x}^T(t)\mathbf{P}(t)\dot{\mathbf{x}}(t)$$

is made negative definite, leaving

$$\frac{1}{2}\mathbf{x}^T(t)\dot{\mathbf{P}}(t)\mathbf{x}(t)$$

undermined, as the result, $\dot{v}(t)$ cannot be negative definite.

3.3   Infinite Quadratic Cost Problem

The design of a linear time varying controller is the primary goal of this section. The first approach refers to the optimal control problem. Precisely, an issue of a periodic solution to the Riccati equation derived from the infinite quadratic cost problem is analysed in the sequel.

There are only few methods constructing a stabilizing periodic control law

$$\mathbf{u}(t) = \mathbf{K}(t)\mathbf{x}(t) \tag{3.20}$$

for the system in Eq. (3.1). One method which is most commonly used, relies on minimization of the infinite time quadratic cost function

$$J(u) = \int_{\tau}^{\infty} [\mathbf{x}^T(t)\mathbf{Q}(t)\mathbf{x}(t) + \mathbf{u}^T(t)\mathbf{u}(t)] dt, \tag{3.21}$$

where $\mathbf{Q}(t)$ is a T-periodic, piecewise continuous positive semidefinite $n \times n$ matrix function.

According to Anderson and Moore (1989) the optimal and stabilizing solution to the time-varying regulator problem is given by

$$\mathbf{u}(t) = \Leftrightarrow \mathbf{B}(t)\mathbf{P}(t)\mathbf{x}(t), \tag{3.22}$$

where $\mathbf{P}(t)$ is a solution to the Riccati equation

$$\Leftrightarrow \dot{\mathbf{P}}(t) = \mathbf{P}(t)\mathbf{A}(t) + \mathbf{A}^T(t)\mathbf{P}(t) \Leftrightarrow \mathbf{P}(t)\mathbf{B}(t)\mathbf{B}^T(t)\mathbf{P}(t) + \mathbf{Q}(t), \tag{3.23}$$

with a certain final condition.

The computational burden to calculate this controller is very heavy. The aim of the next subsections is to find a periodic solution to the Riccati equation providing a stable control law. This approach limits necessary calculations to only one period. The analysis of the Riccati equation is complex due to its nonlinear (quadratic) nature, however a numeric algorithm can be successfully implemented as described below.

3.3.1   Quasi Linearization of Riccati Equation

Lack of linear features of the Riccati equation makes its analysis complex. An iterative method for finding the solution to the Riccati equation based on a Newton-type algorithm (Bellman's quasi linearization) is given in Bittanti (1991). The solution of the Riccati equation is reduced to an iterative solution to the Lyapunov equation, which is linear and has analytic solution.

Consider an operator

$$Ric: \ \mathbf{P}(t) \Leftrightarrow \dot{\mathbf{P}}(t) + \mathbf{A}^T(t)\mathbf{P}(t) + \mathbf{P}(t)\mathbf{A}(t) \Leftrightarrow \mathbf{P}(t)\mathbf{B}(t)\mathbf{B}^T(t)\mathbf{P}(t) + \mathbf{Q}(t).$$
(3.24)

A symmetric solution to the Riccati equation satisfies the operator equation

$$Ric(\mathbf{P}(t)) = 0.$$
(3.25)

Suppose that $\mathbf{P}_i(t)$ is a symmetric matrix function approximating the solution to Eq. (3.25) with a certain accuracy. A Newton algorithm can then be used for computing a new and more accurate approximation

$$\mathbf{P}_{i+1}(t) = \mathbf{P}_i(t) + \Delta\mathbf{P}_i(t).$$
(3.26)

Precisely, $\mathbf{P}_{i+1}(t)$ is computed from $\mathbf{P}_i(t)$ by solving the differential equation

$$\Leftrightarrow \dot{\mathbf{P}}_{i+1}(t) = \mathbf{A}_i^T(t)\mathbf{P}_{i+1}(t) + \mathbf{P}_{i+1}(t)\mathbf{A}_i(t) + \mathbf{Q}(t) + \mathbf{K}_i^T(t)\mathbf{K}_i(t),$$
(3.27)

where

$$\mathbf{A}_i(t) = \mathbf{A}(t) \Leftrightarrow \mathbf{B}(t)\mathbf{K}_i(t),$$
$$\mathbf{K}_i(t) = \mathbf{B}^T(t)\mathbf{P}_i(t).$$
(3.28)

It turns out that Eq. (3.27) is a Lyapunov equation. A number of features of this type of differential equations are given in the next section. Some of these properties can be extended to the Riccati equation as a limit of the series of the Lyapunov equations.

3.3.2 Periodic Lyapunov Equation

The Lyapunov equation plays an important role in the analysis of the Riccati equation. Therefore, some space in this thesis is devoted to its analysis. The major issue is whether a periodic solution to the Lyapunov equation exists.

Consider a system described by Eq. (3.3). The Lyapunov equation is defined as

$$\Leftrightarrow \dot{\mathbf{P}}(t) = \mathbf{A}^T(t)\mathbf{P}(t) + \mathbf{P}(t)\mathbf{A}(t) + \mathbf{Q}(t),$$
(3.29)

where $\mathbf{Q}(t)$ is a positive semidefinite matrix function. The solution to the Lyapunov equation is given by the celebrated formula

$$\mathbf{P}(t) = \mathbf{\Phi}_A^T(t_f, t)\mathbf{P}(t_f)\mathbf{\Phi}_A(t_f, t) + \int_t^{t_f} \mathbf{\Phi}_A^T(\sigma, t)\mathbf{Q}(\sigma)\mathbf{\Phi}_A(\sigma, t)d\sigma.$$
(3.30)

Let us now refer to the periodic Lyapunov lemma, which states that a T-periodic solution to the Lyapunov equation exists.

Lemma 3.3.1 (Extended Lyapunov Lemma in Bittanti (1991)) $\mathbf{A}(t)$ *is stable if and only if, for any symmetric periodic, and positive semidefinite* $\mathbf{Q}(t)$ *such that* $(\mathbf{A}(t), \mathbf{Q}(t))$ *is detectable, there exists a symmetric, periodic and positive definite solution* $\tilde{\mathbf{P}}(t)$ *to the Lyapunov equation.*

It is worthwhile to examine whether the steady state solution to the Lyapunov equation is periodic. The answer is provided in the next lemma.

Lemma 3.3.2 *Let* $\mathbf{P}(t_0)$ *be a solution to the Lyapunov Equation (3.29) at time* t_0 *for the final condition* $\mathbf{P}(t_0 + kT) = \mathbf{P}_f$, *where k is a natural number,* $k \to \infty$, *and* $\mathbf{P}_f$ *is any* $n \times n$ *matrix. Furthermore, let* $\tilde{\mathbf{P}}(t_0)$ *be the periodic solution to Eq. (3.29) defined in the Extended Lyapunov Lemma (Lemma 3.3.1) at time* t_0, *then*

$$\mathbf{P}(t_0) = \tilde{\mathbf{P}}(t_0).$$

Proof of Lemma 3.3.2 According to Eq. (3.30) the solution $\mathbf{P}(t_0)$ to the Lyapunov Equation (3.29) for the final condition $\mathbf{P}(t_0 + T)$ is given by

$$\mathbf{P}(t_0) = \mathbf{\Psi}_A^T(t_0)\mathbf{P}(t_0 + T))\mathbf{\Psi}_A(t_0) + \int_{t_0}^{t_0+T} \mathbf{\Phi}_A^T(\sigma, t_0)\mathbf{Q}(\sigma)\mathbf{\Phi}_A(\sigma, t_0)d\sigma \tag{3.31}$$

and the T-periodic solution $\tilde{\mathbf{P}}(t_0)$ to Eq. (3.29) is

$$\tilde{\mathbf{P}}(t_0) = \mathbf{\Psi}_A^T(t_0)\tilde{\mathbf{P}}(t_0)\mathbf{\Psi}_A(t_0) + \int_{t_0}^{t_0+T} \mathbf{\Phi}_A^T(\sigma, t_0)\mathbf{Q}(\sigma)\mathbf{\Phi}_A(\sigma, t_0)d\sigma \tag{3.32}$$

Now, define $\mathbf{e}(t_0) = \mathbf{P}(t_0) \Leftrightarrow \tilde{\mathbf{P}}(t_0)$, and notice that

$$\mathbf{e}(t_0 + T) = \mathbf{P}(t_0 + T) \Leftrightarrow \tilde{\mathbf{P}}(t_0 + T) = \mathbf{P}(t_0 + T) \Leftrightarrow \tilde{\mathbf{P}}(t_0).$$

Eq. (3.32) is subtracted from Eq. (3.31) and the following formulas are apparent

$$\mathbf{e}(t_0) = \mathbf{\Psi}_A^T(t_0)\mathbf{e}(t_0 + T)\mathbf{\Psi}_A(t_0) \tag{3.33}$$

and

$$\mathbf{e}(t_0 + (k \Leftrightarrow 1)T) = \mathbf{\Psi}_A^T(t_0)\mathbf{e}(t_0 + kT)\mathbf{\Psi}_A(t_0), \tag{3.34}$$

but

$$lim_{k \to \infty}\mathbf{e}(t_0 + kT) = \mathbf{P}_f \Leftrightarrow \tilde{\mathbf{P}}(t_0).$$

Moreover, $\mathbf{A}(t)$ is stable, thus characteristic multipliers of the monodromy matrix $\mathbf{\Psi}_A(t)$ lie in the open unit circle, thus $\mathbf{e}(t_0) = \mathbf{0}$.   ∎

In other words, the lemma says that for any final condition the solution to the Lyapunov equation will pointwise converge to the periodic solution.

Having established conditions for the existence of a periodic solution to the Lyapunov equation, the question of the existence of a periodic solution to the Riccati equation is posed in the next subsection.

3.3.3 Periodic Riccati Equation

This subsection is devoted to the analysis of a symmetric positive semidefinite solution to the Riccati Equation (3.23). The main objective is to demonstrate that the steady state solution to the Riccati equation is periodic.

Firstly, it is shown that the stabilizability of $(\mathbf{A}(t), \mathbf{B}(t))$ is sufficient for the existence of a periodic solution to the Riccati equation.

Theorem 3.3.1 (Theorem 6.2 in Bittanti (1991)) *Suppose that $(\mathbf{A}(t), \mathbf{B}(t))$ is stabilizable and consider the sequence of periodic Lyapunov equations defined in (3.27) and (3.28). Let $\mathbf{K}_0(t)$ be a T-periodic matrix such that $\mathbf{A}_0(t)$ is stable. Then*

1. *For each $i \geq 0$, there exists a unique symmetric periodic and semidefinite solution $\tilde{\mathbf{P}}_{i+1}(t)$ to (3.27) and $\mathbf{A}_{i+1}(t)$ is stable.*

2. *The sequence $\{\tilde{\mathbf{P}}_i(t)\}$ is a monotonically non increasing sequence of symmetric periodic positive semidefinite matrices, i.e., $\mathbf{0} \leq \tilde{\mathbf{P}}_{i+1}(t) \leq \tilde{\mathbf{P}}_i(t)$.*

3. *The sequence $\{\tilde{\mathbf{P}}_i(t)\}$ is such that $\lim_{i \to \infty} \tilde{\mathbf{P}}_i(t) = \tilde{\mathbf{P}}_M(t)$, where $\tilde{\mathbf{P}}_M(t)$ is a maximal and strong solution to the Riccati equation (i.e. the characteristic multipliers of $\mathbf{A}_c(t) \equiv \mathbf{A}(t) \Leftrightarrow \mathbf{B}(t)\mathbf{B}^T(t)\tilde{\mathbf{P}}_M(t)$ belong to the closed unit disk).*

Remark 3.3.1 *Similar theorem can be formulated for convergence of the sequence $\{\mathbf{P}_i(t)\}$ in Eqs. (3.27) and (3.28) towards $\mathbf{P}(t)$, where $\mathbf{P}(t)$ is a strong solution to the Riccati equation for positive semidefinite final condition $\mathbf{P}_f$ (the solution $\mathbf{P}(t)$ need not be periodic). The proof of this statement is analogous to the proof of Theorem 3.1.1, Bittanti (1991). This remark will be used in the proof of Theorem 3.4.2*

Notice, that the solution $\tilde{\mathbf{P}}_M(t)$ need not guarantee stability of $\mathbf{A}_c(t)$, since there may exist characteristic multipliers on the unit circle. The following theorem gives an answer to the question whether a periodic and stabilizing solution to the Riccati equation exists.

Theorem 3.3.2 (Theorem 6.3 in Bittanti (1991)) *There exists a stabilizing symmetric periodic solution $\tilde{\mathbf{P}}_+(t)$ to the Riccati Equation (3.23) if, and only if $((\mathbf{A}(t), \mathbf{B}(t)))$ is stabilizable and no unit-modulus characteristic multipliers of $\mathbf{A}(t)$ are $(\mathbf{A}(t), \mathbf{Q}(t))$ unobservable.*

The ultimate objective of this section is to show that the steady state solution to the Riccati equation is periodic. This statement is a conclusion from Lemma 3.3.2 and Theorem 3.3.1. This is formalized in the following theorem.

Theorem 3.3.3 *Let* $\mathbf{P}(t)$ *be solution to the Riccati Equation (3.23) for positive semidefinite final condition defined at infinity and* $\tilde{\mathbf{P}}_M(t)$ *be the periodic solution to the Riccati equation defined in Theorem 3.3.1, then*

$$\lim_{t \to 0} \mathbf{P}(t) = \tilde{\mathbf{P}}_M(t).$$

Proof of Theorem 3.3.3 Consider the sequence $\{\mathbf{P}_i(t)\}$ defined in Eqs. (3.27) and (3.28), such that

$$\lim_{i \to \infty} \mathbf{P}_i(t) = \mathbf{P}(t),$$

and the sequence $\{\tilde{\mathbf{P}}_i(t)\}$ defined in Theorem 3.3.1 such that

$$\lim_{i \to \infty} \tilde{\mathbf{P}}_i(t) = \tilde{\mathbf{P}}_M(t).$$

According to Lemma 3.3.2

$$\lim_{t \to 0} \mathbf{P}_i(t) = \tilde{\mathbf{P}}_i(t)$$

and thus

$$\lim_{t \to 0} \mathbf{P}(t) = \tilde{\mathbf{P}}_M(t).$$

∎

Theorem 3.3.3 will be used in the next chapter for design of a periodic attitude controller.

3.4 Finite Quadratic Cost Problem

Computation of the periodic steady state equilibrium is demanding, especially when on board calculation of the controller gain is necessary. Therefore, a new controller based on a transient solution to the Riccati equation is proposed in this section. The control law consists of two subsequent steps:

1. Calculate off-line time varying solution to the Riccati equation within one period subject to a given final condition.

2. Apply an optimal controller based on the solution to the Riccati equation calculated in the first step.

This control procedure is recognized in the literature on optimal control as a receding horizon control. However, the name, periodic receding horizon will be used in the sequel to emphasize that the controller is evaluated for one period. The contents of this section is based on Wisniewski (1995*b*).

Consider again the Riccati Equation (3.23). Let $\mathbf{P}(t)$ be its solution evaluated on an interval $(\tau - T, \tau]$ subject to the final condition $\mathbf{P}(\tau) = \mathbf{P}_f$. Furthermore, define the following matrix function $\hat{\mathbf{P}}(t)$

$$\hat{\mathbf{P}}(t) \equiv \begin{cases} \mathbf{P}(t) & \text{if } \tau - T < t \leq \tau \\ \mathbf{0} & \text{otherwise.} \end{cases} \qquad (3.35)$$

The periodic extension, $\tilde{\mathbf{P}}(t)$ is now defined as

$$\tilde{\mathbf{P}}(t) \equiv \sum_{k=0}^{\infty} \hat{\mathbf{P}}(t - kT), \ k = 0, 1, 2, \cdots \qquad (3.36)$$

Notice that the periodic extension is a solution to the Riccati equation calculated for one period, and then applied not only during this period but also extended to subsequent ones.

The control law based on the periodic extension, i.e the periodic receding horizon control is given by

$$\mathbf{u}(t) = -\mathbf{B}^T(t)\tilde{\mathbf{P}}(t)\mathbf{x}(t). \qquad (3.37)$$

The control algorithm then has two steps. The first is to calculate the time varying solution to the Riccati equation within one period subject to the final condition $\mathbf{P}(\tau) = \mathbf{P}_f$. The second is to apply the control law (3.37).

It is important to recognize that the control law in Eqs. (3.35) to (3.37) minimizes the performance index

$$J(\mathbf{u}) = \sum_{k=0}^{\infty} \mathbf{x}^T(\tau - kT)\mathbf{P}_f\mathbf{x}(\tau - kT) + \int_0^{\infty} [\mathbf{x}^T(t)\mathbf{Q}(t)\mathbf{x}(t) + \mathbf{u}^T(t)\mathbf{u}(t)]dt. \qquad (3.38)$$

The system with this control law is not energy optimal, since it has an extra part, i.e. the first summand of Eq. (3.38), which appears owing to the solution to the Riccati equation is forced to have value $\mathbf{P}_f$ at each time $\tau - kT$, where $k = 0, 1, 2, \dots$

Further investigation focuses on an issue whether such a control law is stable. The answer is that the periodic receding horizon may not provide stabilizing control law in general. The necessary condition for stability is that the difference $\mathbf{P}(\tau) - \mathbf{P}(\tau - T)$ is positive semidefinite. A formal description of this statement is formulated in the following theorem below, which was first established in DeNicolao (1994).

Theorem 3.4.1 *Let* $\mathbf{P}(t)$ *be the solution to the Riccati Equation (3.23) with final conditions* $\mathbf{P}(\tau) = \mathbf{P}_f \geq \mathbf{0}$ *(positive semidefinite) and assume that*

1. $(\mathbf{A}(t), \mathbf{B}(t))$ *is stabilizable*

2. $(\mathbf{A}(t), \mathbf{Q}(t))$ *is detectable*

3. $\mathbf{F} \equiv \mathbf{P}(\tau) \Leftrightarrow \mathbf{P}(\tau \Leftrightarrow T)$ *is positive semidefinite*

Then the periodic matrix function $\tilde{\mathbf{P}}(t)$ (see Eqs. (3.35) and (3.36)) is stabilizing, i.e. the control law (3.37) is stable.

Proof of Theorem 3.4.1 The proof of Theorem 3.4.1 is equivalent to the proof of Theorem 3 in DeNicolao (1994) if the following property is applied: if $(\mathbf{A}(t), \mathbf{Q}(t))$ is detectable then $(\mathbf{A}(t), \mathbf{Q}(t), \mathbf{F})$ is D-detectable. ∎

Remark 3.4.1 *In the next chapter on implementation of the finite and infinite quadratic cost problems, the weight matrix $\mathbf{Q}$ will be time invariant. Notice that the pair $(\mathbf{A}(t), \mathbf{Q})$ is detectable if $\mathbf{Q}$ has the full rank n. Consider the observability gramian*

$$\mathbf{G}_o(t, \tau) \equiv \int_\tau^t \mathbf{\Phi}^T(s, \tau) \mathbf{Q}^T \mathbf{Q} \mathbf{\Phi}(s, \tau) ds. \tag{3.39}$$

The matrix $\mathbf{G}_o(\tau, t)$ has rank n, since

$$rank(\mathbf{G}_o(\tau, t)) >= rank(\mathbf{\Phi}^T(\tau, \tau) \mathbf{Q}^T \mathbf{Q} \mathbf{\Phi}(\tau, \tau)) = rank(\mathbf{Q}^T \mathbf{Q}) = n. \tag{3.40}$$

3.4.1 Choice of Final Condition

The critical issue of a periodic receding horizon controller design is the choice of the final condition $\mathbf{P}_f$ such that $\mathbf{F} \geq \mathbf{0}$ ($\mathbf{F}$ is positive semidefinite). A suitable value of the final condition can be found via numerical simulation. Lemma 3.4.1 gives a hint for a heuristic final condition search algorithm, which is given at the end of this subsection. The lemma states that if a periodic solution and a solution to the Riccati equation are given such that the difference between the final conditions is positive semidefinite, then the difference between these solutions is positive semidefinite for all time.

Lemma 3.4.1 *Suppose that $(\mathbf{A}(\cdot), \mathbf{B}(\cdot))$ is stabilizable and let $\tilde{\mathbf{P}}_M(t)$ be the T-periodic solution to the Riccati Equation (3.23) and let $\mathbf{P}(t)$ be a solution to the Riccati equation. Moreover let $\mathbf{P}(\tau) \geq \tilde{\mathbf{P}}_M(\tau)$ for some τ then $\mathbf{P}(t) \geq \tilde{\mathbf{P}}_M(t)$ for all $t \leq \tau$.*

Proof of Lemma 3.4.1 Let $\mathbf{P}_{12}^{(i)}(t) = \mathbf{P}(t) \Leftrightarrow \tilde{\mathbf{P}}_i(t)$, where $\tilde{\mathbf{P}}_i(t)$ is defined in Theorem 3.3.1 and let

$$\tilde{\mathbf{P}}_M(t) = \lim_{i \to \infty} \tilde{\mathbf{P}}_i(t) \tag{3.41}$$

Comparing Eqs. (3.23) and (3.27), (3.28) the following Lyapunov equation is derived

$$
\begin{aligned}
-\dot{\mathbf{P}}_{12}^{(i+1)}(t) &= (\mathbf{A}(t) - \mathbf{B}(t)\mathbf{B}^T(t)\tilde{\mathbf{P}}_i(t))^T \mathbf{P}_{12}^{(i+1)}(t) + \mathbf{P}_{12}^{(i+1)}(t)(\mathbf{A}(t) \quad (3.42)\\
&\quad - \mathbf{B}(t)\mathbf{B}^T(t)\tilde{\mathbf{P}}_i(t)) + (\tilde{\mathbf{P}}_i(t) - \mathbf{P}(t))\mathbf{B}(t)\mathbf{B}^T(t)(\mathbf{P}_i(t) - \mathbf{P}(t)).
\end{aligned}
$$

The Lyapunov Equation (3.42) has positive semidefinite finite condition, $\mathbf{P}_{12}^{(i+1)}(\tau) \geq \mathbf{0}$. According to Theorem 3.3.1 the closed loop system $(\mathbf{A}(t) - \mathbf{B}(t)\mathbf{B}^T(t)\tilde{\mathbf{P}}_i(t))$ is stable. The matrix $\mathbf{P}_{12}^{(i+1)}(t)$ is positive semidefinite as the solution to the Lyapunov equation, see Extended Lyapunov Lemma in Section 1.1.2. Thus, the quantity $\mathbf{P}(t) - \mathbf{P}_M(t) = \lim_{i\to\infty} \mathbf{P}_{12}^{(i)}(t)$ is also positive semidefinite, and $\mathbf{P}(t) \geq \mathbf{P}_M(t)$ for all $t \leq \tau$. ∎

A procedure for finding the final conditions of the Riccati equation stabilizing the receding horizon will be derived in the following. According to Lemma 3.3.3 the periodic equilibrium $\tilde{\mathbf{P}}_M(t)$ is

$$
\lim_{t\to 0} \mathbf{P}(t) = \tilde{\mathbf{P}}_M(t). \tag{3.43}
$$

Recognize that, if $\mathbf{P}(\tau) \geq \tilde{\mathbf{P}}_M(\tau)$ then from Lemma 3.4.1 and Eq. (3.43), $\mathbf{P}(\tau - T) \leq \mathbf{P}(\tau)$, i.e. $\mathbf{F} = \mathbf{P}(\tau) - \mathbf{P}(\tau - T)$ is positive semidefinite. In other words, the necessary condition for stability of the periodic receding horizon control is that the difference between $\mathbf{P}_f$ and the periodic equilibrium of the Riccati equation at time τ is positive definite.

Remark 3.4.2 *The final condition matrix, $\mathbf{P}(\tau)$ can be chosen such that it is positive definite and converges to infinity, then $\mathbf{F}$ is positive definite, indeed.*

Kwon and Pearson (1977) demonstrate that instead of considering $\mathbf{P}_f$ infinitely large one can choose $\mathbf{S}_f = \mathbf{P}_f^{-1} = \mathbf{0}$. The matrix $\mathbf{S}(\cdot) = \mathbf{P}^{-1}(\cdot)$ satisfies the following Riccati differential equation

$$
-\dot{\mathbf{S}}(t) = -\mathbf{A}(t)\mathbf{S}(t) - \mathbf{S}(t)\mathbf{A}^T(t) + \mathbf{B}(t)\mathbf{B}^T(t) - \mathbf{S}(t)\mathbf{Q}(t)\mathbf{S}(t),
$$
$$(3.44)$$

with the final condition

$$
\mathbf{S}(\tau) = \mathbf{0}.
$$

The solution $\mathbf{S}(\tau - nT)$ is positive definite according to Kwon and Pearson (1977), thus $\mathbf{P}(\tau - nT) = \mathbf{S}^{-1}(\tau - nT)$ is defined.

Large $\mathbf{P}_f$ is desired to fulfill stability conditions, but it indicates that the resultant control signal is unnecessarily large, therefore a tradeoff between these two issues shall be found. The following design procedure for finding an appropriate final condition can now be adopted.

Procedure 3.1

1. *Choose large value of the final condition,* $\mathbf{P}(\tau) \geq \mathbf{0}$.

2. *Find the solution to the Riccati equation backwards for* $\tau \Leftrightarrow nT$ $(n \geq 1)$.

3. *Apply this solution as the final condition* $\mathbf{P}_f$ *in the receding horizon controller.*

3.4.2 Quasi Periodic Receding Horizon

An issue of applicability of the periodic receding horizon to a system, where either the system or the control matrices are not perfectly periodic, is in the focus of this subsection. The investigation is motivated by the magnetic attitude control problem. The control matrix, $\mathbf{B}(t)$ in Eq. (2.38) is not ideally periodic within one orbit, due to certain perturbations caused by rotation of the Earth in the World CS. A quasi periodic horizon controller investigated in this subsection corresponds to the periodic horizon controller except that the Riccati equation is computed for each interval of time $t \in (\tau + iT, \tau + (i+1)T]$ separately.

Formally, a quasi periodic system is of the form

$$\dot{\mathbf{x}}(t) = \mathbf{A}(t)\mathbf{x}(t) + \mathbf{B}(t)\mathbf{u}(t), \tag{3.45}$$

where $\mathbf{x}(t) \in \mathbb{R}^n$, $\mathbf{u}(t) \in \mathbb{R}^m$, the system matrix, $\mathbf{A}(t)$ and the control matrices, $\mathbf{B}(t)$ are time varying and limited.

The objective of this subsection is to show when the following control law is stable.

Procedure 3.2

1. *Calculate the solution* $\mathbf{P}^{(i)}(t)$ *to the Riccati Equation (3.23) in the interval* $t \in (\tau + iT, \tau + (i+1)T]$ *with the final condition* $\mathbf{P}^{(i)}(\tau + (i+1)T) = \mathbf{P}_f$, *where* $i = 1, 2, 3, \ldots$

2. *Apply the control law*

$$\mathbf{u}(t) = \Leftrightarrow \mathbf{B}(t)\breve{\mathbf{P}}(t)\mathbf{x}(t). \tag{3.46}$$

   where

$$\breve{\mathbf{P}}(t) \equiv \mathbf{P}^{(i)}(t) \text{ for } t \in (\tau + iT, \tau + (i+1)T]. \tag{3.47}$$

The control law given above will be called the quasi periodic receding horizon control. It is essentially the same as the periodic receding horizon control, except that it is applied to a quasi periodic system. It is demonstrated in Theorem 3.4.2 that the quasi periodic receding horizon control is stable if $\mathbf{F}_i \equiv \mathbf{P}_f \Leftrightarrow \mathbf{P}_i(\tau + iT)$ is positive semidefinite for all i.

Theorem 3.4.2 *Consider a quasi periodic system in Eq. (3.45). Let $(\mathbf{A}(t), \mathbf{B}(t))$ be stabilizable and $(\mathbf{A}(t), \mathbf{Q}(t))$ observable. Let $\breve{\mathbf{P}}(t)$ be defined as*

$$\breve{\mathbf{P}}(t) \equiv \mathbf{P}^{(i)}(t) \, for \, t \in (\tau + iT, \tau + (i+1)T],$$

where $\mathbf{P}^{(i)}(t)$ is the solution to the Riccati Equation (3.23) with the final condition $\mathbf{P}^{(i)}(\tau + (i+1)T) = \mathbf{P}_f$. Furthermore, if $\mathbf{F}^{(i)} \equiv \mathbf{P}_f \Leftrightarrow \mathbf{P}^{(i)}(\tau + iT)$ is positive semidefinite, then the control law (3.46) is stable.

Proof of Theorem 3.4.2 The theorem is proved using Lyapunov's direct method, Section 5.2.

For each solution to the Riccati equation $\mathbf{P}^{(i)}$ consider a sequence $\{\mathbf{P}_k^{(i)}\}$ of the solutions to the Lyapunov equations defined in Eqs. (3.27) and (3.28). In accordance with Remark 3.3.1

$$\mathbf{0} \leq \mathbf{P}_{k+1}^{(i)}(t) \leq \mathbf{P}_k^{(i)}(t) \text{ and } \lim_{k \to \infty} \mathbf{P}_k^{(i)}(t) = \mathbf{P}^{(i)}(t),$$

where $\mathbf{P}_{k+1}^{(i)}$ is computed from $\mathbf{P}_k^{(i)}$ by solving the Lyapunov differential equation

$$\Leftrightarrow \dot{\mathbf{P}}_{k+1}^{(i)}(t) = \mathbf{A}_k^{(i)}(t)^T \mathbf{P}_{k+1}^{(i)}(t) + \mathbf{P}_{k+1}^{(i)}(t)\mathbf{A}_k^{(i)}(t) + \mathbf{Q}(t) + \mathbf{K}_k^{(i)}(t)^T \mathbf{K}_k^{(i)}(t),$$
(3.48)

and

$$\begin{aligned}
\mathbf{A}_k^{(i)}(t) &= \mathbf{A}(t) \Leftrightarrow \mathbf{B}(t)\mathbf{K}_k^{(i)}(t), \\
\mathbf{K}_k^{(i)}(t) &= \mathbf{B}^T(t)\mathbf{P}_k^{(i)}(t)
\end{aligned}$$
(3.49)

Choose k such that

$$\mathbf{F}_k^{(i)} \equiv \mathbf{P}_f \Leftrightarrow \mathbf{P}_k^{(i)}(\tau + iT)$$

is positive semidefinite for all i. This index, k exists since the difference

$$\mathbf{F} \equiv \mathbf{P}_f \Leftrightarrow \mathbf{P}^{(i)}(\tau + iT)$$

is positive semidefinite for all i and $\mathbf{P}_k^{(i)}(t)$ converges to $\mathbf{P}^{(i)}(t)$.

Define a Lyapunov candidate function

$$v(t) = \mathbf{x}(t)\breve{\mathbf{P}}_{k+1}(t)\mathbf{x}(t),$$

where

$$\breve{\mathbf{P}}_k(t) \equiv \mathbf{P}_k^{(i)}(t) \text{ for } t \in (\tau + iT, \tau + (i+1)T]$$

and let $t_0 \leq t_f$, $t_0 \in [\tau + (l \Leftrightarrow 1)T, \tau + lT)$ and $t_f \in [\tau + (j \Leftrightarrow 1)T, \tau + jT), l \leq j$.
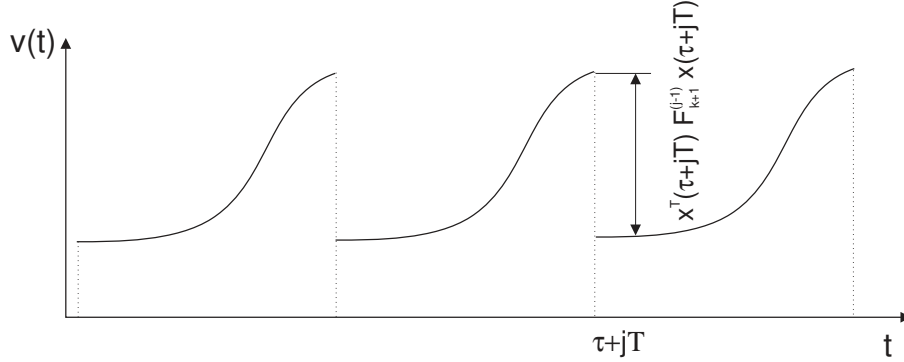
Figure 3.1: The Lyapunov function $v(t) = \mathbf{x}^T(t)\breve{\mathbf{P}}(t)\mathbf{x}(t)$ is discontinuous at time $t = \tau + jT$.

Now, it is demonstrated that $v(t_f) \Leftrightarrow v(t_0)$ is negative definite

$$v(t_f) \Leftrightarrow v(t_0) =$$
$$\int_{t_0}^{\tau+lT} \frac{d}{dt}[\mathbf{x}^T(t)\mathbf{P}_{k+1}^{(l-1)}(t)\mathbf{x}(t)]dt + \int_{\tau+lT}^{\tau+(l+1)T} \frac{d}{dt}[\mathbf{x}^T(t)\mathbf{P}_{k+1}^{(l)}(t)\mathbf{x}(t)]dt + \cdots$$
$$+ \int_{\tau+(j-1)T}^{t_f} \frac{d}{dt}[\mathbf{x}^T(t)\mathbf{P}_{k+1}^{(j-1)}(t)\mathbf{x}(t)]dt + \mathbf{x}^T(\tau+lT)\mathbf{F}_{k+1}^{(l-1)}\mathbf{x}(\tau+lT)$$
$$+ \mathbf{x}^T(\tau+(l+1)T)\mathbf{F}_{k+1}^{(l)}\mathbf{x}(\tau+(l+1)T) + \cdots \tag{3.50}$$
$$+ \mathbf{x}^T(\tau+(j\Leftrightarrow 1)T)\mathbf{F}_{k+1}^{(j-2)}\mathbf{x}(\tau+(j\Leftrightarrow 1)T).$$

The last three summands on the r.h.s of Eq.(3.50) are due to discontinuity of the matrix function $\breve{\mathbf{P}}(t)$ at time $\tau + iT$, see Fig. 3.1.

Furthermore, the difference $v(t_f) \Leftrightarrow v(t_0)$ is bounded from above

$$v(t_f) \Leftrightarrow v(t_0) \le \Leftrightarrow \int_{t_0}^{\tau+lT} \mathbf{x}^T(t)[\mathbf{P}_k^{(l-1)}(t)\mathbf{B}(t)\mathbf{B}^T(t)\mathbf{P}_k^{(l-1)}(t) + \mathbf{Q}(t)]\mathbf{x}(t)dt$$
$$\Leftrightarrow \int_{\tau+lT}^{(\tau+l+1)T} \mathbf{x}^T(t)[\mathbf{P}_k^{(l)}(t)\mathbf{B}(t)\mathbf{B}^T(t)\mathbf{P}_k^{(l)}(t) + \mathbf{Q}(t)]\mathbf{x}(t)dt \Leftrightarrow \cdots \tag{3.51}$$
$$\Leftrightarrow \int_{\tau+(j-1)T}^{t_f} \mathbf{x}^T(t)[\mathbf{P}_k^{(j-1)}(t)\mathbf{B}(t)\mathbf{B}^T(t)\mathbf{P}_k^{(j-1)}(t) + \mathbf{Q}(t)]\mathbf{x}(t)dt.$$

Notice that the following equality was used in Eq. (3.51)

$$\frac{d}{dt}\mathbf{x}^T(t)\mathbf{P}_{k+1}^{(l-1)}(t)\mathbf{x}(t) = 2\mathbf{x}^T(t)\mathbf{P}_{k+1}^{(l-1)}(t)\mathbf{A}_k^{(i)}(t)\mathbf{x}(t)$$

$$\Leftrightarrow \mathbf{x}^T(t)(\mathbf{A}_k^{(i)}(t)\mathbf{P}_{k+1}^{(l-1)}(t) + \mathbf{P}_{k+1}^{(l-1)}(t)\mathbf{A}_k^{(i)}(t) + \mathbf{Q} + \mathbf{P}_k^{(l-1)}(t)\mathbf{B}(t)\mathbf{B}^T(t)\mathbf{P}_{k+1}^{(l-1)}(t))\mathbf{x}(t)$$

$$= \mathbf{x}^T(t)(\mathbf{Q} + \mathbf{P}_k^{(l-1)}(t)\mathbf{B}(t)\mathbf{B}^T(t)\mathbf{P}_{k+1}^{(l-1)}(t))\mathbf{x}(t).$$

If the state $\mathbf{x}(t)$ in Eq. (3.51) is substituted by

$$\mathbf{x}(t) = \mathbf{\Phi}_k(t, t_0)\mathbf{x}(t_0), \tag{3.52}$$

where

$$\mathbf{\Phi}_k(t, t_0) \equiv \mathbf{\Phi}_k^{(i)}(t, t_0), \text{ for } t \in (\tau + iT, \tau + (i+1)T] \tag{3.53}$$

and $\mathbf{\Phi}_k^{(i)}(\cdot)$ is the state transition matrix of the closed loop system, $\mathbf{A}_k^{(i)}$ in Eq. (3.49), then

$$v(t_f) \Leftrightarrow v(t_0) \le$$

$$\Leftrightarrow \mathbf{x}^T(t_0)\int_{t_0}^{\tau+lT}\mathbf{\Phi}_k^T(t, t_0)[\mathbf{P}_k^{(l-1)}(t)\mathbf{B}(t)\mathbf{B}^T(t)\mathbf{P}_k^{(l-1)}(t) + \mathbf{Q}(t)]\mathbf{\Phi}_k(t, t_0)dt\, \mathbf{x}(t_0)$$

$$\Leftrightarrow \mathbf{x}^T(\tau+lT)\int_{\tau+lT}^{\tau+(l+1)T}\mathbf{\Phi}_k^T(t, \tau+lT)[\mathbf{P}_k^{(l)}(t)\mathbf{B}(t)\mathbf{B}^T(t)\mathbf{P}_k^{(l)}(t)$$

$$+ \mathbf{Q}(t)]\mathbf{\Phi}_k(t, \tau+lT)dt\, \mathbf{x}(\tau+lT) \Leftrightarrow \cdots \tag{3.54}$$

$$\Leftrightarrow \mathbf{x}^T(\tau+(j\Leftrightarrow1)T)\int_{\tau+(j-1)T}^{t_f}\mathbf{\Phi}_k^T(t, \tau+(j\Leftrightarrow1)T)[\mathbf{P}_k^{(j-1)}(t)\mathbf{B}(t)\mathbf{B}^T(t)\mathbf{P}_k^{(j-1)}(t)$$

$$+ \mathbf{Q}(t)]\mathbf{\Phi}_k(t, \tau+(j\Leftrightarrow1)T)dt\, \mathbf{x}(\tau+(j\Leftrightarrow1)T).$$

Finally, from Eq. (3.54) the following inequality is true

$$v(t_f) \Leftrightarrow v(t_0) \le \Leftrightarrow \mathbf{x}^T(t_0)\int_{t_0}^{\tau+lT}\mathbf{\Phi}_k^T(t, t_0)\mathbf{Q}(t)\mathbf{\Phi}_k(t, t_0)dt\, \mathbf{x}(t_0)$$

$$\Leftrightarrow \mathbf{x}^T(\tau+lT)\int_{\tau+lT}^{\tau+(l+1)T}\mathbf{\Phi}_k^T(t, \tau+lT)\mathbf{Q}(t)\mathbf{\Phi}_k(t, \tau+lT)dt\, \mathbf{x}(\tau+lT) \Leftrightarrow \cdots$$

$$\tag{3.55}$$

$$\Leftrightarrow \mathbf{x}^T(\tau+(j\Leftrightarrow1)T)\int_{\tau+(j-1)T}^{t_f}\mathbf{\Phi}_k^T(t, \tau+(j\Leftrightarrow1)T)\mathbf{Q}(t)\mathbf{\Phi}_k(t, \tau+(j\Leftrightarrow1)T)dt$$

$$\cdot \mathbf{x}(\tau+(j\Leftrightarrow1)T).$$

The system $(\mathbf{A}(\cdot), \mathbf{Q}(\cdot))$ is observable thus also the closed loop system $(\mathbf{A}_i(\cdot), \mathbf{Q}(\cdot))$ is observable, and the gramian matrix

$$\mathbf{G}_{(A,Q)}(t, t_0) = \int_{t_0}^{t}\mathbf{\Phi}_k^T(\tau, t_0)\mathbf{Q}(t)\mathbf{\Phi}_k(\tau, t_0)d\tau$$

is positive definite. According to Lyapunov's direct method, Section 5.2. $\breve{\mathbf{P}}_k(t)$ is stabilizing, and

$$\lim_{k \to \infty} \breve{\mathbf{P}}_k(t) = \breve{\mathbf{P}}(t),$$

thus $\breve{\mathbf{P}}(t)$ is stabilizing as well.   ∎

So far, time varying controllers have been investigated. Their common feature is that a solution to the Riccati differential equation specifies the control gain. The computer burden associated with these controllers is very heavy. It is thus worthwhile to design a constant gain controller stabilizing a linear periodic periodic system.

3.5   Constant Gain Control for Linear Periodic Systems

This section gives theoretical fundamentals for the design of a constant gain controller for a periodic system. The constant gain control is very attractive for satellites, which computer capacity is limited. The concepts investigated in this section are applied in Section 4.4 dealing with constant gain controller for a LEO satellite with a gravity gradient boom.

The work is motivated by Zhang *et al.* (1996), where it is proved that there exists a time invariant controller for every linear periodic system, that provides better H_2 and H_∞ performance than that of the periodically time varying controller.

It seems promising to base the design of a controller for the system (3.1) on the Floquet theory. The objective is to design a linear constant gain controller such that the characteristic multipliers belong to the open unit circle. The method presented in the sequel is derived from Picard's method of Successive Approximations. The contents of this section is based on Wisniewski (1995*b*).

Consider system (3.1) actuated according to a constant gain control law

$$\dot{\mathbf{x}}(t) = \mathbf{A}_c(t)\mathbf{x}(t), \tag{3.56}$$

where

$$\mathbf{A}_c(t) = \mathbf{A}(t) + \mathbf{B}(t)\mathbf{K}.$$

It is necessary to calculate the monodromy matrix $\mathbf{\Psi}_{A_c}(t_0)$ and its characteristic multipliers to check stability of the system (3.56). Deriving an analytic formula for the monodromy matrix is in general tedious and often even impossible [1]. Hence, an approximate solution to (3.56) is of the interest. Picard's method of successive approximations is then applied in the sequel.

---

[1] Notice that the monodromy matrix $\mathbf{\Psi}_A(t_0)$ of system 3.3 is $\mathbf{\Psi}_A(t_0) = exp \int_{t_0}^{t_0+T} A(\sigma)d\sigma$ if and only if $\mathbf{A}(t_1)\mathbf{A}(t_2) = \mathbf{A}(t_2)\mathbf{A}(t_1)$, which is not the case in general (certainly not for the magnetic actuated satellite).

3.5.1 Picard's Method of Successive Approximations

Solution to an ordinary differential equation can by calculated using Picard's method of successive approximations Matwiejew (1982).

Consider two continuous, Lipschitz ordinary differential equations

$$\frac{dy}{dt} = f_1(t, y, z), \ \frac{dz}{dt} = f_2(t, y, z) \tag{3.57}$$

with initial conditions

$$y(t_0) = y_0, \ z(t_0) = z_0. \tag{3.58}$$

The solutions $y(t)$, $z(t)$ are given by the following iterative procedure

- First approximation is

$$y^{(1)}(t) = y_0 + \int_{t_0}^{t} f_1(t, y_0, z_0)dt,$$

$$z^{(1)}(t) = z_0 + \int_{t_0}^{t} f_2(t, y_0, z_0)dt \tag{3.59}$$

- Second approximation is

$$y^{(2)}(t) = y_0 + \int_{t_0}^{t} f_1(t, y^{(1)}, z^{(1)})dt,$$

$$z^{(2)}(t) = z_0 + \int_{t_0}^{t} f_2(t, y^{(1)}, z^{(1)})dt \tag{3.60}$$

- n-th approximation is

$$y^{(n)}(t) = y_0 + \int_{t_0}^{t} f_1(t, y^{(n-1)}, z^{(n-1)})dt,$$

$$z^{(n)}(t) = z_0 + \int_{t_0}^{t} f_2(t, y^{(n-1)}, z^{(n-1)})dt \tag{3.61}$$

- The solutions $y(t)$, $z(t)$ are

$$y(t) = \lim_{n \to \infty} y^{(n)}, \ z(t) = \lim_{n \to \infty} z^{(n)} \tag{3.62}$$

Now, the monodromy matrix $\Psi_{A_c}(t_0)$ is approximated by the Picard's method of successive approximations.

3.5.2 Monodromy Matrix Approximation

The following differential equation describes the time propagation of the transition matrix $\mathbf{\Phi}_{A_c}(t, t_0)$ of the system (3.56)

$$\dot{\mathbf{\Phi}}_{A_c}(t, t_0) = \mathbf{A}_c(t)\mathbf{\Phi}_{A_c}(t, t_0)$$

with the initial condition

$$\mathbf{\Phi}_{A_c}(t_0, t_0) = \mathbf{I}. \tag{3.63}$$

Application of Picard's method of successive approximation gives

- First approximations is

$$\mathbf{\Phi}_{A_c}^{(1)}(t, t_0) = \mathbf{I} + \int_{t_0}^{t} \mathbf{A}_c(t)dt \tag{3.64}$$

- n-th approximation is

$$\mathbf{\Phi}_{A_c}^{(n)}(t, t_0) = \mathbf{I} + \int_{t_0}^{t} \mathbf{A}_c(t)\mathbf{\Phi}_{A_c}^{(n-1)}(t, t_0)dt \tag{3.65}$$

As mentioned in Section 3.1, the transition matrix evaluated within one period i.e. for $t = t_0 + T$ is defined as the monodromy matrix, which characteristic multipliers determine stability of the periodic system (3.56). The n-th approximation of the monodromy matrix $\mathbf{\Psi}_{A_c}^{(n)}(t_0)$ can be related to the monodromy matrix of the system with constant coefficients

$$\dot{\mathbf{x}} = \tilde{\mathbf{A}}\mathbf{x}, \tag{3.66}$$

where

$$\tilde{\mathbf{A}} = \frac{1}{T}\int_{t_0}^{t_0+T} \mathbf{A}_c(t)\mathbf{\Phi}_{A_c}^{(n-1)}(t, t_0)dt. \tag{3.67}$$

Notice that the monodromy matrix of the system (3.66) is

$$\mathbf{\Psi}_{\tilde{A}} = e^{\tilde{\mathbf{A}}T} = \mathbf{I} + \tilde{\mathbf{A}} + \frac{1}{2}\tilde{\mathbf{A}}^2 T^2 + \dots \tag{3.68}$$

Comparing Eq. (3.65) with Eq. (3.68) it is concluded that the monodromy matrix $\mathbf{\Psi}_{A_c}^{(n)}$ is the first order approximation of the monodromy matrix $\mathbf{\Psi}_{\tilde{A}}$.

An interesting issue is whether stability of the system (3.66) implies stability of the monodromy matrix $\mathbf{\Psi}_{A_c}^{(n)}$. The eigenvalues of the system (3.68) are given by the equation

$$det(\lambda_{\tilde{A}}\mathbf{E} \Leftrightarrow \tilde{\mathbf{A}}) = 0, \tag{3.69}$$

whereas

$$det(\lambda_{\Psi}\mathbf{E} \Leftrightarrow \mathbf{E} \Leftrightarrow T\tilde{\mathbf{A}}) = 0 \tag{3.70}$$

is the equation of the characteristic multiplier of the monodromy matrix $\boldsymbol{\Psi}_{A_c}^{(n)}$.

It follows from Eqs. (3.69) and (3.70) that

$$\lambda_{\Psi} = T\lambda_{\tilde{A}} + 1, \tag{3.71}$$

but the monodromy matrix $\boldsymbol{\Psi}_{A_c}^{(n)}$ is stable if its characteristic multipliers satisfies $|\lambda_{\Psi}| < 1$, thus

$$\Leftrightarrow \frac{2}{T} < \lambda_{\tilde{A}} < 0. \tag{3.72}$$

Hence, the time constants of the time invariant counterpart (3.66) shall be larger than $\frac{T}{2}$ in order to fulfill the stability condition for the periodic system, or in other words the band width in all channels of the system (3.66) shall be less than $\frac{2}{T}$.

3.5.3 Calculation of Constant Gain Control

The first order approximation of the monodromy matrix derived in the previous subsection is used in the following to generate a constant gain control law.

Consider the time invariant system (3.66) for $n = 1$

$$\dot{\mathbf{x}}(t) = \left(\frac{1}{T}\int_{t_0}^{t_0+T}\mathbf{A}(t)dt\right)\mathbf{x}(t) + \left(\frac{1}{T}\int_{t_0}^{t_0+T}\mathbf{B}(t)dt\,\mathbf{K}\right)\mathbf{x}(t). \tag{3.73}$$

The system in Eq. (3.73) is time invariant, and the standard methods of the linear control theory can be applied for finding a stabilizing control law.

Note that stability of the system (3.1) is not guaranteed, since the systems (3.1) and (3.73) are equivalent only to the first order approximation. Therefore, additionally Floquet stability analysis is to be performed.

Consider the procedure below for the design of a constant gain controller.

Procedure 3.3
   1. *Calculate the equivalent system with constant coefficients*

$$\dot{\mathbf{x}}(t) = \hat{\mathbf{A}}\mathbf{x}(t) + \hat{\mathbf{B}}\mathbf{u}(t), \tag{3.74}$$

   where

$$\hat{\mathbf{A}} = \frac{1}{T}\int_{t_0}^{t_0+T}\mathbf{A}(t)dt, \ \hat{\mathbf{B}} = \frac{1}{T}\int_{t_0}^{t_0+T}\mathbf{B}(t)dt. \tag{3.75}$$

2. *Find the control gain* **K** *for the system (3.74).*

3. *Compute the characteristic multipliers for the system (3.56).*

4. *If the characteristic multipliers do belong to the open unit circle then the feedback system is stable.*

Practical realization of the Procedure 3.3 is provided in the next chapter.

Remark 3.5.1 *The system (3.1) is equivalent to the system (3.74) if the matrices* **A** *and* **B** *are time invariant.*

Remark 3.5.2 *The differential Equation (3.74) can be viewed as a system with averaged parameters within one period relative to the periodic system (3.1). The effects of low frequency disturbances on a periodic system and its time invariant counterpart are similar, whereas high frequency responses are very much different. The periodic system may not even be controllable at fixed time (magnetic attitude control problem).*

3.6   Discussion of Results

The theoretical foundations for the magnetic attitude controller design were provided in this chapter. First, time varying optimal control was investigated. The infinite horizon controller was presented, which gain was calculated based on the periodic solution to the Riccati equation. This solution can be calculated off-line and stored in the computer memory. The controller assumed ideally periodic system parameters. This is violated in the magnetic attitude control problem, since the geomagnetic field is not ideally periodic during one orbital passage. In order to overcome this baseline, quasi periodic receding horizon was proposed, which can solve the Riccati equation for a realistic geomagnetic field model. The computer power associated with this controller is heavy. The most attractive for satellites with limited computer resources was the constant gain controller, which theoretical basis was thoroughly elaborated. The findings are implement to a LEO satellite with a gravity gradient boom in the next chapter.

Chapter 4

Three Axis Attitude Control: Linear Approach

The satellite trajectory during the science observation mission phase must remain in a window of $10\ deg$ pitch/roll, and $20\ deg$ yaw about the reference and the angular velocity must remain quite small.. Therefore, it is reasonable to base design of the attitude controller on a linear approach. Later chapters will discuss operation outside the specified window.

The system adopted in this chapter is linear and time varying. It was mentioned already in Chapter 2 that the satellite is not controllable when considered at fixed time. Availability of design methods for time varying systems is very limited. Nevertheless, a solution of the Riccati equation gives an excellent frame for further investigations.

An observation that the geomagnetic field changes approximately periodically when a satellite is on a near polar LEO is used throughout this chapter. Confined computer capacity and a limit on electrical power supply are factors which constrains possible solutions. Computational simplicity and power optimality are therefore required from the attitude control system. The design of optimal controllers for a real-time implementation is the subject of this chapter. Three types of attitude controllers are proposed: a) an infinite horizon, a finite horizon, and a constant gain controller. Time varying controllers, i.e. the infinite horizon controller, and the finite horizon controller are developed in Sections 4.2 and 4.3. The constant gain controller is designed in Section 4.4. Performance of the attitude controllers is validated via simulation. Simulation tests are performed for the Ørsted satellite on its elliptic orbit. The satellite motion is influenced by a moderate aerodynamic drag torque corresponding to normal solar activity.

The contents of this chapter is based on Wisniewski (1994a) and Wisniewski (1995b). The theoretical background for the design and analysis was elaborated in Chapter 3.

4.1   Satellite as Linear Periodic System

It has been mentioned several times that the control torque of the magnetic actuated satellite always lies perpendicular to the geomagnetic field vector, and a magnetic moment generated in the direction parallel to the local geomagnetic field has no influence on the satellite motion. This can be explained by the following equality

$$
{}^{c}\mathbf{N}_{ctrl}(t) = ({}^{c}\mathbf{m}_{\parallel}(t) + {}^{c}\mathbf{m}_{\perp}(t)) \times {}^{c}\mathbf{B} = {}^{c}\mathbf{m}_{\perp}(t) \times {}^{c}\mathbf{B}, \tag{4.1}
$$

where ${}^{c}\mathbf{m}_{\parallel}$ is the component of ${}^{c}\mathbf{m}$ parallel to ${}^{c}\mathbf{B}$, whereas ${}^{c}\mathbf{m}_{\perp}$ is perpendicular to the local geomagnetic field.

Concluding, the necessary condition for power optimality of a control law is that the magnetic moment lies on a 2-dimensional manifold perpendicular to the geomagnetic field vector.

Consider the following mapping

$$
{}^{c}\tilde{\mathbf{m}} \mapsto {}^{c}\mathbf{m} \ : \ {}^{c}\mathbf{m} \ = \ \frac{{}^{c}\tilde{\mathbf{m}} \times {}^{c}\mathbf{B}}{\| \, {}^{c}\mathbf{B} \, \|}, \tag{4.2}
$$

where ${}^{c}\tilde{\mathbf{m}}$ represents a new control signal for the satellite. Now, the magnetic moment, ${}^{c}\mathbf{m}$, is perpendicular to the local geomagnetic field vector and control theory for a system with unconstrained input ${}^{c}\tilde{\mathbf{m}}$ can be applied. The direction of the signal vector ${}^{c}\tilde{\mathbf{m}}$ (contrary to ${}^{c}\mathbf{m}$) can be chosen arbitrary by the controller. From practical point of view, the mapping (4.2) selects the component of ${}^{c}\tilde{\mathbf{m}}$ which is perpendicular to the local geomagnetic field vector. The efficiency of the control is improved by this re-formulation. The reason is that currents sent into the magnetorquer coils will always give rise to a magnetic control moment which is exactly perpendicular to ${}^{c}\mathbf{B}$.

Linearization of the satellite motion in terms of the first three components of the attitude quaternion was elaborated in Section 2.6. The only difference between the linear satellite model in Section 2.6 and the linear system with the new control signal ${}^{c}\tilde{\mathbf{m}}$ is that the cross product operation ${}^{c}\mathbf{m} \times {}^{c}\mathbf{B}$ is substituted by the double cross product $({}^{c}\tilde{\mathbf{m}} \times {}^{c}\mathbf{B}) \times {}^{c}\mathbf{B}$.

The linearized equation of motion from Eqs. (2.38) and (4.2) is

$$
\frac{d}{dt} \left[\begin{array}{c} \delta\mathbf{\Omega} \\ \delta\mathbf{q} \end{array} \right] = \mathbf{A} \left[\begin{array}{c} \delta\mathbf{\Omega} \\ \delta\mathbf{q} \end{array} \right] + \mathbf{B}(t){}^{c}\tilde{\mathbf{m}}, \tag{4.3}
$$

where

$$
\mathbf{A} = \left[\begin{array}{cccccc} 0 & 0 & 0 & \Leftrightarrow 2k\sigma_x & 0 & 0 \\ 0 & 0 & \omega_o\sigma_y & 0 & 2k\sigma_y & 0 \\ 0 & \omega_o\sigma_z & 0 & 0 & 0 & 0 \\ \frac{1}{2} & 0 & 0 & 0 & 0 & 0 \\ 0 & \frac{1}{2} & 0 & 0 & 0 & \omega_o \\ 0 & 0 & \frac{1}{2} & 0 & \Leftrightarrow\omega_o & 0 \end{array} \right],
$$

$$\sigma_x = \frac{I_y \Leftrightarrow I_z}{I_x}, \ \sigma_y = \frac{I_z \Leftrightarrow I_x}{I_y}, \ \sigma_z = \frac{I_x \Leftrightarrow I_y}{I_z},$$

$$\mathbf{B}(t) = \left[\mathbf{I}^{-1} \begin{bmatrix} \Leftrightarrow^o B_y^2(t) \Leftrightarrow^o B_z^2(t) & {}^o B_x(t)^o B_y(t) & {}^o B_x(t)^o B_z(t) \\ {}^o B_x(t)^o B_y(t) & \Leftrightarrow^o B_x^2(t) \Leftrightarrow^o B_z^2(t) & {}^o B_y(t)^o B_z(t) \\ {}^o B_x(t)^o B_z(t) & {}^o B_y(t)^o B_z(t) & \Leftrightarrow^o B_x^2(t) \Leftrightarrow^o B_y^2(t) \end{bmatrix} \begin{bmatrix} 0 & 0 & 0 \\ 0 & 0 & 0 \\ 0 & 0 & 0 \end{bmatrix} \right]$$

Our attention is on the matrix $\mathbf{B}(t)$ consisting of a time varying and a constant part. The time varying part represents the double cross product operation $\Leftrightarrow^o\mathbf{B}(t) \times ({}^o\mathbf{B}(t) \times)$. The matrix $\mathbf{B}(t)$ is approximated by a periodic matrix $\hat{\mathbf{B}}(t)$ in the next subsections.

4.2   Infinite Horizon Periodic Controller

The geomagnetic field is essentially that of a magnetic dipole with the largest anomalies over Brazil and Siberia. The geomagnetic field in the Orbit CS, has large y and z components, while the x component is comparatively small. The rotation of the Earth is visible via fluctuations of the geomagnetic field vector's x component with frequency $1/24 \ 1/hours$, see Fig. 2.4 in Subsection 2.7.2. The following observation is used for the design of an attitude controller. The geomagnetic field on a near polar orbit is approximately periodic with a period $T = 2\pi/\omega_0$.

Due to periodic nature of the geomagnetic field, seen from the Orbit CS, the linearized model of the satellite can be considered as periodic. It is though necessary to find an ideally periodic counterpart of the real magnetic field of the Earth. This is done by averaging the geomagnetic field over $N = 15$ number of orbits covering $24 \ hours$. Furthermore, the geomagnetic field is parameterized by the mean anomaly M, since the geomagnetic field and the mean anomaly have the common period T

$$^o\mathbf{B}_{ave}(M) = \frac{1}{N} \sum_{i=1}^{N} {}^o\mathbf{B}(M). \tag{4.4}$$

An averaged B-field vector $\mathbf{B}_{ave}(M(t))$ is depicted in Fig. 4.1. The resultant linear periodic system is

$$\frac{d}{dt} \begin{bmatrix} \delta\mathbf{\Omega} \\ \delta\mathbf{q} \end{bmatrix} = \mathbf{A} \begin{bmatrix} \delta\mathbf{\Omega} \\ \delta\mathbf{q} \end{bmatrix} + \hat{\mathbf{B}}(M)^c\tilde{\mathbf{m}}, \tag{4.5}$$

where $\hat{\mathbf{B}}(M)$ is given in Eq. (4.5) after substituting the symbol $\mathbf{B}(t)$ for $\hat{\mathbf{B}}(M)$, and the components of the vector $^o\mathbf{B}(t)$ for the components of $^o\mathbf{B}_{ave}(M)$.
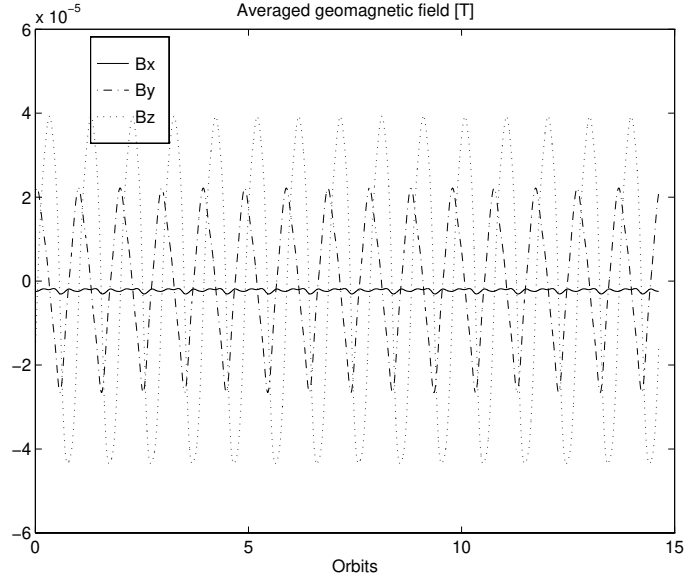
Figure 4.1: An averaged B-field vector in the Orbit CS. Compare with the realistic magnetic field of the Earth in Fig. 2.4 .

The difference between the time varying matrix $\mathbf{B}(t)$ and the ideal periodic counterpart $\hat{\mathbf{B}}(M(t))$ used for the controller design is considered an additional external disturbance torque acting on the satellite.

The controller gain is calculated from the steady state solution of the Riccati equation, which is periodic. The solution to the Riccati equation is calculated off-line and stored in the computer memory.

The results from Section 3.3 are applied for the design of a periodic attitude controller. According to Theorem 3.3.2, if the pair $\left(\mathbf{A}, \hat{\mathbf{B}}(M)\right)$ is stabilizable then there exists a stabilizing symmetric periodic solution $\mathbf{P}_+(t)$ of the Riccati equation

$$\Leftrightarrow \dot{\mathbf{P}}_+(t) = \mathbf{P}_+(t)\mathbf{A} + \mathbf{A}^T\mathbf{P}_+(t) \Leftrightarrow \mathbf{P}_+(t)\hat{\mathbf{B}}(M)\hat{\mathbf{B}}^T(M)\mathbf{P}_+(t) + \mathbf{Q}. \tag{4.6}$$

The periodic solution of the Riccati equation, $\mathbf{P}_+(t)$ is found from the periodic extension of the steady state solution $\mathbf{P}_\infty(t)$.

$$\hat{\mathbf{P}}(t) = \left\{ \begin{array}{ll} \mathbf{P}_\infty(t) & \text{if } 0 \leq t < T \\ \mathbf{0} & \text{otherwise} \end{array} \right. \tag{4.7}$$
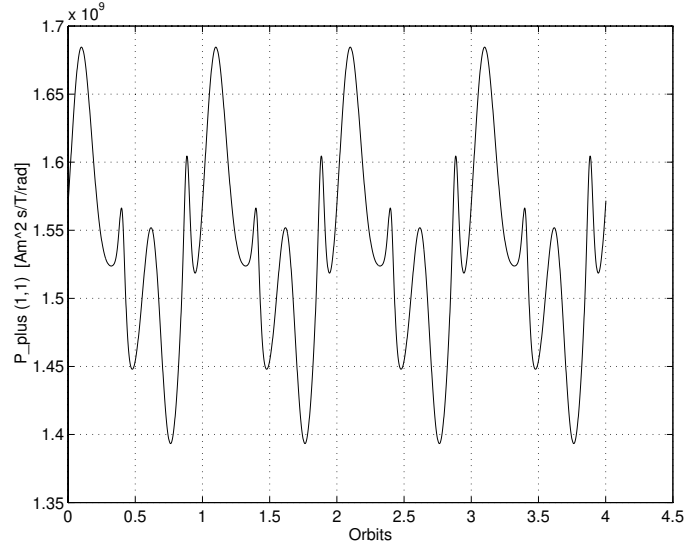
Figure 4.2: The time history of the (1,1) component of $\mathbf{P}_+$. Notice that $\mathbf{P}_+$ has a period equivalent to the orbit period.

$$\mathbf{P}_+(t) = \sum_{k=0}^{\infty} \hat{\mathbf{P}}(t \Leftrightarrow kT) \tag{4.8}$$

The solution $\mathbf{P}_\infty(t)$ is calculated using backward integration of the Riccati equation for an arbitrary final condition. This solution converges to the periodic solution. The matrix function $\mathbf{P}_\infty(t)$ corresponding to one orbital passage is stored in the computer memory, and then used for the subsequent orbits.

An example of the periodic matrix function $\mathbf{P}_+(t)$ is illustrated in Fig. 4.2. $\mathbf{P}_+(t_0)$ at fixed time t_0 is a 6 x 6 positive definite matrix. The figure depicts the time history of $P_+(1, 1)$, which is typical for the diagonal components. Off-diagonal components change their amplitudes between positive and negative values.

Again, the mean anomaly M can be used for parameterization of $\mathbf{P}_+(M)$, since both $\mathbf{P}_+(t)$ and $M(t)$ are T-periodic. Furthermore, the controller gain matrix is also T-periodic and parameterized with respect to $\mathbf{M}$

$$\mathbf{K}_+(M) = \Leftrightarrow\mathbf{B}(M)\mathbf{P}_+(M). \tag{4.9}$$

4.2.1   Implementation

The mean anomaly dependent control gain matrix $\mathbf{K}_+(M)$ is computed off-line and stored in the computer memory. The control signal $^c\tilde{\mathbf{m}}(t)$ is then calculated according to

$$^c\tilde{\mathbf{m}}(t) = \mathbf{K}_+(M) \begin{bmatrix} ^c\mathbf{\Omega}_{co}(t) \\ \mathbf{q}(t) \end{bmatrix}, \tag{4.10}$$

and finally, the magnetic moment, $^c\mathbf{m}(t)$ is obtained by

$$^c\mathbf{m}(t) = \frac{^c\tilde{\mathbf{m}}(t) \times {^c}\mathbf{B}(t)}{\parallel {^c}\mathbf{B}(t) \parallel}. \tag{4.11}$$

Another option is to represent $\mathbf{K}_+(M)$ in terms of the Fourier coefficients, benefiting in a reduction of the data stored. A satisfactory approximation of the gain matrix $\mathbf{K}_+$ has been obtained with 16th order Fourier series, see Fig. 4.3. The required capacity of computer memory given in floating point numbers is

$$Memory = \frac{Period \ * \ No.\ of\ elemnts\ in\ \mathbf{K}_+ \ * \ Order\ of\ Fourier\ series}{Sampling\ time}.$$

For example with a sampling time of 10 sec and the orbital period 6000 sec , then 172800 floating point memory is required.

Simulation results of the infinite horizon attitude control are presented in Figs. 4.4, 4.5 and 4.6. Fig. 4.4 illustrates performance of the attitude controller for the linear model of the satellite motion with an ideally periodic geomagnetic field simulator. Fig. 4.5 depicts performance of the infinite horizon attitude controller for the Ørsted satellite in a circular orbit. In Fig. 4.6, the Ørsted satellite is simulated in its elliptic orbit. The satellite motion is affected by the aerodynamic drag for normal solar activity. Additionally, the realistic geomagnetic field is applied in both Figs. 4.5 and 4.6.

Disturbances due to eccentricity of the orbit and the aerodynamic drag torque act in the pitch direction. Therefore, both the first component of the quaternion and the first component of the angular velocity, which for small angles correspond to the pitch and pitch rate, are punished slightly more than the remaining components of the state. A diagonal weight matrix $\mathbf{Q}$ with the diagonal $[10\ 6\ 6\ 10\ 6\ 6]^T$ has been implemented for both linear and nonlinear models of the satellite. Initial values of the attitude are the same in both examples corresponding to $40\ deg$ pitch, $\Leftrightarrow 40\ deg$ roll, and $80\ deg$ yaw.

The simulations show that the controller is stable for a wide range of operating points, also very much outside the reference. However, the performance of the infinite horizon controller is relatively poor outside vicinity of the reference, due to influence of the non-linearities. This can be observed as large variations of the third and fourth component of the attitude quaternion, q_3 and q_4 in Figs. 4.5 and 4.6. The result of the disturbance torque
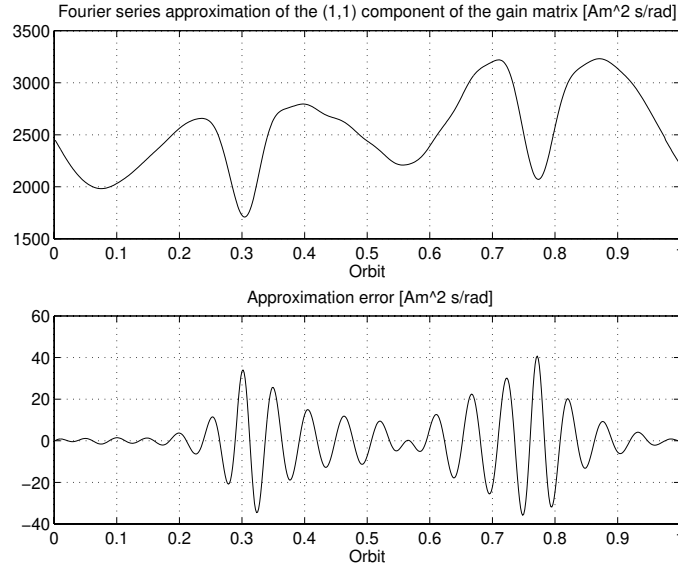
Figure 4.3: An approximation of the (1,1) component of the gain matrix $\mathbf{K}_+$ by 16th order Fourier series. The discrepancy between $\mathbf{K}_+$ and its Fourier approximation reaches 1.5 per cents at most.

due to a difference between the geomagnetic field and its periodic counterpart implemented in the attitude controller is the steady state attitude error in Fig. 4.5. Performance of the infinite horizon attitude controller for the Ørsted satellite affected by the aerodynamic torque is illustrated in Fig. 4.6. The satellite motion is influenced by a moderate aerodynamic drag torque corresponding to normal solar activity. The aerodynamic drag is equal $0.9\,10^{-5}\,Nm$ at perigee. The attitude error is $3\,deg$ of pitch and roll, whereas yaw angle varies within $6\,deg$.

A computational expense for the infinite horizon controller lies in the off-line numeric solution to the Riccati equation, but relatively large computer memory is required for keeping the gain data for one orbit. The controller gives a nonzero steady state error also for simulations without external disturbance torques. It is concluded that the infinite horizon magnetic controller is applicable for missions with low pointing requirements. The steady state performance could be improved by the finite horizon controller, which incorporates a realistic model of the geomagnetic field.
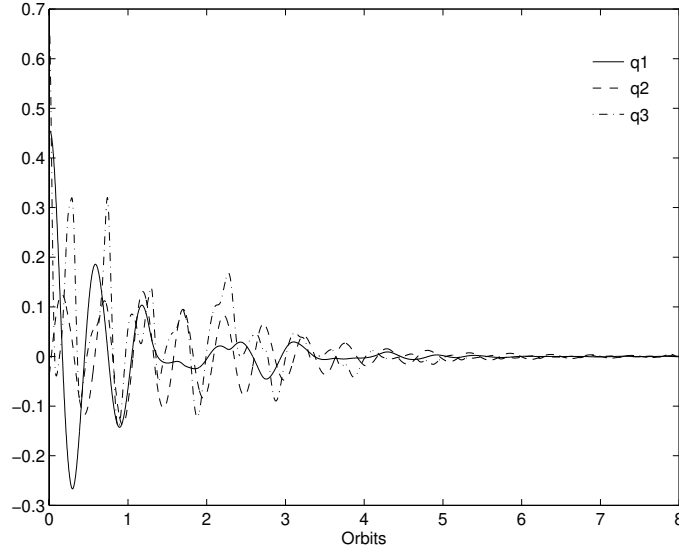
Figure 4.4: Performance of the infinite horizon controller for a satellite modeled as a linear object. The simulation is carried out for "ideally periodic" geomagnetic field. The initial attitude is $40\ deg$ pitch, $\Leftrightarrow 40\ deg$ roll and $80\ deg$ yaw.

4.3   Finite Horizon Periodic Controller

The linearized model of the satellite motion is only approximately periodic. There is a certain difference between the ideal periodic model of the geomagnetic field developed in Section 4.2, and the real magnetic field of the Earth. The controller performance could be improved by incorporating the time history of the real geomagnetic field into the controller structure.

A new attitude controller based on a transient solution of the Riccati equation is therefore investigated. Theoretical basis for the quasi periodic receding horizon controller was given in Section 3.4. The control algorithm is summarized as:

Procedure 4.1

1. *Calculate the time varying solution of the Riccati differential equation in the time interval* $t \in (\tau \Leftrightarrow T, \tau]$

$$\Leftrightarrow \dot{\mathbf{P}}(t) = \mathbf{A}^T \mathbf{P}(t) + \mathbf{P}(t)\mathbf{A} \Leftrightarrow \mathbf{P}(t)\mathbf{B}(t)\mathbf{B}^T(t)\mathbf{P}(t) + \mathbf{Q}(t) \tag{4.12}$$

   with the final condition

$$\mathbf{P}(\tau) = \mathbf{P}_f. \tag{4.13}$$
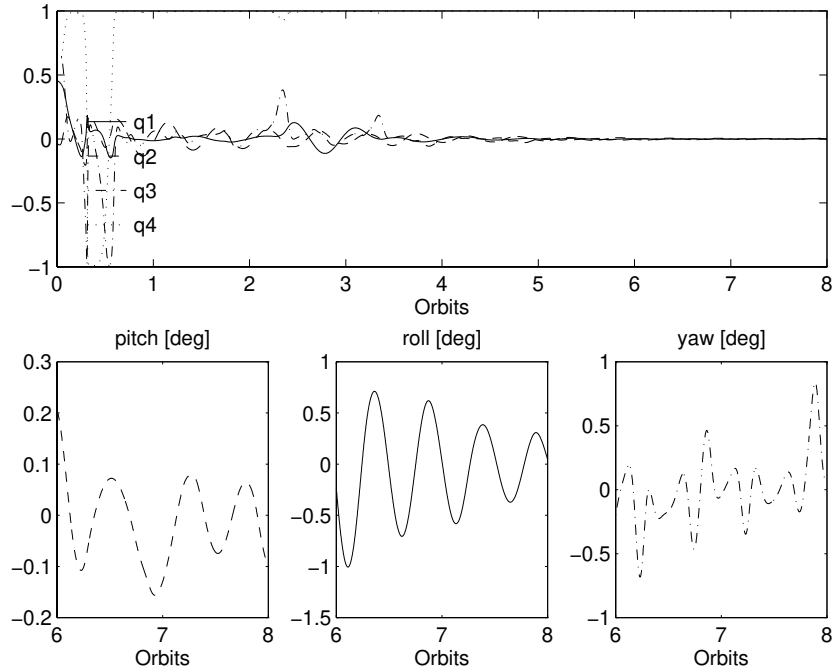
Figure 4.5: Performance of the infinite horizon controller for the Ørsted satellite on a circular orbit. The initial attitude is the same as in Fig. 4.4. The steady state attitude error is below $1\ deg$.

2. *Implement controller*

$$\tilde{\mathbf{m}}(t) = \Leftrightarrow\mathbf{B}^T(t)\mathbf{P}(t) \begin{bmatrix} {}^c\mathbf{\Omega}_{co} \\ \mathbf{q} \end{bmatrix} \tag{4.14}$$

for $t \in (\tau \Leftrightarrow T, \tau]$.

3. *Calculate magnetic moment from the equation*

$${}^c\mathbf{m}(t) = \frac{{}^c\tilde{\mathbf{m}}(t) \times {}^c\mathbf{B}(t)}{\|\ {}^c\mathbf{B}(t)\ \|}.$$

4. *τ becomes $\tau + T$.*

5. *go to 1.*

It was stated in Section 3.4 that if the difference $\mathbf{F} = \mathbf{P}_f \Leftrightarrow \mathbf{P}(\tau \Leftrightarrow kT)$ is positive semidefinite for $k \geq 0$ then the procedure given above provides a stable control law (Theorem 3.4.1). The final condition, $\mathbf{P}_f$ is chosen sufficiently large such that $\mathbf{F}$ is positive
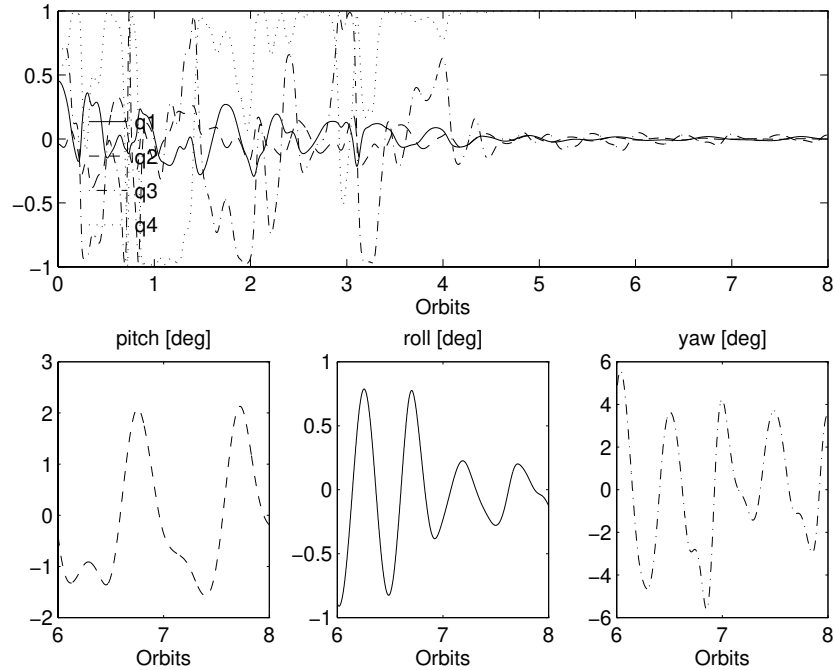
Figure 4.6: Performance of the infinite horizon controller for the Ørsted satellite on its elliptic orbit. The initial attitude is the same as in Fig. 4.4. The satellite is influenced by the aerodynamic drag for normal solar activity. The attitude error is below $3\ deg$ of pitch and roll. Yaw varies within $6\ deg$.

semidefinite independently on the deviation of the geomagnetic field from its periodic model. It should be noted that the larger $\mathbf{P}_f$, the larger is the control torque. The controller shall comply with the power constraints imposed on the attitude control system, therefore the maximum value of the final condition shall be confined. A heuristic algorithm searching for an acceptable $\mathbf{P}_f$ was given in Subsection 3.4.1. The final condition is considered as a design parameter, that can be iterated by means of computer simulation.

The attitude control system based on the final horizon control is illustrated in Fig. 4.7. The orbit model provides position of the satellite in orbit in terms of longitude, latitude and altitude. This information is used by the on board geomagnetic field model (here 10th order spherical harmonic model). The Riccati equation is computed for the subsequent orbit. The controller gain is computed and parameterized by the mean anomaly. The controller gain is stored in a buffer. This procedure is activated once per orbit. The control gain matrix is taken from the buffer on the basis of the mean anomaly associated
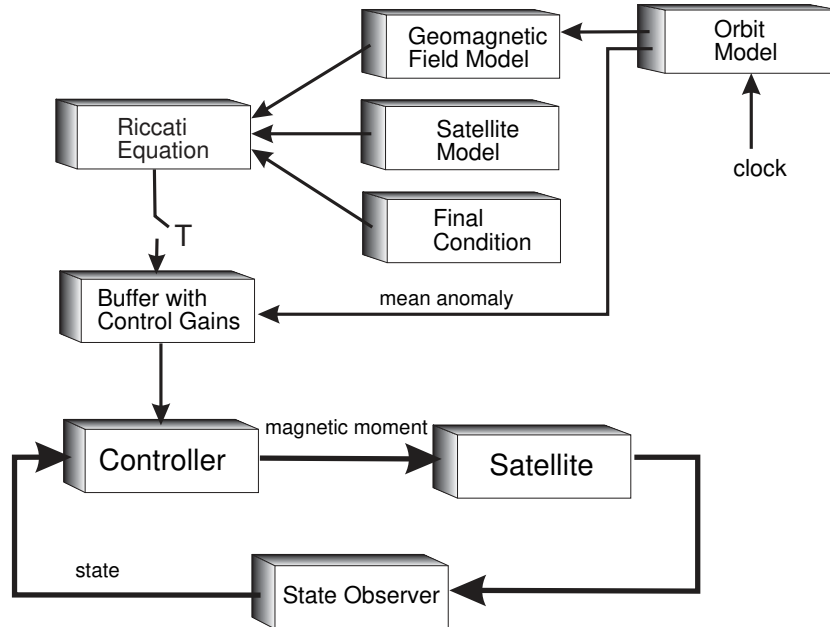
Figure 4.7: Attitude control system based on finite horizon control.

with position of the satellite in orbit. The controller gain is updated every sampling cycle, and is implemented in the control loop.

4.3.1 Implementation

The quasi periodic receding horizon controller has been validated through computer simulation. The results are depicted in Figs. 4.8 and 4.9. Control parameters have been found empirically. Weight matrix $\mathbf{Q}$ has been set to $10\,\mathbf{E}$, and the final condition $\mathbf{P}_f$ has been calculated from the steady state solution: $\mathbf{P}_f = \mathbf{P}(\tau) = 2\mathbf{P}_\infty(\tau)$. Initial values of the attitude have again been assigned to $40\,deg$ pitch, $\Leftrightarrow\!40\,deg$ roll and $80\,deg$ yaw.

Fig. 4.8 depicts the Ørsted satellite motion on a circular orbit, i.e. there are no external disturbances. The satellite attitude is seen to converge asymptotically to the reference. The performance of the quasi periodic receding horizon controller for the satellite disturbed by the aerodynamic torque is comparable with the performance of the infinite horizon controller, see Figs. 4.9 and 4.6. This is due to the impact of the aerodynamic torque is seen to be much larger than the influence of the torque due to the discrepancy between the geomagnetic field and its periodic counterpart.

The steady state performance of the infinite horizon controller on a circular orbit is much
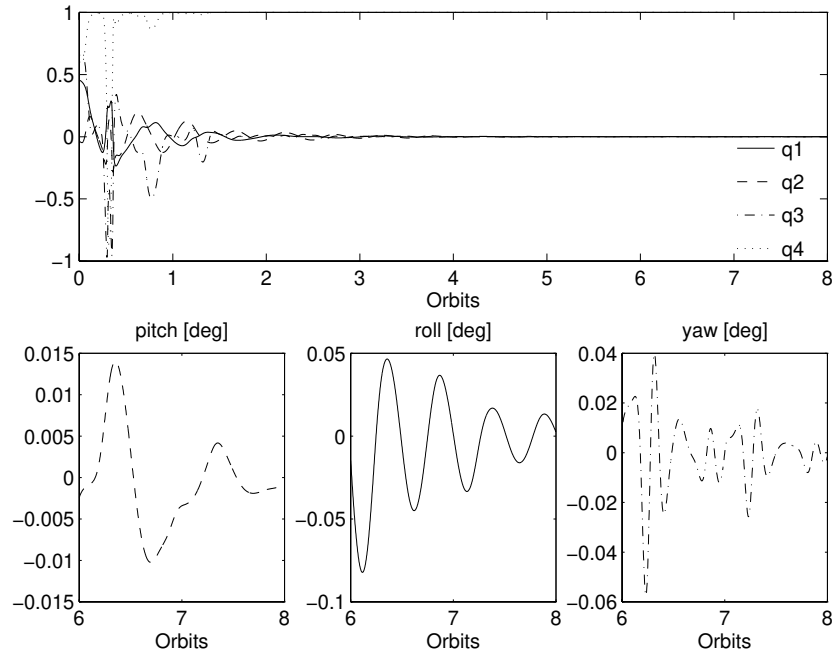
Figure 4.8: Performance of the quasi periodic receding horizon controller for the Ørsted satellite on circular orbit. The attitude converges asymptotically to the reference, i.e. ${}_{o}^{c}\mathbf{q} \rightarrow [0\ 0\ 0\ 1]^{T}$.

better than infinite horizon, however they are seen to have the same performance for a satellite in an elliptic orbit effected by the aerodynamic drag. The computational burden for the finite horizon controller is heavy due to the Riccati equation shall be solved on board (alternatively uploaded to the on board computer during every ground station passage). Therefore, the infinite horizon controller is preferable for the missions like Ørsted with low pointing accuracy. The necessary computer power could be additionally limited if the constant controller was implemented, and had the same performance as the time varying controllers.

4.4   Constant Gain Control

Computation of the infinite and finite horizon attitude controllers are tedious and difficult to implement on a real-time platform. A simple constant gain attitude controller could be an alternative which is investigated in this section.
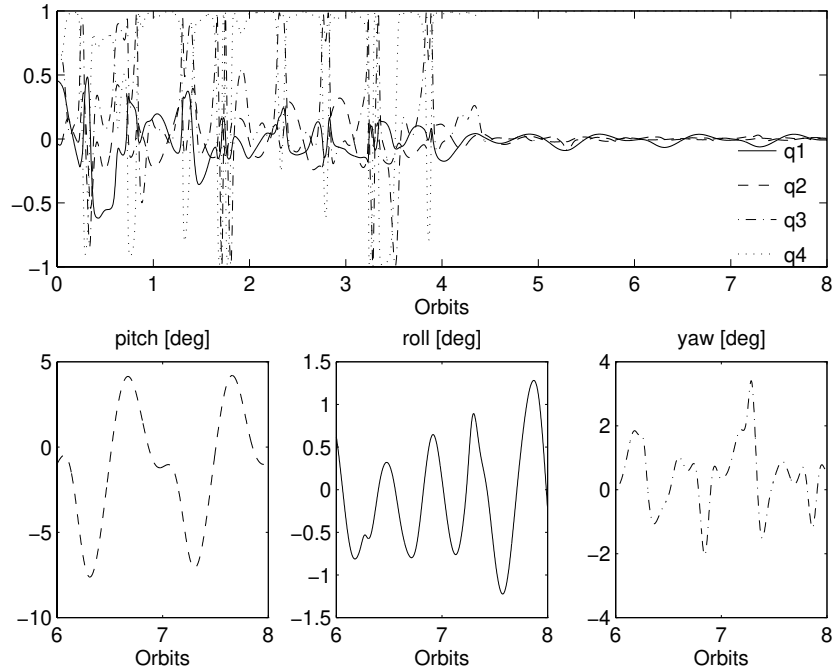
Figure 4.9: Performance of the quasi periodic receding horizon controller for the Ørsted satellite on the elliptic orbit. The satellite is influenced by the aerodynamic torque. Performance of the receding horizon is comparable with efficiency of the infinite horizon attitude controller in Fig. 4.6.

The design algorithm consists of replacing the time varying parameters of the satellite by its averaged values evaluated over a period of one orbit. The theoretical basis of the method was given in Section 3.5, and the design procedure was outlined in Subsection 3.5.3.

The time invariant counterpart of the time varying linearized satellite motion was

$$\frac{d}{dt}\left[\begin{array}{c} \delta\mathbf{\Omega} \\ \delta\mathbf{q} \end{array}\right] = \mathbf{A}\left[\begin{array}{c} \delta\mathbf{\Omega} \\ \delta\mathbf{q} \end{array}\right] + \mathbf{B}^c\tilde{\mathbf{m}}, \tag{4.15}$$

where

$$\mathbf{B} = \frac{1}{T}\int_o^T \hat{\mathbf{B}}(M(t))dt, \tag{4.16}$$

and T is the orbit period, and $\hat{\mathbf{B}}(M)$ is the control matrix in Eq. (4.5).

A linear quadratic regulator (LQR) is used for the constant gain controller design. The system is linear, time invariant and controllable thus a control law can be based on the solution of the steady state Riccati equation, see Kwakernaak and Sivan (1972). The optimal control is given by

$$^{c}\tilde{\mathbf{m}} = \Leftrightarrow \mathbf{B}^{T} \mathbf{P} \left[\begin{array}{c} \delta \mathbf{\Omega} \\ \delta \mathbf{q} \end{array} \right], \qquad (4.17)$$

where $\mathbf{P}$ satisfies the Riccati algebraic equation

$$\mathbf{P} \mathbf{A} + \mathbf{A}^{T} \mathbf{P} \Leftrightarrow \mathbf{P} \mathbf{B} \mathbf{B}^{T} \mathbf{P} + \mathbf{Q} = \mathbf{0}. \qquad (4.18)$$

Once the control vector $^{c}\tilde{\mathbf{m}}$ in Eq. (4.17) is calculated, the magnetic moment, $^{c}\mathbf{m}$ is computed according to Eq. (4.2).

Stability of the control law in Eqs. (4.17) and (4.2) for the time varying linear model of the satellite in Eq. (2.38) is determined using Floquet theory. This check is necessary, since stability of the time varying system and its time invariant counterpart are not equivalent. The time invariant system is only the first order approximation of the satellite. Furthermore, the sensitivities of those systems are not equivalent neither, e.g. the disturbance torque acting on the satellite in the direction of yaw in a zone near the North nor South poles remains unaffected by the attitude controller (due to lack of controllability), whereas it can be arbitrarily damped by an LQ controller for the time invariant counterpart.

The following closed-loop system is considered for the Floquet analysis

$$\frac{d}{dt} \left[\begin{array}{c} \delta \mathbf{\Omega} \\ \delta \mathbf{q} \end{array} \right] = (\mathbf{A} \Leftrightarrow \hat{\mathbf{B}}^{T} (M(t)) \mathbf{P}) \left[\begin{array}{c} \delta \mathbf{\Omega} \\ \delta \mathbf{q} \end{array} \right]. \qquad (4.19)$$

As seen from Eqs. (4.18) and (4.19) stability of the closed-loop system is dependent on the weight matrix $\mathbf{Q}$. Fig. 4.10 depicts locus of the characteristic multipliers for $\mathbf{Q}(\epsilon) \equiv \epsilon \mathbf{E}_{6 \times 6}$, where ϵ changes from 1 to 80 [1]. The satellite becomes unstable for $\epsilon = 52$. For $\epsilon = 18$, the largest characteristic multiplier is closest to the origin.

Notice that the averaged geomagnetic field is implemented for the Floquet analysis. Therefore, an ultimate test is the Monte Carlo simulation for the nonlinear model of the satellite with realistic disturbances.

4.4.1 Simulation

The constant gain control demonstrated stability for the entire envelope of the expected satellite initial attitudes and angular velocities in the science observation mission phase.

---

[1] The weight matrix $\mathbf{Q}(\epsilon)$ acts on the state space $[\delta \mathbf{\Omega} \ \delta \mathbf{q}]^{T}$. $\delta \mathbf{\Omega}$ is provided in rad/s and $\delta \mathbf{q}$ is given without units.
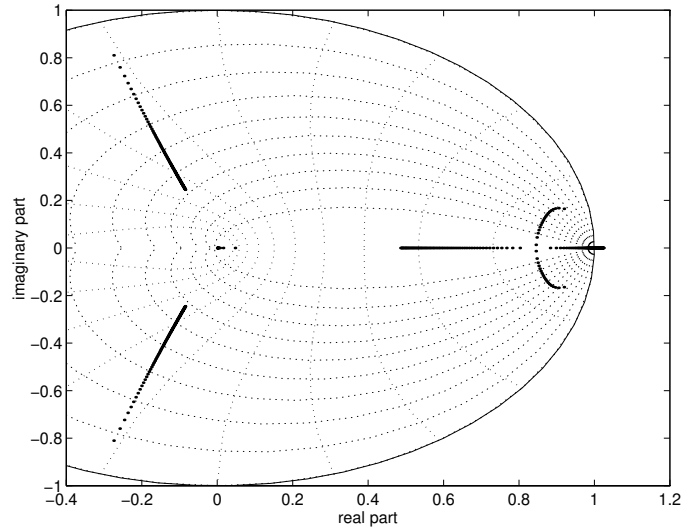
Figure 4.10: Locus of the characteristic multipliers $\lambda(\epsilon)$ for ϵ changing from 1 to 80 is evaluated for the closed loop system in Eq. (4.19).The satellite becomes unstable for $\epsilon = 52$, for $\epsilon = 18$ the largest characteristic multiplier is closest to the origin.

The control parameter: the weight matrix, $\mathbf{Q}$ has been found empirically. Its value has been set to $18 \cdot \mathbf{E}_{6 \times 6}$. The simulation results for the Ørsted satellite on the circular orbit in Fig. 4.11 show large amplitude of yaw oscillations. A new diagonal weigh matrix with diagonal $[18\ 18\ 90\ 18\ 18\ 90]^T$ is proposed. The amplitude of the yaw fluctuations is reduced, see Fig. 4.12. The last Fig. 4.13 illustrates the satellite motion on impact of the aerodynamic drag and the torque due to the eccentricity of the Ørsted orbit. The performance of the constant gain controller is very much the same as the infinite and finite horizon attitude controllers in Figs. 4.6 and 4.9. The attitude error is within $8\ deg$, which complies with required bond of $\pm 10\ deg$ of pitch and roll, $20\ deg$ of yaw.

4.5 Discussion of Results

Three attitude controllers were designed and evaluated in this chapter: the finite horizon, the infinite horizon, and the constant gain controllers. Their performances were comparable for a satellite in an elliptic orbit effected by the aerodynamic drag. The computer expense was however smallest for the constant gain controller, which is chosen for on board implementation. This controller is seen to be stable for a wide envelope of initial values of the attitude. This satisfactory performance achieved for the nonlinear model of the satellite inspired an investigation of attitude controllers with PD type structure in
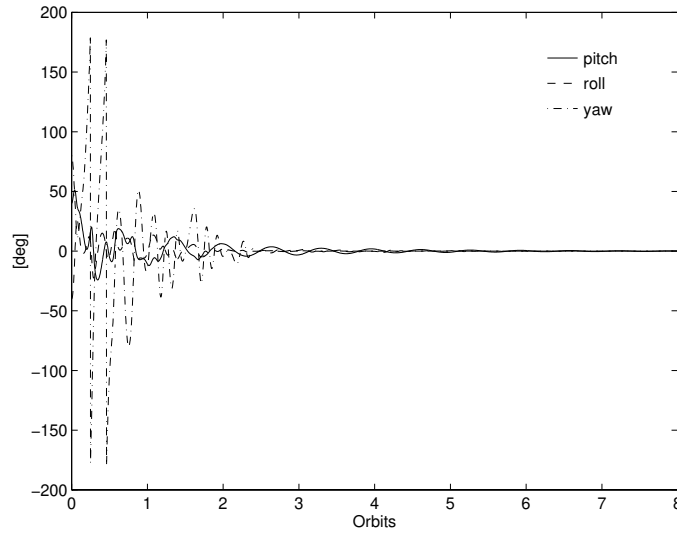
Figure 4.11: Performance of the constant gain controller for the Ørsted satellite on circular orbit, i.e. without external disturbances. The weigh matrix, $\mathbf{Q}$ has value $18 \cdot \mathbf{E}_{6 \times 6}$. Large amplitude of the yaw oscillations is encountered. The initial attitude is $40 \ deg$ pitch, $\Leftrightarrow\!40 \ deg$ roll and $80 \ deg$ yaw.
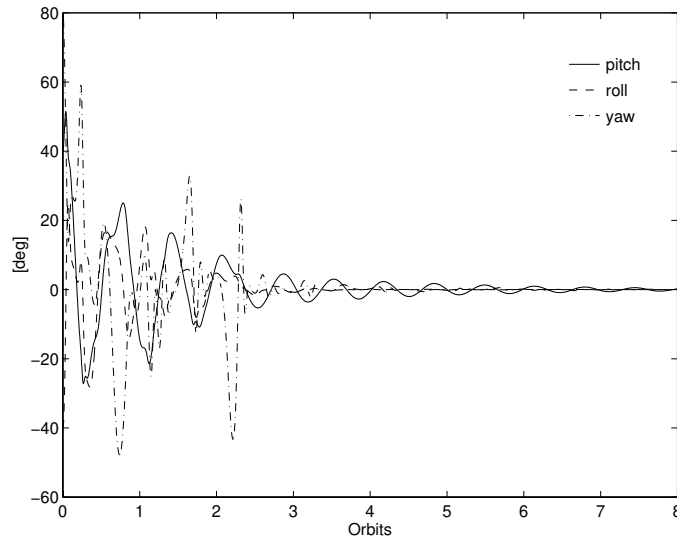
Figure 4.12: Performance of the constant gain controller for Ørsted satellite on circular orbit. The initial conditions are the same as in Fig. 4.11. The diagonal weight matrix $\mathbf{Q}$ with diagonal $[18\,18\,90\,18\,18\,90]^{T}$ is implemented. The amplitude of the yaw oscillation is reduced comparing with. Fig. 4.11.
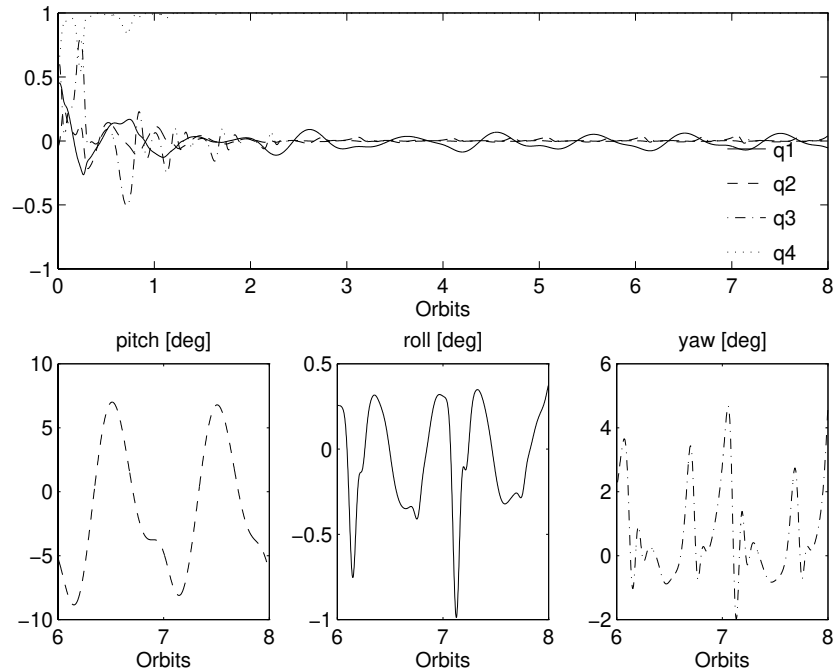
Figure 4.13: Performance of the constant gain controller for the Ørsted satellite on the elliptic orbit influenced by the aerodynamic drag. The initial conditions are as in Fig. 4.11. The resultant attitude is within $8\ deg$.

Chapter 7. The approach presented here was tested for a broad range of initial values such that the instrument boom was upright. There are, however, certain transitions and contingency phases that the satellite can not be considered as the rotation about the reference, owing to the nonlinear terms in the equations of kinematics and dynamics become dominant, e.g. a tumbling satellite or a satellite in a boom upside-down orientation. Nonlinear methods for magnetic attitude control are investigated in the next part of this work.

Chapter 5

Periodic Nonlinear Systems

A considerable part of the thesis has been devoted to development of the linear methods for the satellite attitude control. The nonlinear magnetic control techniques presented in this and the next two chapters comprise the central part of the work however. The nonlinear theory provides not only methods for globally stable control law but fused with the knowledge of the nature of the satellite motion it explains why simple linear controllers developed in the previous chapter are stable for initial values of the attitude very much outside the reference.

The satellite trajectory is expected to be in the vicinity of the reference for the most of the operational time, but there are certain transitions and contingency phases, where the satellite motion cannot be considered as rotation in the neighbourhood of a reference, and the nonlinear terms in Eqs. (2.12) to (2.20) become dominant. The problem is, thus, inherently nonlinear and nonlinear control methods are needed. The most important of the transition phases is when the satellite is released from the launcher, and will experience a random tumbling motion in space, with known bounds on the angular velocity.

A background of the nonlinear control theory is established in this chapter. However, it is not intended, that the chapter comprises a thorough tutorial, but it consists of a number of theorems, findings and conclusions, that are used in the subsequent part treating the design issues of a nonlinear controller for a near polar LEO satellite. The reader is also referred to the literature listed in the text.

Fundamental definitions of stability and asymptotic stability are first recalled in Section 5.1. Afterwards, Lyapunov's direct method is presented in Section 5.2. This is a basic tool for satellite motion analysis used throughout the remainder of the thesis. This method is extended to periodic nonlinear systems in Section 5.3. The reason for this effort is to utilize an observation that the satellite actuated by a set of electromagnetic coils can be modeled as a system, with the period of the geomagnetic field.

5.1   Concepts of Stability

The concept of stability of nonlinear systems differs remarkably from the definition of stability used for the linear plants. Stability and asymptotic stability are introduced. Furthermore, the variation of the system parameters in time demands an application of new notions of the uniform stability and the uniform asymptotic stability.

A concept of local stability defines properties of the system near the equilibrium. Global stability is an extension of the previous notion to the entire state space.

A general description of a nonlinear time varying (non autonomous) system is given in a form

$$\dot{\mathbf{x}}(t) = \mathbf{f}(t, \mathbf{x}(t)), \tag{5.1}$$

where $\mathbf{x}(t) \in \mathbb{R}^n$. The function $\mathbf{f} : \mathbb{R}_+ \times \mathbb{R}^n \to \mathbb{R}^n$ is continuous and satisfies a global Lipschitz condition, thus the solution to the differential equation (5.1) exists and is unique.

Furthermore, the solution to Eq. (5.1) for the initial condition $\mathbf{x}(t_0) = \mathbf{x}_0$ is denoted as $\mathbf{x}(t, t_0, \mathbf{x}_0)$. Recall that a vector $\mathbf{x}_e$ is an equilibrium if

$$\forall t \geq 0 \; \mathbf{f}(t, \mathbf{x}_e) = \mathbf{0}, \tag{5.2}$$

i.e. if the system starts in the equilibrium, then it stays there.

The fundamental definition of the stability is provided below.

Definition 5.1.1 (Definitions 9,10 in Vidyasagar (1993)) *The equilibrium, $\mathbf{x}_e$ is stable if, for each $\epsilon > 0$ and each $t_o \in \mathbb{R}_+$, there exists a $\delta = \delta(\epsilon, t_0)$ such that*

$$\| \mathbf{x}_0 \Leftrightarrow \mathbf{x}_e \| < \delta(\epsilon, t_0) \Rightarrow \forall t > 0 \; \| \mathbf{x}(t, t_0, \mathbf{x}_0) \Leftrightarrow \mathbf{x}_e \| < \epsilon. \tag{5.3}$$

It is uniformly stable if, for each $\epsilon > 0$, there exists a $\delta = \delta(\epsilon)$ such that

$$\| \mathbf{x}_0 \Leftrightarrow \mathbf{x}_e \| < \delta(\epsilon) \Rightarrow \forall t > 0 \; \| \mathbf{x}(t, t_0, \mathbf{x}_0) \Leftrightarrow \mathbf{x}_e \| < \epsilon. \tag{5.4}$$

The equilibrium is unstable if it is not stable.

Definition 5.1.1 states that if the solution trajectory $x(t, t_0, \mathbf{x}_0)$ starts inside a ball of radius δ and centre $\mathbf{x}_e$ then it always stays inside a new ball of radius ϵ, and the same centre, $\mathbf{x}_e$, see Figure 5.1. Uniform stability is a special case of stability, for which the radius δ is only dependent on ϵ (independent on the initial time).

For uniformly stable systems the following is true, an arbitrary small perturbations of the initial state, $\mathbf{x}_0$ from $\mathbf{x}_e$ results in arbitrary small perturbations of the corresponding solution trajectory, $\mathbf{x}(t, t_0, \mathbf{x}_0)$.

stability   *asymptotic stability*
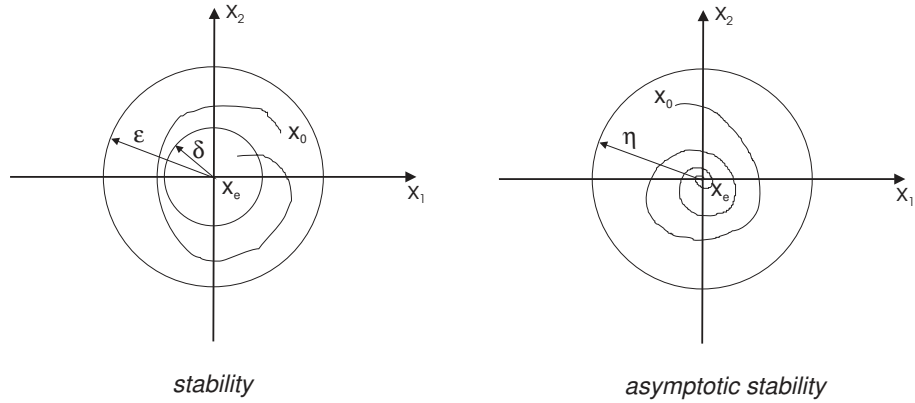
Figure 5.1: An illustration of stability and asymptotic stability

It is often interesting to investigate if the solution trajectory with the initial conditions outside the equilibrium, $\mathbf{x}_e$, finally will converge toward the equilibrium. The system having this property is recognized as asymptotically stable.

Definition 5.1.2 (Definition 31 in Vidyasagar (1993)) *The equilibrium x_e is asymptotically stable if it is stable and for each $t_0 \in \mathbf{R}_+$ there is an $\eta(t_0) > 0$ such that*

$$\| \mathbf{x}_0 \Leftrightarrow \mathbf{x}_e \| < \eta(t_0) \Rightarrow \mathbf{x}(t + t_0, t_0, \mathbf{x}_0) \to \mathbf{x}_e \text{ as } t \to \infty. \tag{5.5}$$

The equilibrium x_e is uniformly asymptotically stable if it is uniformly stable and there is a number $\eta > 0$ such that

$$\| \mathbf{x}_0 \Leftrightarrow \mathbf{x}_e \| < \eta \Rightarrow \mathbf{x}(t + t_0, t_0, \mathbf{x}_0) \to \mathbf{x}_e \text{ as } t \to \infty \text{ uniformly in } \mathbf{x}_0, \ t_0. \tag{5.6}$$

The nature of Definition 5.1.2 is local since only the behaviour of the solution trajectories starting from initial states near the equilibrium is taken into account. The definition of a globally uniformly asymptotically stable system is given below.

Definition 5.1.3 (Definitions 38 in Vidyasagar (1993)) *The equilibrium $\mathbf{x}_e$ is globally uniformly asymptotically stable if it is uniformly stable, for each arbitrarily large M. Furthermore, there exists a finite $T(M, \epsilon)$ for each arbitrarily small ϵ, such that*

$$\| \mathbf{x}_0 \Leftrightarrow \mathbf{x}_e \| < M, \ t_0 \Rightarrow \forall t \geq T(M, \epsilon), \| \mathbf{x}(t, t_0, \mathbf{x}_0) \| < \epsilon. \tag{5.7}$$

As mentioned in the introduction to this chapter the satellite, actuated by the set of electromagnetic coils with a certain state feedback, is periodic due to periodic nature of the

geomagnetic field. Therefore, a vital part of this chapter will be devoted to investigation of stability of a periodic system.

Formally, the satellite may be described by Eq. (5.1) with an additional property

$$\forall t \geq 0, \mathbf{x} \in \mathbb{R}^n \ \mathbf{f}(t + T, \mathbf{x}) = \mathbf{f}(t, \mathbf{x}), \tag{5.8}$$

where T is the period of the geomagnetic field.

Notice also that for periodic systems, the following is true

$$\forall t \geq t_0 \geq 0, \forall \mathbf{x}_0 \in \mathbb{R}^n \ \mathbf{x}(t + T, t_0 + T, \mathbf{x}_0) = \mathbf{x}(t, t_0, \mathbf{x}_0). \tag{5.9}$$

The solution to the system in Eq. (5.1) at time t for the initial conditions, $\mathbf{x}(t_0) = \mathbf{x}_0$, is the same as the solution to the same system at time $t + T$ for the initial conditions, $\mathbf{x}(t_0 + T) = \mathbf{x}_0$.

The concept of stability for periodic systems is in many details like that for time invariant (autonomous) systems. It will be shown that the behaviour of a periodic system resembles more an autonomous system than a non autonomous one. This statement is confirmed in the following theorem, which was first proposed by Hahn (1967).

Theorem 5.1.1 *Consider a periodic system fulfilling Eq. (5.8). Then an equilibrium is uniformly asymptotically stable if and only if it is asymptotically stable.*

Mostly the concept of asymptotically stable periodic systems will be investigated in the sequel. Note that the autonomous systems can be considered as periodic with an arbitrary period.

5.2 Lyapunov's Direct Method

Lyapunov's direct method is comparatively simple, but involves well understanding of the system in hand. The idea is to define a continuously differentiable, positive definite function reflecting energy in the system. This function is called a Lyapunov candidate function in the following. If the initial energy is dissipated the system is considered as stable.

Without loss of generality the equilibrium $\mathbf{0}$ is considered instead of an arbitrary equilibrium $\mathbf{x}_e$. As a motivation, consider a substitution $\tilde{\mathbf{x}} = \mathbf{x} \Leftrightarrow \mathbf{x}_e$. Recognize that if $\mathbf{x}$ has the equilibrium $\mathbf{x}_e$, then $\tilde{\mathbf{x}}$ has $\mathbf{0}$ as an equilibrium.

First, the celebrated theorem on stability of a general class of time-varying systems is provided.

Theorem 5.2.1 (Theorem 38 in Vidyasagar (1993)) *The equilibrium $\mathbf{0}$ of the system in Eq. (5.1) is stable if there exists a function $v : \mathbb{R}_+ \times \mathbb{R}^n \rightarrow \mathbb{R}$, which is continuously*

differentiable and locally positive definite. Furthermore, there exists a constant $r > 0$ such that

$$\forall \parallel \mathbf{x} \parallel < r, \ \dot{v}(t, \mathbf{x}) \leq 0.$$

The fundamental theorem on global asymptotic uniform stability of the equilibrium $\mathbf{0}$ is as follows.

Theorem 5.2.2 (Theorem 56 in Vidyasagar (1993)) *The equilibrium $\mathbf{0}$ of the system in Eq. (5.1) is globally uniformly asymptotically stable if there exists a C^1 function v: $\mathbb{R}_+ \times \mathbb{R}^n \rightarrow \mathbb{R}$, that is positive definite, decrescent and radially unbounded, and $\dot{v}$ is negative definite.*

Remark 5.2.1 *Recognize that if the positive definiteness is substituted by local positive definiteness, and the condition on radially unboundedness is released, Theorem 5.2.2 gives conditions for a local asymptotically stable equilibrium.*

5.3   Periodic Extension of Lyapunov Stability

So far, the standard Lyapunov method was recaptulated. The technique is applicable to the general class of nonlinear systems. Our attention in this section is, however, on periodic systems. It will be demonstrated that more specific stability tools can be developed for this class of systems, like in a theorem below stating that if the solution trajectory of a periodic system belongs to an L_2-space then the system is uniformly asymptotically stable to $\mathbf{0}$.

Theorem 5.3.1 *Consider a periodic system described by the non autonomous differential equation (5.1) with bounded r.h.s. Furthermore, let $\mathbf{x}(t, t_0, \mathbf{x}_0) \in L_2[0, \infty)$ for all $t_0 \geq 0$ and $\parallel \mathbf{x}_0 \parallel < \eta$, then $\mathbf{0}$ is a locally uniformly asymptotically stable equilibrium.*

Barbalat's lemma is used in the proof of Theorem 5.3.1.

Lemma 5.3.1 (Barbalat's lemma in Popov (1973)) *If ϕ is a real function of the real variable t, defined and uniformly continuous for $t > 0$, and if the limit of the integral $\int_0^t \phi(\tau) d\tau$ as t tends to infinity exists and is a finite number, then*

$$\lim_{t \to \infty} \phi(t) = 0. \tag{5.10}$$

Proof of Theorem 5.3.1 From the definition of the L_2-space, the following inequality involving the solution to the differential equation (5.1) is valid

$$\forall \mathbf{x}_0, t_0, t \geq t_0, \ \int_{t_0}^{\infty} \parallel \mathbf{x}(t, t_0, \mathbf{x}_0) \parallel^2 dt < \infty. \tag{5.11}$$

The r.h.s of the differential equation (5.1) is limited, hence the solution $\mathbf{x}(t, t_0, \mathbf{x}_0)$ is uniformly continuous. Then according to Barballat's lemma

$$\lim_{t \to \infty} \parallel \mathbf{x}(t, t_0, \mathbf{x}_0) \parallel^2 = 0, \tag{5.12}$$

thus

$$\lim_{t \to \infty} \mathbf{x}(t, t_0, \mathbf{x}_0) = \mathbf{0}, \tag{5.13}$$

The inequality (5.11) implies that

$$\forall \mathbf{x}_0, t_0, t \geq t_0 \parallel \mathbf{x}(t, t_0, \mathbf{x}_0) \parallel < \infty. \tag{5.14}$$

Therefore, it is concluded that the system is asymptotically stable, but the differential equation (5.1) was assumed to be periodic, hence according to Theorem 5.1.1 the system is also uniformly asymptotically stable.   ∎

Before introducing the next lemma dealing with stability of nonlinear periodic systems a definition of an invariant set will be given. The invariant set is characterized as a set, such that for every initial state in the set and some appropriate initial time t_0, the entire solution trajectory belongs to this set. A formal definition is given below.

Definition 5.3.1 *[Definition 25 in Vidyasagar (1993)] A set $W \subseteq \mathbb{R}^n$ is called an invariant set of the differential equation (5.1) if for each $\mathbf{x}_0 \in W$ there exists a $t_0 \in \mathbb{R}_+$ such that*

$$\forall t \geq t_0, \ \mathbf{x}(t, t_0, \mathbf{x}_0) \in W.$$

Another vital notion is a concept of a level set, which is defined below.

Definition 5.3.2 *A level set $L_v(c)$ is the connected subset of a set*

$$M_v(c) = \{\mathbf{x} \in \mathbb{R}^n : \exists t \geq 0 \ such \ that \ v(t, \mathbf{x}) \leq c\}, \tag{5.15}$$

that contains the equilibrium $\mathbf{0}$.

An example of the level set, $L_v(c)$ is depicted in Figure 5.2. The set $M_v(c)$ consists of two subsets. The level set, $L_v(c)$ is the subset of $M_v(c)$, which contains the equilibrium.

The major findings of this section are stated in the lemma and the theorem below treating stability analysis of a periodic nonlinear system. The foundations of this investigation are given in Krasovskii (1963)
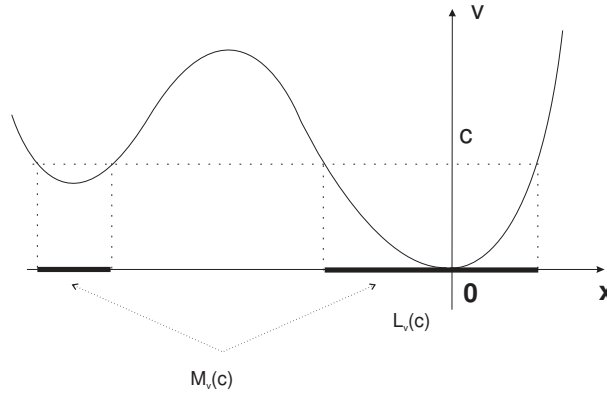
Figure 5.2: An example of level set $L_v(c)$. The set $M_v(c)$ consists of two subsets, whereas the level set, $L_v(c)$ is the subset of $M_v(c)$, which is containing the equilibrium.

Lemma 5.3.2 (Krasovskii-LaSalle) *Consider the periodic system in Eq. (5.1) with the property as in Eq. (5.8). Suppose there exists a C^1 function $v : \mathbb{R}_+ \times \mathbb{R}^n \to \mathbb{R}$ such that v is periodic with the same period as the system, v is locally positive definite, moreover there exists an open neighbourhood N of $\mathbf{0}$ such that*

$$\forall t \geq 0, \forall \mathbf{x} \in N, \ \dot{v}(t, \mathbf{x}) \leq 0. \tag{5.16}$$

Choose a constant $c > 0$ such that the level set $L_v(c)$ is bounded and contained in N. Finally let

$$U = \{\mathbf{x} \in L_v(c) : \exists t \geq 0 \ such \ that \ \dot{v}(t, \mathbf{x}) = 0\}, \tag{5.17}$$

and

$$A_v(c) = \{\mathbf{x} \in L_v(c) : \forall t \geq 0 \ v(t, \mathbf{x}) \leq c\}, \tag{5.18}$$

and let W denotes the largest invariant set of the system in hand contained in U. Then

$$\mathbf{x}_0 \in A_v(c), t_0 \geq 0 \Rightarrow \lim_{t \to \infty} d(\mathbf{x}(t, t_0, \mathbf{x}_0), W) = 0, \tag{5.19}$$

where $d(\mathbf{y}, W)$ denotes the distance from the point $\mathbf{y}$ to the set W.

It is beneficial to combine Lemma 5.3.2 with Theorem 5.2.1 to give a very useful result of uniformly asymptotic stability of periodic nonlinear systems.

Theorem 5.3.2 (Krasovskii-LaSalle) *Suppose the system (5.1) is periodic. Suppose there exists a C^1 locally positive definite function $v : \mathbb{R}_+ \times \mathbb{R}^n \to \mathbb{R}$ having the same*

period as the system, and an open neighbourhood N of $\mathbf{0}$ such that Eq. (5.16) holds. Choose a constant $c > 0$ such that the level set $L_v(c)$ is bounded and contained in N, and define U as in Eq. (5.17). Under these conditions, if U contains no trajectories of the system other than the trivial trajectory $\forall t_0 \geq 0$ $\mathbf{x}(t) \equiv \mathbf{0}$, then the equilibrium $\mathbf{0}$ is uniformly asymptotically stable.

In other words Theorem 5.3.2 states that if the stable system converges to a certain set U, instead of being convergent to the equilibrium $\mathbf{0}$, then it is essential to check what the largest invariant set W, a subset of the set U, is. If the set W has only one component $\mathbf{x} \equiv \mathbf{0}$, then $\mathbf{0}$ is a locally asymptotically stable equilibrium. This interpretation will be used in the next sections treating the attitude controller design.

The theoretical findings from this section will be applied in the next two chapters dealing with satellite magnetic attitude control using nonlinear methods.

Chapter 6

Three Axis Attitude Control: Sliding Mode Control

The last but not least approach to the attitude control for a magnetic actuated satellite is based on nonlinear methods. The control strategy presented in this chapter is based on the sliding mode control. The controller is developed for a satellite without appendages, since the concept was originally formulated for the Ørsted satellite during the boom pre-release phase. A characteristic feature of this configuration is that the principal moments of inertia are of the same order of magnitude.

After release from the launch vehicle the satellite is tumbling randomly with known bounds on the initial angular velocity. The objectives of the attitude control are to first damp the high angular velocity, then to stabilize the satellite in three axis with respect to the Orbit CS. Linearized equations of motion cannot be applied, since a control strategy satisfying global stability of the satellite motion is necessary.

The essence of the sliding controller design is outlined in Section 6.1. The design algorithm is split into two steps: the sliding manifold design and the sliding condition design. A three dimensional sliding manifold is proposed in Section 6.2. Furthermore, motion of the satellite on the sliding manifold is shown to be asymptotically stable. An ideal case of the sliding condition development is when the control torque is producible in x, y, and z directions independently. A solution to this control problem is given in Section 6.3. Sections 6.4 and 6.5 consider a sliding condition for the magnetic generated control torque. It is illustrated that a stable discontinuous sliding condition cannot be generated by the magnetorquers, therefore a continuous sliding condition must be applied. Furthermore, it is proved that a control design strategy, consisting of a sliding manifold design and a continuous sliding condition development, provides an asymptotically stable attitude controller. Finally, a control law for the magnetic actuated satellite is stated in Section

6.5. The simulation study shows that the sliding control is stable for satellites, which the principal moments of inertia are of the same order of magnitude. The contents of this chapter is based on the findings from Wisniewski (1994*b*) and Wisniewski and Blanke (1996*a*).

6.1   Sliding Mode Control

A sliding mode controller is implemented for the attitude corrections using magnetic torquing. The objective of the attitude control is to turn the satellite such that the Control CS coincides with the Orbit CS, i.e. $\mathbf{\Omega}_{co}$ converges to $\mathbf{0}$, the vector part of the attitude quaternion, $\mathbf{q}$, converges to $\mathbf{0}$, and the scalar part, q_4, approaches 1.

The design strategy of the sliding mode controller adopted in this thesis consists of two steps, see Utkin (1992), Slotine and Li (1991):

1. Sliding manifold design.

2. Sliding condition design.

Consider a manifold, a 3 dimensional hyperplane, in the state space of a 6th order system $[^c\mathbf{\Omega}_{co} \ \mathbf{q}]^T$. The sliding manifold is designed in such a way that the satellite trajectory, if on the hyperplane, converges to the reference. However, the satellite motion is not confined to the 3 dimensional hyperplane in general. Therefore, a control law forcing the satellite motion towards the manifold is necessary for achieving stable satellite motion. The sliding condition keeps decreasing the distance from the state to the sliding manifold, such that every solution $^c\mathbf{\Omega}_{co}$, $\mathbf{q}$ originating outside the sliding manifold tends to it. The manifold is an invariant set of the satellite motion and the trajectory of the system converges to the reference.

The result of the sliding condition design is a desired control torque. When the desired control torque is implemented the satellite trajectory converges to the sliding manifold. Now, the trajectory converges to the reference, since the satellite motion is stable on the sliding manifold.

The magnetic actuated satellite possesses one serious obstacle: the magnetic control torque is confined to lie perpendicular to the geomagnetic field vector and may not comply with the control torque which is desired to turn the satellite towards the sliding manifold. This control problem is addressed in Section 6.5

6.2   Sliding Manifold Design

It will be shown that the satellite motion on a certain 3 dimensional hyperplane in the 6-dimensional state space of the vector part of the attitude quaternion, $\mathbf{q}$, and the satellite

angular velocity, ${}^{c}\mathbf{\Omega}_{co}$, is stable.

First, let a sliding variable, ${}^{c}\mathbf{s}$, be defined as in Eq. (6.1)

$$
{}^{c}\mathbf{s} \equiv {}^{c}\mathbf{\Omega}_{co} + \mathbf{\Lambda}_{q}\mathbf{q}, \tag{6.1}
$$

where $\mathbf{\Lambda}_{q}$ is a positive definite matrix.

The sliding manifold is the subspace of the state space, where the sliding variable equals $\mathbf{0}$

$$
\mathbf{S} \equiv \{\mathbf{q}, {}^{c}\mathbf{\Omega}_{co} : {}^{c}\mathbf{s} = \mathbf{0}\}. \tag{6.2}
$$

The definition of the sliding variable, ${}^{c}\mathbf{s}$, in Eq. (6.1) guarantees convergence of $\mathbf{q}$ to zero and q_4 to 1 with an exponential rate. To show this, consider a Lyapunov candidate function

$$
v_q = \mathbf{q}^T\mathbf{q} + (1 \Leftrightarrow q_4)^2, \tag{6.3}
$$

which is equivalent to

$$
v_q = 2(1 \Leftrightarrow q_4), \tag{6.4}
$$

since $\mathbf{q}^T\mathbf{q} + q_4^2 = 1$.

The time derivative of the Lyapunov candidate function is calculated applying the kinematics in Eq. (2.18)

$$
\dot{v}_q = \mathbf{q}^T \, {}^{c}\mathbf{\Omega}_{co}, \tag{6.5}
$$

but ${}^{c}\mathbf{\Omega}_{co} = \Leftrightarrow\mathbf{\Lambda}_{q}\mathbf{q}$ thus

$$
\dot{v}_q = \Leftrightarrow\mathbf{q}^T\Lambda_q\mathbf{q}. \tag{6.6}
$$

The time derivative of the Lyapunov function is negative definite, since $\mathbf{\Lambda}_q$ is the positive definite matrix. According to Lyapunov's direct method Theorem 5.2.2, the equilibrium ${}^{c}_{o}\mathbf{q} = [0\ 0\ 0\ 1]^T$, ${}^{c}\mathbf{\Omega}_{co} = \mathbf{0}$ is asymptotically stable if the satellite is on the sliding manifold, ${}^{c}\mathbf{s}$.

Remark 6.2.1 *Recognize that only the vector part of the attitude quaternion is used in the definition of the sliding variable. Therefore, it is sufficient to describe satellite motion in the state space of $[{}^{c}\mathbf{\Omega}_{co}^{T}\ \mathbf{q}^T]^T$, and the order of the differential equation describing satellite motion is thus reduced from 7 to 6.*

Remark 6.2.2 *Notice that the equilibrium ${}^{c}_{o}\mathbf{q} = [0\ 0\ 0\ \Leftrightarrow 1]^T$, ${}^{c}\mathbf{\Omega}_{co} = \mathbf{0}$ is unstable even though ${}^{c}_{o}\mathbf{q} = [0\ 0\ 0\ \Leftrightarrow 1]^T$ and ${}^{c}_{o}\mathbf{q} = [0\ 0\ 0\ 1]^T$ represent the same attitude (Control CS coincides with Orbit CS). Furthermore, if the sliding variable is defined as*

$$
{}^{c}\mathbf{s} \equiv \mathbf{\Omega}_{co} \Leftrightarrow \mathbf{\Lambda}_{q}\mathbf{q}, \tag{6.7}
$$

it is possible to show using the Lyapunov candidate function

$$v_q = \mathbf{q}^T \mathbf{q} + (1 + q_4)^2,$$

(6.8)

that the equilibrium $^c_o\mathbf{q} = [0\ 0\ 0\ \Leftrightarrow 1]^T$, $^c\mathbf{\Omega}_{co} = \mathbf{0}$ is asymptotically stable and the equilibrium $^c_o\mathbf{q} = [0\ 0\ 0\ 1]^T$, $^c\mathbf{\Omega}_{co} = \mathbf{0}$ is unstable.

6.3 Sliding Condition Development

The objective of the analysis covered in this section is to derive the desired control torque turning the satellite trajectory towards the sliding manifold. An ideal case is considered first: It is assumed that the control torque is producible independently in the direction of the x, y, and z axes. In the next sections the magnetic generated control torque will be considered.

The satellite motion can be described in the space of the sliding variable, $^c\mathbf{s}$. A salient feature of this approach is that a reduced 3rd order system is considered. The attitude control problem is equivalent to that of making stable the equilibrium $^c\mathbf{s} = \mathbf{0}$. The representation of the satellite motion in the space of the sliding variable is calculated by differentiation of the sliding variable, $^c\mathbf{s}(t)$ w.r.t. time, which describes projection of the satellite motion on the space of the sliding variable (the s-space)

$$^c\dot{\mathbf{s}} = {^c\dot{\mathbf{\Omega}}_{cw}} \Leftrightarrow \omega_o {^c\mathbf{i}_o} + \mathbf{\Lambda}_q \dot{\mathbf{q}}.$$

(6.9)

The derivatives of the satellite angular velocity and the attitude quaternion are calculated according to the equations of kinematics and dynamics, Eqs. (2.18) and (2.12)

$$\mathbf{I}^c\dot{\mathbf{s}} = \Leftrightarrow {^c\mathbf{\Omega}_{cw}} \times \mathbf{I}^c\mathbf{\Omega}_{cw} + 3\omega_o^2 {^c\mathbf{k}_o} \times \mathbf{I}^c\mathbf{k}_o \Leftrightarrow \omega_o \mathbf{I}({^c\mathbf{i}_o} \times {^c\mathbf{\Omega}_{co}})$$
$$+ \quad \frac{1}{2}\mathbf{I}\mathbf{\Lambda}_q({^c\mathbf{\Omega}_{co}}q_4 + {^c\mathbf{\Omega}_{co}} \times \mathbf{q}) + {^c\mathbf{N}_{ctrl}}.$$

(6.10)

Assume that the satellite trajectory is on the sliding manifold. An equivalent torque is a control torque necessary to keep the satellite on the sliding manifold. In other words, if the control torque is equal to the equivalent torque then the time derivative of the sliding variable equals zero. If the satellite is not on the sliding manifold, a desired control torque equals the sum of the equivalent torque and a part making the sliding variable converge to $\mathbf{0}$ in finite time

$$^c\mathbf{N}_{des} \equiv {^c\mathbf{N}_{eq}} \Leftrightarrow \lambda_s\ sign\ {^c\mathbf{s}},$$

(6.11)

where λ_s is a positive constant number, and the equivalent torque, $^c\mathbf{N}_{eq}$ is

$$^c\mathbf{N}_{eq} = {^c\mathbf{\Omega}_{cw}} \times \mathbf{I}^c\mathbf{\Omega}_{cw} \Leftrightarrow 3\omega_o^2({^c\mathbf{k}_o} \times \mathbf{I}^c\mathbf{k}_o) + \omega_o \mathbf{I}({^c\mathbf{i}_o} \times {^c\mathbf{\Omega}_{co}})$$
$$\Leftrightarrow \quad \frac{1}{2}\mathbf{I}\mathbf{\Lambda}_q({^c\mathbf{\Omega}_{co}}q_4 + {^c\mathbf{\Omega}_{co}} \times \mathbf{q}).$$

(6.12)

If the control torque was producible in the x, y, and z directions independently the desired control torque, $^c\mathbf{N}_{des}$ could be substituted in Eq. (6.10) for the control torque, $^c\mathbf{N}_{ctrl}$. As the result, the time derivative of the sliding variable, $^c\mathbf{s}$ would be

$$^c\dot{\mathbf{s}} = \Leftrightarrow \lambda_s \mathbf{I}^{-1} \, sign \, {}^c\mathbf{s}. \tag{6.13}$$

The system described by the differential equation (6.13) is stable, hence the sliding condition is fulfilled. According to Utkin (1992) a system is stable if the control torque complies with the desired torque in Eq. (6.11). However, the magnetic generated torque is perpendicular to the local geomagnetic field vector and can only partly conform with the desired torque. A modified sliding condition for magnetic actuated satellite is provided in Section 6.5.

Remark 6.3.1 *Consider a design case such that the moments of inertia are known with a known tolerance $\mathbf{\Delta}_I$. Then $\mathbf{\Delta}_I$ will propagate in Eq. (6.12) resulting in an error $\mathbf{\Delta}_{eq}$ of the equivalent torque. The design parameter λ_s can be chosen sufficiently large such that*

$$\lambda_s > \bar{\sigma}(\mathbf{\Delta}_{eq}), \tag{6.14}$$

where $\bar{\sigma}$ is maximum singular value, and the resultant $\dot{\mathbf{s}}(t)$ is guaranteed to be negative definite.

6.4   Continuous Sliding Condition Development

Before a sliding condition for a magnetic actuated satellite will be formulated it is illustrated that the electromagnetic torque cannot generate stable discontinuous sliding condition. Instead a continuous sliding condition is proposed.

A compensation of the desired torque applying the magnetorquer coils is in the focus of this section. The desired torque may be given by a discontinuous function like in Eq. (6.11) or a continuous counterpart

$$^c\mathbf{N}_{des} \equiv {}^c\mathbf{N}_{eq} \Leftrightarrow \lambda_s \, {}^c\mathbf{s}.$$

It was concluded in Chapter 4 that a magnetic moment providing nonzero control torque lies on a 2-dimensional manifold perpendicular to the local geomagnetic field.

The following control law fulfills this requirement

$$^c\mathbf{m} = \frac{{}^c\mathbf{N}_{des} \times {}^c\mathbf{B}}{\| \, {}^c\mathbf{B} \, \|^2}. \tag{6.15}$$

The magnetic moment, $^c\mathbf{m}$ in Eq. (6.15) is $\mathbf{0}$ if the desired torque is parallel to the local geomagnetic field. In this case the the control torque cannot be generated in the direction

of the desired torque due to lack of controllability in the direction of $^c\mathbf{B}$. If $^c\mathbf{N}_{des}$ and $^c\mathbf{B}$ are perpendicular the control torque complies with the desired torque.

Stability of the magnetic actuation according to Eq. (6.15) is investigated both for continuous and discontinuous formulation of the desired torque. It is assumed in this section that the equivalent torque, i.e. $^c\mathbf{N}_{eq} = \mathbf{0}$ can be disregarded. This baseline is imposed only for the sake of simplicity and corresponds to a statement that the equivalent control can always be compensated by the control torque (ideal case).

6.4.1 Discontinuous Sliding Condition

The desired control torque, the result of the discontinuous sliding condition design from Eq. (6.11) is

$$^c\mathbf{N}_{des} = \Leftrightarrow \lambda_s \; sign \; ^c\mathbf{s}, \qquad (6.16)$$

since $^c\mathbf{N}_{eq}$ was assumed to be $\mathbf{0}$. The control torque which is to compensate the desired control torque is generated according to

$$^c\mathbf{N}_{ctrl} = {}^c\mathbf{m} \times {}^c\mathbf{B},$$

where the magnetic moment $^c\mathbf{m}$ is given in Eq. (6.15). Then the projection of the satellite motion on the s-space is

$$^c\dot{\mathbf{s}} = \frac{1}{\| \, ^c\mathbf{B} \, \|^2} \mathbf{I}^{-1} \left({}^c\mathbf{B} \times \lambda_s \; sign \; ^c\mathbf{s} \right) \times {}^c\mathbf{B}. \qquad (6.17)$$

The following Lyapunov candidate function is suggested

$$v_s = \frac{1}{2} {}^c\mathbf{s}^T \mathbf{I} \, {}^c\mathbf{s}. \qquad (6.18)$$

The derivative of v_s w.r.t. time gives

$$\dot{v}_s = \Leftrightarrow \frac{\lambda_s}{\| \, ^c\mathbf{B} \, \|^2} \left({}^c\mathbf{B} \times {}^c\mathbf{s} \right) \cdot \left({}^c\mathbf{B} \times \; sign \; ^c\mathbf{s} \right). \qquad (6.19)$$

It will be shown that there exist vectors $^c\mathbf{s}$ and $^c\mathbf{B}$ such that $\dot{v}_s > 0$. Consider an angle α between the vectors $^c\mathbf{s}$ and $sign \; ^c\mathbf{s}$. Recognize that α belongs to the interval $\left(\Leftrightarrow \frac{\pi}{4}, \frac{\pi}{4} \right)$. If the angle between $^c\mathbf{B}$ and $^c\mathbf{s}$ belongs to $\left(0, \frac{\pi}{4} \right)$ then it is possible to find a satellite attitude (i.e. the Control CS) such that the angle between $^c\mathbf{B}$ and $sign \; ^c\mathbf{s}$ belongs to $\left(\Leftrightarrow \frac{\pi}{4}, 0 \right)$, Fig. 6.1. Therefore, $\left({}^c\mathbf{B} \times {}^c\mathbf{s} \right) \cdot \left({}^c\mathbf{B} \times \; sign \; ^c\mathbf{s} \right) < 0$, and $\dot{v}_s > 0$.

In the next chapter a continuous sliding condition is proposed, and it is shown that it is asymptotically stable.
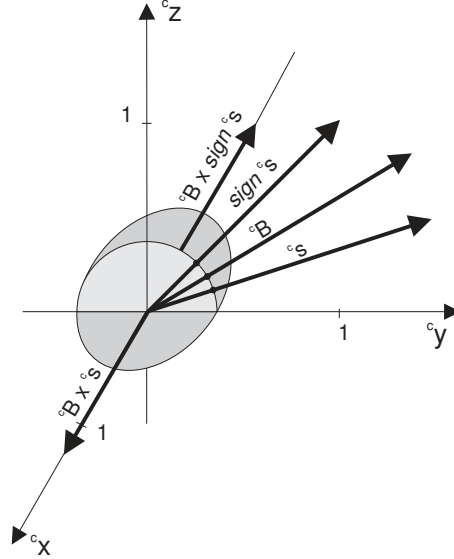
Figure 6.1: The angle between $^c\mathbf{B}$ and $^c\mathbf{s}$ belongs to $(0, \frac{\pi}{4})$. It is possible to find a Control CS such that the angle between $^c\mathbf{B}$ and $sign\ ^c\mathbf{s}$ belongs to $(\Leftrightarrow\frac{\pi}{4}, 0)$, and $(^c\mathbf{B} \times\ ^c\mathbf{s}) \cdot (^c\mathbf{B} \times\ sign\ ^c\mathbf{s}) < 0$.

6.4.2   Continuous Sliding Condition

The discontinuous sliding condition can be substituted by a continuous counterpart

$$^c\mathbf{N}_{des} \equiv\ ^c\mathbf{N}_{eq} \Leftrightarrow\lambda_s\,^c\mathbf{s}, \tag{6.20}$$

where λ_s is a positive scalar. However, it was assumed in the introduction to this chapter that $^c\mathbf{N}_{eq} = \mathbf{0}$, hence

$$^c\mathbf{N}_{des} = \Leftrightarrow\lambda_s\,^c\mathbf{s}. \tag{6.21}$$

Let the magnetic moment be generated according to Eq. (6.15). Now, the projection of the satellite motion on the s-plain is

$$^c\dot{\mathbf{s}} = \frac{1}{\parallel\,^c\mathbf{B}\parallel^2}\mathbf{I}^{-1}(^c\mathbf{B} \times \lambda_s\,^c\mathbf{s}) \times\ ^c\mathbf{B}. \tag{6.22}$$

Again, the stability properties are analyzed using the Lyapunov candidate function in Eq. (6.18). The time derivative of v_s is

$$\dot{v}_s = \Leftrightarrow\frac{\lambda_s}{\parallel\,^c\mathbf{B}\parallel^2}(^c\mathbf{B} \times\ ^c\mathbf{s}) \cdot (^c\mathbf{B} \times\ ^c\mathbf{s}). \tag{6.23}$$

The derivative of the Lyapunov function is negative semidefinite and time varying. It is equal to zero if the vectors ${}^{c}\mathbf{B}$ and ${}^{c}\mathbf{s}$ are parallel. Note that, if these two vectors are parallel then the magnetic moment, and hence the control torque is also equal to zero. The equations of motion of the satellite actuated by a set of electromagnetic coils are periodic because the geomagnetic field changes periodically in the Orbit CS, see Subsection 2.7.2, and the Krasovskii-LaSalle Theorem 5.3.2 can be applied. The set U in Theorem 5.3.2 contains such ${}^{c}\mathbf{s}$ and ${}^{c}_{o}\mathbf{q}$ that ${}^{c}\mathbf{B}$ and ${}^{c}\mathbf{s}$ are parallel

$$U = \{ {}^{c}\mathbf{s}, {}^{c}_{o}\mathbf{q} : \exists t > 0 \; {}^{c}\mathbf{B}(t) \text{ parallel to } {}^{c}\mathbf{s}(t) \}. \tag{6.24}$$

The geomagnetic field vector and the vector ${}^{c}\mathbf{s}$ can be resolved in the Orbit CS, therefore

$$ {}^{c}\mathbf{B} \text{ parallel to } {}^{c}\mathbf{s} \Leftrightarrow {}^{o}\mathbf{B} \text{ parallel to } {}^{o}\mathbf{s}. \tag{6.25}$$

But the statement

$$\exists t_0 \; \forall t > t_0 \; {}^{o}\mathbf{B} \text{ parallel to } {}^{o}\mathbf{s} \text{ for } {}^{c}\mathbf{m} = \mathbf{0} \tag{6.26}$$

is false, since the equation of the torque free motion of the satellite does not correspond to the geomagnetic field variation, see Wertz (1990). The geomagnetic field in the Orbit CS depends only on the satellite position (longitude, latitude, altitude), whereas ${}^{o}\mathbf{s}$ depends on the satellite attitude and angular velocity. It is concluded that the largest invariant set contained in U is ${}^{c}\mathbf{s} \equiv \mathbf{0}$, and according to the Krasovskii-LaSalle theorem the satellite motion projected in the s-space is globally uniformly asymptotically stable to $\mathbf{0}$.

In plain words, the total energy of the satellite is dissipated if ${}^{c}\mathbf{B}$ and ${}^{c}\mathbf{s}$ are not parallel. The energy is maintained constant if the two vectors are parallel. However, this does not hold permanently, since the local geomagnetic field changes its direction in time. Therefore, the total energy of the satellite motion will decrease to zero.

6.4.3 Sliding Mode Control with Continuous Sliding Condition

In the previous subsections a stable sliding manifold was designed, and a continuous sliding condition was formulated. The objective of this subsection is to demonstrate that the design procedure: first design a sliding manifold and then design a continuous sliding condition, provides an asymptotically stable controller with equilibrium in $[{}^{c}\mathbf{\Omega}_{co}^{T} \; \mathbf{q}^{T}]^{T} = \mathbf{0}$.

Consider the following Lyapunov candidate function

$$v = \mathbf{q}^{T}\mathbf{q} + (1 \Leftrightarrow q_4)^2. \tag{6.27}$$

The time derivative of v is

$$\dot{v} = \mathbf{q}^{T} \; {}^{c}\mathbf{\Omega}_{co}.$$

The satellite trajectory converges asymptotically to the sliding manifold, and the sliding variable **s** converges to **0**

$$\dot{v} = \mathbf{q}^T({}^c\mathbf{s} \Leftrightarrow \mathbf{\Lambda}_q\mathbf{q}), \tag{6.28}$$

since ${}^c\mathbf{\Omega}_{co} = {}^c\mathbf{s} \Leftrightarrow \mathbf{\Lambda}_q\mathbf{q}$.

Note that if ${}^c\mathbf{s} = \mathbf{0}$ then Eq. (6.28) is equivalent to Eq. (6.6).

The derivative $\dot{v}_q$ is bounded by

$$\dot{v}_q \leq \parallel \mathbf{q} \parallel \parallel {}^c\mathbf{s} \parallel \Leftrightarrow \lambda_q \parallel \mathbf{q} \parallel^2, \tag{6.29}$$

where λ_q is the minimum singular value of the matrix $\mathbf{\Lambda}_q$.

Both sides of Eq. (6.29) are now integrated

$$v_q(t) \Leftrightarrow v_q(t_0) \leq \Leftrightarrow \lambda_q \int_{t_0}^{t} \parallel \mathbf{q} \parallel^2 dt + \int_{t_0}^{t} \parallel \mathbf{q} \parallel \parallel {}^c\mathbf{s} \parallel dt, \tag{6.30}$$

thus

$$\lambda_q \int_{t_0}^{t} \parallel \mathbf{q} \parallel^2 dt \Leftrightarrow \int_{t_0}^{t} \parallel \mathbf{q} \parallel \parallel {}^c\mathbf{s} \parallel dt \Leftrightarrow v_q(t_0) \leq 0, \tag{6.31}$$

since $v_q(t)$ is positive definite.

According to Hölder's inequality, Rudin (1987), the following holds

$$\int_{t_0}^{t} \parallel \mathbf{q} \parallel \parallel {}^c\mathbf{s} \parallel dt \leq \sqrt{\int_{t_0}^{t} \parallel \mathbf{q} \parallel^2 dt} \sqrt{\int_{t_0}^{t} \parallel {}^c\mathbf{s} \parallel^2 dt}. \tag{6.32}$$

The definition of the norm in L_2-space is

$$\parallel \mathbf{x} \parallel_2 \equiv \sqrt{\int_{t_0}^{t} \parallel \mathbf{x} \parallel^2 dt}. \tag{6.33}$$

Eq. (6.31) is rewritten using Hölder's inequality

$$\lambda_q \parallel \mathbf{q} \parallel_2^2 \Leftrightarrow \parallel \mathbf{q} \parallel_2 \parallel {}^c\mathbf{s} \parallel_2 \Leftrightarrow v_q(t_0) \leq 0. \tag{6.34}$$

Finally,

$$\parallel \mathbf{q} \parallel_2 \leq \frac{\sqrt{\parallel {}^c\mathbf{s} \parallel_2^2 + 4\lambda_q v_q(t_0)}}{2\lambda_q} + \frac{\parallel {}^c\mathbf{s} \parallel_2}{\lambda_q}, \tag{6.35}$$

Recognize that ${}^c\mathbf{s}$ converges to **0**, since the sliding condition is satisfied, now ${}^c\mathbf{s} \in L_2[t_0, \infty)$. From the inequality (6.35) $\mathbf{q} \in L_2[t_0, \infty)$, as well. Furthermore, **q** is uniformly continuous, since r.h.s. of the kinematic equation (2.18) is bounded w.r.t. the

time variable (due to $^c\mathbf{s},\ \mathbf{q} \in L_2[t_0, \infty)$). Therefore, it is claimed that according to Theorem 5.3.1, the reference $[^c\mathbf{\Omega}_{co}^T\ _o^c\mathbf{q}^T]^T = [0\,0\,0\,0\,0\,0\,1]^T$ is globally uniformly asymptotically stable. The design procedure consisting of the sliding manifold and the continuous sliding condition design provides a stable attitude controller, indeed.

Remark 6.4.1 *It is worthwhile mentioning that the design algorithm for the sliding mode controller with continuous sliding condition resembles the feedback linearization techniques in Isidori (1994).*

6.4.4 Influence of Modeling Errors

A model of the satellite motion is provided with a certain parametric uncertainty, e.g. the moments of inertia are determined with finite accuracy. This indicates that the equivalent torque in Eq. (6.12) is not perfectly known. An influence of modeling errors on the sliding mode controller design was already discussed in Remark 6.3.1. A discontinuous sliding condition that rejects the influence of uncertainty in moments of inertia was proposed. Influence of the modeling errors on a continuous sliding controller is addressed in this subsection.

The sliding control introduced in the previous section provides the desired control torque that equals the sum of the equivalent torque and the part making the sliding variable convergent to zero. An effect of this uncertainty can be modeled by a certain limit value on the sliding variable, such that the desired control torque makes the sliding variable convergent to some nonzero constant vector $\mathbf{s}_0$. This implies that the satellite attitude converges to the reference with a bias vector $\mathbf{q}_0$.

Let the sliding variable, $^c\mathbf{s}(t)$ converge to a vector $\mathbf{s}_0$, then the satellite trajectory is on a manifold given by

$$^c\mathbf{\Omega}_{co} + \mathbf{\Lambda}_q\mathbf{q} \Leftrightarrow \mathbf{s}_0 = \mathbf{0}. \tag{6.36}$$

The objective of the following analysis is to provide approximate value of the bias vector $\mathbf{q}_0$. The vector $\mathbf{s}_0$ is considered to be small, therefore it is appropriate to analyze the satellite motion in the vicinity of the reference. The satellite angular velocity, $^c\mathbf{\Omega}_{co}$ and the first three components of the attitude quaternion, $\mathbf{q}$ are small, while the scalar component q_4 can be approximated by 1. It was shown in Subsection 2.6.2 that the first order approximation of the kinematics is given by

$$\dot{\mathbf{q}} = \frac{1}{2}{}^c\mathbf{\Omega}_{co}. \tag{6.37}$$

The linear approximation of the sliding manifold is then

$$2\dot{\mathbf{q}} + \mathbf{\Lambda}_q\mathbf{q} \Leftrightarrow \mathbf{s}_0 = \mathbf{0}. \tag{6.38}$$

Finally, the satellite motion on the sliding manifold is given by

$$\mathbf{q} = \mathbf{\Lambda}_q^{-1}\mathbf{s}_0 + e^{-\frac{1}{2}\mathbf{\Lambda}_q(t-t_0)}\mathbf{q}(t_0), \qquad (6.39)$$

thus the bias $\mathbf{q}_0$ equals

$$\mathbf{q}_0 = \mathbf{\Lambda}_q^{-1}\mathbf{s}_0. \qquad (6.40)$$

Recognize that the larger the components of the matrix $\mathbf{\Lambda}_q$ are, the smaller is the bias, $\mathbf{q}_0$.

6.5 Modified Sliding Condition

An ultimate sliding condition for a magnetic stabilized satellite is discussed in this section. Preliminary results were already established in the last chapter, and superiority of a continuous over discontinuous sliding condition was demonstrated.

The satellite appears uncontrollable if fixed at any instant of time due to the magnetic torque vector is constrained to always lie perpendicular to the local geomagnetic field vector. Therefore, it is necessary to select only those components of the desired control torque, which have an influence on the stability of the satellite motion. The desired control torque is resolved into two components: perpendicular and parallel to the sliding variable vector. Magnetic generated control torque is due to compensate only the component parallel to the sliding variable vector.

The desired control torque is the result of the continuous sliding condition design. The definition of the desired control torque adopted in this section is

$$^c\mathbf{N}_{des} \equiv {}^c\mathbf{N}_{eq} \Leftrightarrow \lambda_s {}^c\mathbf{s}, \qquad (6.41)$$

where λ_s is a positive scalar and $^c\mathbf{N}_{eq}$ is given in Eq. (6.12)

Consider orthogonal projection of the desired control torque, $^c\mathbf{N}_{des}(t)$ onto the instant sliding variable vector, $^c\mathbf{s}(t)$, Fig. 6.2. The desired control torque, $^c\mathbf{N}_{des}(t)$ has two components: parallel: $^c\mathbf{N}_{des}^{prl}(t)$, and perpendicular: $^c\mathbf{N}_{des}^{prp}(t)$, to the vector $^c\mathbf{s}(t)$.

The control torque, $^c\mathbf{N}_{ctrl}$ only needs to compensate $^c\mathbf{N}_{des}^{prl}$, since $^c\mathbf{N}_{des}^{prp}$ does not decrease the distance from the satellite trajectory to the sliding manifold. This control principle has an intuitive interpretation. The component $^c\mathbf{N}_{des}^{prl}$ is responsible for diminishing of the sphere radius in Fig. 6.2, whereas $^c\mathbf{N}_{des}^{prp}$ is responsible for movement on the sphere surface (sphere radius remains unchanged). This claim is formalized in Theorem 6.5.1.

Theorem 6.5.1 *The control torque that compensates $^c\mathbf{N}_{des}^{prl}$ makes the distance from the state $[{}^c\mathbf{\Omega}_{co}(t)\ \mathbf{q}(t)]^T$ to the sliding manifold in Eqs. (6.2) and (6.1) converge to zero, and the sliding condition is satisfied.*
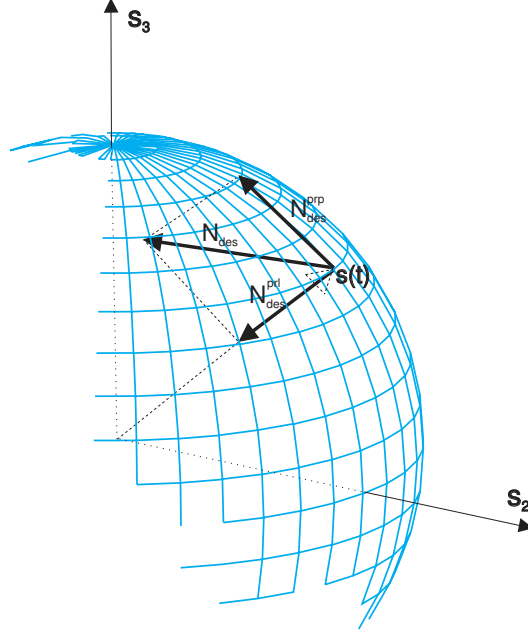
Figure 6.2: The desired control torque is resolved in the s-space. The component $^c\mathbf{N}^{prl}_{des}$ is responsible for diminishing of the sphere radius, whereas $^c\mathbf{N}^{prp}_{des}$ is responsible for movement on the sphere surface.

Proof of Theorem 6.5.1 Construct a Lyapunov candidate function

$$v_s = \frac{1}{2}{}^c\mathbf{s}^T\mathbf{I}^c\mathbf{s}. \tag{6.42}$$

The motion in the s-space is described by the equation

$$\mathbf{I}^c\dot{\mathbf{s}} = \Leftrightarrow{}^c\mathbf{N}_{eq} + {}^c\mathbf{N}_{ctrl}, \tag{6.43}$$

but the control torque compensates only $^c\mathbf{N}^{prl}_{des}$, thus

$$\mathbf{I}^c\dot{\mathbf{s}} = \Leftrightarrow\lambda_s{}^c\mathbf{s} + {}^c\mathbf{N}^{prp}, \tag{6.44}$$

where $^c\mathbf{N}^{prp}$ is the sum of the components of $^c\mathbf{N}_{eq}$ and $^c\mathbf{N}_{ctrl}$ that are perpendicular to the vector $^c\mathbf{s}(t)$.

Finally, the time derivative of the Lyapunov candidate function is given by

$$\dot{v}_s = {}^c\mathbf{s}^T\left(\Leftrightarrow\lambda_s{}^c\mathbf{s} + {}^c\mathbf{N}^{prp}\right) = \Leftrightarrow{}^c\mathbf{s}\lambda_s{}^c\mathbf{s}. \tag{6.45}$$
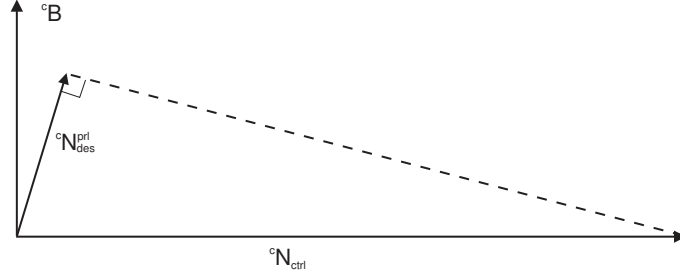
Figure 6.3: Large ${}^c\mathbf{N}_{ctrl}$ is necessary to compensate small ${}^c\mathbf{N}_{des}^{prl}$, if ${}^c\mathbf{B}$ and ${}^c\mathbf{s}$ are near to be parallel, and the magnitude of the control signal can be very large.

The time derivative of the Lyapunov candidate function is negative definite. The conditions of Theorem 5.2.2 are hence fulfilled, and the equilibrium $\mathbf{s} = \mathbf{0}$ is globally uniformly asymptotically stable. ∎

The control law which has to compensate ${}^c\mathbf{N}_{des}^{prl}$ with use of magnetic coils is only feasible if the geomagnetic field is never perfectly aligned with the sliding variable, ${}^c\mathbf{s}$. If ${}^c\mathbf{B}$ and ${}^c\mathbf{s}$ are close to parallel the amplitude of the control signal can be very large, since the large control torque ${}^c\mathbf{N}_{ctrl}$ is desired to compensate even small ${}^c\mathbf{N}_{des}^{prl}$, Fig. 6.3. In practice, the magnetic moment is confined, and ideal compensation of ${}^c\mathbf{N}_{des}^{prl}$ is not possible. Therefore, an approximate compensation is introduced

$$
{}^c\mathbf{m} = \frac{{}^c\mathbf{N}_{des}^{prl} \times {}^c\mathbf{B}}{\|{}^c\mathbf{B}\|^2}, \tag{6.46}
$$

where

$$
{}^c\mathbf{N}_{des}^{prl} = \frac{{}^c\mathbf{N}_{des} \cdot {}^c\mathbf{s}}{\|{}^c\mathbf{s}\|^2}{}^c\mathbf{s}. \tag{6.47}
$$

Notice that the control law in Eq. (6.46) compensates ${}^c\mathbf{N}_{des}^{prl}$ very well, if ${}^c\mathbf{B}$ is perpendicular or nearly perpendicular to ${}^c\mathbf{s}$, and produces small control torque when ${}^c\mathbf{B}$ and ${}^c\mathbf{s}$ are near to be parallel.

The control law based on the approximate compensation of the desired control torque in Eq. (6.46) has been observed to be locally asymptotically stable for small values of the gain Λ_q. Additionally, global stability was obtained when the principal moments of inertia are of the same order of magnitude, i.e. the Ørsted satellite is in the boom stowed configuration. In this case the magnetic moment generated according to Eq. (6.46) consists of the cross product of ${}^c\boldsymbol{\Omega}_{co}$ with the local geomagnetic field vector, ${}^c\mathbf{B}$, plus a small perturbation of the satellite attitude, since the equivalent control torque is small.

This phenomenon inspired further work on proportional-derivative feedback cross product with the local geomagnetic field vector treated in the next chapter.
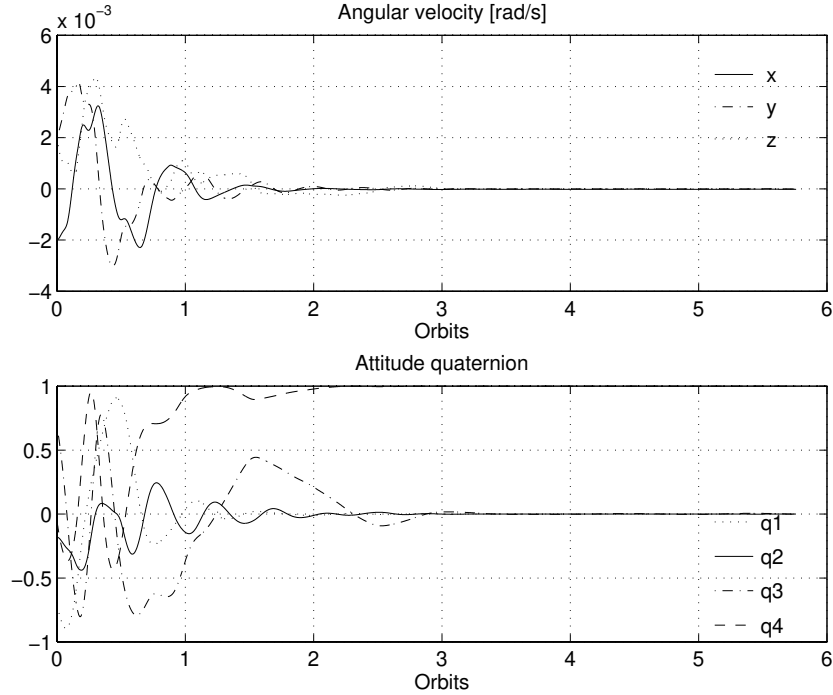
Figure 6.4: Performance of the sliding mode attitude controller in Eq. (6.46) for a satellite in a circular orbit. The plot shows the angular velocity, $^c\mathbf{\Omega}_{co}$ and the attitude quaternion,$^c_o\mathbf{q}$. The attitude quaternion converges to the reference $[0\ 0\ 0\ 1]^T$.

Remark 6.5.1 *It was mentioned that the large gain $\mathbf{\Lambda}_q$ can provide unstable satellite motion, but according to Section 6.4.4 large value of $\mathbf{\Lambda}_q$ is necessary to maintain the required accuracy of convergence. This tradeoff can be solved by Monte Carlo simulation.*

6.6   Validation of Sliding Mode Attitude Control

The sliding mode attitude controller in Eq. (6.46) was validated by the Monte Carlo simulation for the Ørsted satellite in boom stowed configuration. Various initial values of the angular velocity and the attitude were tested. The controller was evaluated for the initial values of the attitude, both in the neighbourhood of the reference and for the z principal axis pointing up-side down w.r.t. the z axis of the Orbit CS.

The control parameters were found empirically: $\mathbf{\Lambda}_q = 0.002 \cdot \mathbf{E} \frac{rad}{sec}$, $\mathbf{\Lambda}_s = 0.003 \frac{N\ sec}{rad}$. Fig. 6.4 shows simulation of the angular velocity and the attitude quaternion. The at-
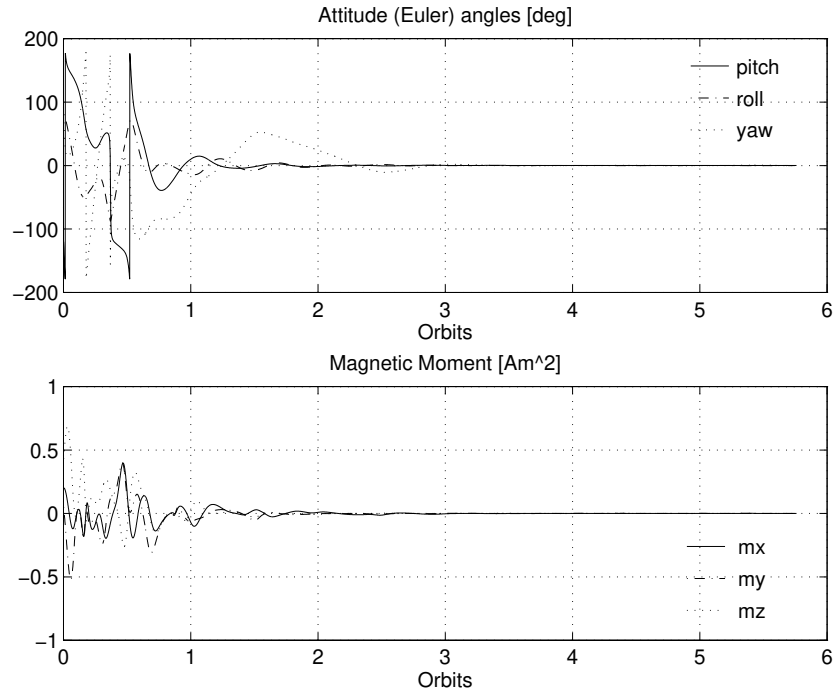
Figure 6.5: The simulation test corresponds to Fig. 6.4. The attitude is represented by the Euler angles. Already after 2 orbits pitch, roll and yaw are within $10\ deg$. Plot of magnetic moment refers to power utilization of the sliding mode attitude controller.

titude is represented by pitch, roll, and yaw angles in Fig. 6.5. The initial value of pitch is $60\ deg$, roll is 100 deg, and yaw is $\Leftrightarrow 100\ deg$. Initial angular velocity ${}^c\mathbf{\Omega}_{co}$ is $[\Leftrightarrow 0.002\ 0.002\ 0.002]^T\ \frac{rad}{sec}$. Already after 2 orbits pitch, roll and yaw are within $10\ deg$. The plot of the magnetic moment used for attitude correction depicted in Fig. 6.5 shows that the sliding mode attitude controller is power efficient.

Simulation of the Ørsted satellite motion in its elliptic orbit with the aerodynamic drag torque acting on the satellite structure is depicted in Fig. 6.6. The sliding mode attitude controller keeps the steady state attitude error within $\pm 3\ deg$.

6.7 Discussion of Results

The sliding control law for three axis stabilization of a tumbling satellite was described and analysed in this chapter. Both sliding manifold and continuous sliding condition
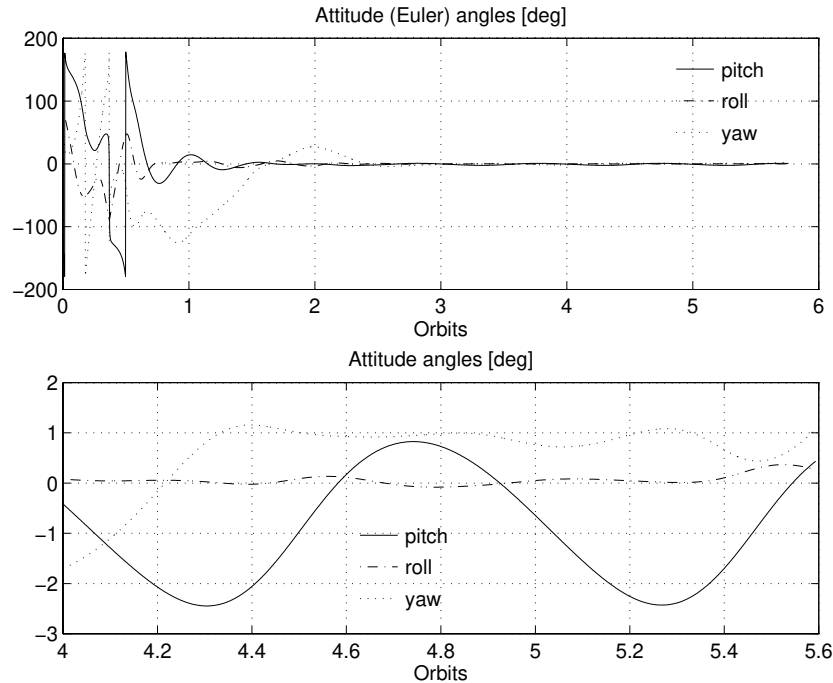
Figure 6.6: Performance of the sliding mode attitude controller in Eq. (6.46) for the Ørsted satellite on its elliptical orbit. Motion is influenced by the aerodynamic drag. The initial values of the attitude and the angular velocity are the same as in Fig. 6.5. The steady state attitude error is within $\pm 3\ deg$.

were designed. The properties of the moments of inertia of a satellite body, when a gravity gradient boom is stowed, were used to provide the final control law. The controller was evaluated by simulations for the Ørsted satellite in realistic space environment. The controller shows to be applicable for satellites with pointing accuracy larger than $3\ deg$. The controller is seen in the Monte Carlo simulation to be globally stable, however only approximate stability study was given.

There is still an unsolved issue, stabilization of the satellite after boom deployment for initial values of the attitude such that the boom is pointing upside-down. The sliding mode controller does not provide satisfactory results, since large influence of the gravity gradient in the boom deployed configuration heavily perturbs the satellite motion from the sliding manifold, and the magnetic control torque is not capable to compensate for this disturbances. A globally stabilizing controller based on an energetic approach for the satellite in this configuration is investigated in the next chapter.

Chapter 7

Three Axis Attitude Control: Energy Approach

An attitude with the boom pointing upside-down in the science observation phase is likely. This could be caused by a considerable impact of the aerodynamic torque on the satellite body or an unexpected behaviour during the boom deployment phase. A globally stable attitude controller is therefore necessary. The development of nonlinear strategies for the satellite attitude control is addressed in this chapter.

Complete comprehension of the nature of the satellite control problem requires a new approach merging the control theory with physics of the rigid body motion and an extension of the earlier results in these fields using findings from the theory of periodic systems. The Lyapunov stability theory is employed, and a Lyapunov function based on the potential and kinetic energy of the satellite motion is formulated. Section 7.1 considers attitude stabilization at large, introduces a velocity controller applying a vector product between the angular velocity and the local geomagnetic field. The velocity controller contributes to dissipation of both kinetic and potential energy. It provides four stable equilibria of the system, one of which is the reference. It is shown how the equilibria depend on the ratio of the satellite moments of inertia. The resultant controller is shown to be only locally asymptotically stable. The reason not to achieve global three axis stabilization is found to be the lack of attitude information in the control law. The extension with attitude information is made in Section 7.2. The energy necessary to change the satellite attitude between the equilibria is calculated in Section 7.3. Section 7.4 provides the desired stability properties and presents a family of controllers which can achieve three axis attitude stabilization using only magnetorquers. Simulations are shown to confirmed the performance of the proposed controllers to be very satisfactory and applicable in two mission phases: the velocity controller in a tumbling phase of the satellite, and three axis attitude stabilization in the normal science observation phase. These results are presented

in Section 7.7.

The energy based approach to magnetic attitude control covered in this section is based on Wisniewski and Blanke (1996*b*) and Wisniewski and Blanke (1996*c*).

7.1   Attitude Stability at Large

A magnetic generated mechanical torque is always perpendicular to the geomagnetic field vector as seen from Eq. (2.15). The consequence is that the satellite is only controllable in two directions at any single point in time. With the geomagnetic field varying along an orbit this implies, e.g. that in the Earth's polar regions the yaw angle is uncontrollable, whereas it can be controlled again when the satellite is in the equatorial regions. Since the control torque is always perpendicular to the geomagnetic field vector, it is desirable that the magnetic moment is also perpendicular to the geomagnetic field vector, as only this component produces a non-zero control torque, Section 4.1.

It is concluded that magnetic control moment must include information about the angular velocity of the satellite, and also about time propagation of the geomagnetic field. A candidate for generation of the magnetic moment is an angular velocity feedback

$$ {}^c\mathbf{m}(t) = h\, {}^c\mathbf{\Omega}_{co}(t) \times {}^c\mathbf{B}(t), \tag{7.1} $$

where h is a positive constant.

There are two main reasons to suggest this feedback:

1. It contributes to dissipation of kinetic energy of the satellite.

2. It provides four stable equilibria depicted in Fig. 7.1. The equilibria are such that the z axis of the Control CS (the axis of the minimal moment of inertia) points in the direction of the z axis of the Orbit CS, and the unit vector of the x axis of the Control CS (the axis of the largest moment of inertia) is parallel to the x axis of the Orbit CS. One of these equilibria is the desired reference.

These claims will be proved below.

The magnetic torquing obviously introduces time dependency in the equations of the satellite motion. This time variation has periodic nature, see Fig. 2.4. Therefore, the theory of nonlinear periodic systems introduced in Section 5.3 can also be applied in this chapter.

Global stability of the control law (7.1) can be expressed in the following theorem.

Theorem 7.1.1 *Consider the control law*

$$ {}^c\mathbf{m}(t) = h\, {}^c\mathbf{\Omega}_{co}(t) \times {}^c\mathbf{B}(t), $$
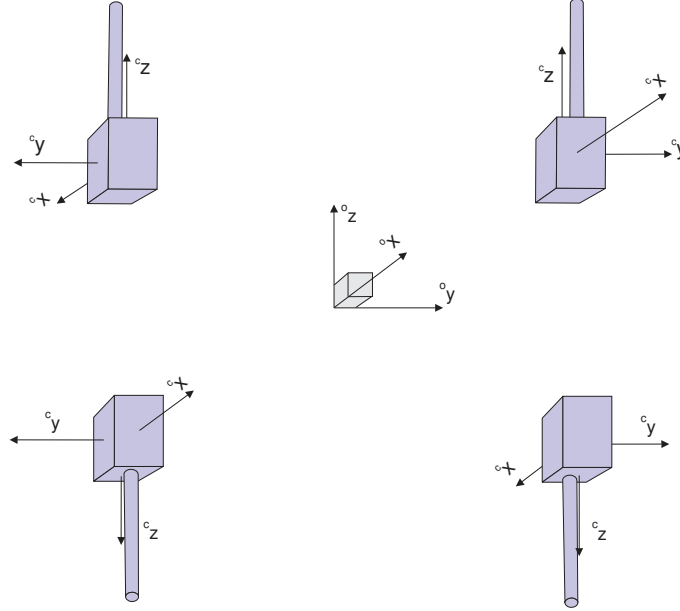
Figure 7.1: Four locally stable equilibria of the angular velocity feedback (7.1)

then the satellite, Eqs. (2.12) to (2.20) has 4 asymptotically stable local equilibria

$$\{({}^c\mathbf{\Omega}_{co}, {}^c\mathbf{k}_o, {}^c\mathbf{i}_o) : (\mathbf{0}, \pm{}^o\mathbf{k}_o, \pm{}^o\mathbf{i}_o)\}. \tag{7.2}$$

Proof of Theorem 7.1.1 Consider a Lyapunov candidate function expressing the total energy of the satellite. The total energy derived in Section 2.4 is the sum of kinetic energy of rotary motion, potential energy generated by the gravity gradient and the energy originating from revolution of the satellite around the Earth

$$E_{tot} = E_{kin} + E_{gg} + E_{gyro}.$$

This leads to

$$E_{tot} = \frac{1}{2}{}^c\mathbf{\Omega}_{co}^T\mathbf{I}^c\mathbf{\Omega}_{co} + \frac{3}{2}\omega_o^2({}^c\mathbf{k}_o^T\mathbf{I}^c\mathbf{k}_o \Leftrightarrow I_z) + \frac{1}{2}\omega_o^2(I_x \Leftrightarrow {}^c\mathbf{i}_o^T\mathbf{I}^c\mathbf{i}_o). \tag{7.3}$$

Recall that I_x is the satellite maximal moment of inertia, and I_z is the minimal one, thus positive definiteness of the Lyapunov function is fulfilled.

The time derivative of E_{tot} will be shown to be negative semidefinite

$$\dot{E}_{tot} = {}^c\mathbf{\Omega}_{co}^T\mathbf{I}^c\dot{\mathbf{\Omega}}_{co} + 3\omega_o^2{}^c\mathbf{k}_o^T\mathbf{I}^c\dot{\mathbf{k}}_o + \omega_o^2{}^c\mathbf{i}_o^T\mathbf{I}^c\dot{\mathbf{i}}_o. \tag{7.4}$$

Eqs. (2.12) to (2.20) are substituted into Eq. (7.4) yielding

$$
\begin{aligned}
\dot{E}_{tot} \quad = \quad & {}^c\boldsymbol{\Omega}_{co}^T(\Leftrightarrow{}^c\boldsymbol{\Omega}_{cw} \times \mathbf{I}{}^c\boldsymbol{\Omega}_{cw} + 3\omega_o^2\,{}^c\mathbf{k}_o^T \times \mathbf{I}{}^c\mathbf{k}_o + {}^c\mathbf{N}_{ctrl}) \Leftrightarrow \\
& \omega_o\,{}^c\boldsymbol{\Omega}_{co}^T\mathbf{I}({}^c\mathbf{i}_o \times {}^c\boldsymbol{\Omega}_{co}) + 3\omega_o^2\,{}^c\mathbf{k}_o^T\mathbf{I}({}^c\mathbf{k}_o \times {}^c\boldsymbol{\Omega}_{co}) \Leftrightarrow \\
& \omega_o^2\,{}^c\mathbf{i}_o^T\mathbf{I}({}^c\mathbf{i}_o \times {}^c\boldsymbol{\Omega}_{co}).
\end{aligned}
\tag{7.5}
$$

Recognize that from Eq. (2.20) the following equality holds

$$
{}^c\boldsymbol{\Omega}_{co}^T({}^c\boldsymbol{\Omega}_{cw} \times \mathbf{I}{}^c\boldsymbol{\Omega}_{cw}) = \omega_o\,{}^c\boldsymbol{\Omega}_{co}^T({}^c\mathbf{i}_o \times \mathbf{I}{}^c\boldsymbol{\Omega}_{co}) + \omega_o^2\,{}^c\boldsymbol{\Omega}_{co}^T({}^c\mathbf{i}_o \times \mathbf{I}{}^c\mathbf{i}_o),
\tag{7.6}
$$

hence Eq. (7.5) is reduced to a simple expression

$$
\dot{E}_{tot} = {}^c\boldsymbol{\Omega}_{co}^T\,{}^c\mathbf{N}_{ctrl}.
\tag{7.7}
$$

If the proposed control law (7.1) is applied then Eq. (7.7) becomes

$$
\dot{E}_{tot} = \Leftrightarrow h({}^c\mathbf{B} \times {}^c\boldsymbol{\Omega}_{co})^T({}^c\mathbf{B} \times {}^c\boldsymbol{\Omega}_{co}),
\tag{7.8}
$$

or

$$
\dot{E}_{tot} = \Leftrightarrow h\,{}^c\boldsymbol{\Omega}_{co}^T\tilde{\mathbf{B}}^T\tilde{\mathbf{B}}{}^c\boldsymbol{\Omega}_{co}.
\tag{7.9}
$$

Here $\tilde{\mathbf{B}}$ is the skew symmetric matrix representing a cross product operator: ${}^c\mathbf{B}\times$. The matrix $\tilde{\mathbf{B}}^T\tilde{\mathbf{B}}$ is positive semidefinite and h was a positive constant. The derivative of the total energy is thus negative semidefinite.

The Krasovskii-LaSalle theorem is applicable in this proof since the control law (7.1) is periodic. The set U in Theorem 5.3.2 contains such elements ${}^c\boldsymbol{\Omega}_{co}$, ${}^c_o\mathbf{q}$ that ${}^c\boldsymbol{\Omega}_{co}$ and ${}^c\mathbf{B}$ are parallel (${}^c\mathbf{B} \times {}^c\boldsymbol{\Omega}_{co} = \mathbf{0}$)

$$
U = \{{}^c\boldsymbol{\Omega}_{co}, {}^c_o\mathbf{q} : \exists t > 0\ {}^c\mathbf{B} \text{ parallel to } {}^c\boldsymbol{\Omega}_{co}\}.
\tag{7.10}
$$

It will be proved by contradiction that the set U is not an invariant set.

Assume that the vector ${}^c\mathbf{B}(t)$ was parallel to ${}^c\boldsymbol{\Omega}_{co}(t)$ for each $t > t_0$. This could be described by

$$
\forall t > t_0 \geq 0,\ {}^c\mathbf{B}(t) = \alpha\,{}^c\boldsymbol{\Omega}_{co}(t),\ \alpha \neq 0.
\tag{7.11}
$$

Expressing Eq. (7.11) in the Orbit CS gives

$$
\forall t > t_0 \geq 0,\ {}^o\mathbf{B}(t) = \alpha\mathbf{A}^T({}^c_o\mathbf{q}){}^c\boldsymbol{\Omega}_{co}(t).
\tag{7.12}
$$

Recognize the magnetic moment and hence the control torque are equal zero since

$$
{}^c\mathbf{m} = h\,{}^c\boldsymbol{\Omega}_{co} \times {}^c\mathbf{B} = h\alpha\,{}^c\boldsymbol{\Omega}_{co} \times {}^c\boldsymbol{\Omega}_{co} = \mathbf{0}.
\tag{7.13}
$$

The angular velocity, $^c\mathbf{\Omega}_{co}$, is given by the dynamic equations (2.12), (2.15), and (2.20) for $^c\mathbf{N}_{ctrl} = \mathbf{0}$. The geomagnetic field determines the vector $^o\mathbf{B}$. Its time propagation in the Orbit CS is depicted in Fig. 2.4. The geomagnetic field is only dependent on the satellite position in orbit, whereas the angular velocity $^c\mathbf{\Omega}_{co}$ depends on the state $[^c\mathbf{\Omega}_{co}^T\; _o^c\mathbf{q}^T]^T$, and is completely independent on the orbital position. Hence, $^c\mathbf{B}$ and $^c\mathbf{\Omega}_{co}$ cannot be parallel all the time, and Eq. (7.11) is not valid. This shows the contradiction.

Therefore, the largest invariant set contained in U is the trajectory $^c\mathbf{\Omega}_{co} \equiv \mathbf{0}$. The angular velocity is zero for all $t \geq 0$ if the trajectory is in an equilibrium. Finally, it is concluded that the equilibria $\{(^c\mathbf{\Omega}_{co}, {}^c\mathbf{k}_o, {}^c\mathbf{i}_0) : (\mathbf{0}, \pm^o\mathbf{k}_o, \pm^o\mathbf{i}_o)\}$ are locally uniformly asymptotically stable. ∎

Remark 7.1.1 *If h was changed in Eq. (7.1) from a positive scalar to a positive definite matrix $\mathbf{h}$, then the time derivative of the Lyapunov candidate function would be*

$$\dot{E}_{tot} = \Leftrightarrow^c\mathbf{\Omega}_{co}^T\mathbf{h}^T\tilde{\mathbf{B}}^T\tilde{\mathbf{B}}^c\mathbf{\Omega}_{co}. \tag{7.14}$$

Due to the operation: positive definite matrix times positive semidefinite matrix does not necessary give a semipositive definite matrix, it follows that the velocity feedback can only use scalar gain in order to prove asymptotic stability.

Remark 7.1.2 *The control law (7.1) can be used for three axis magnetic stabilization of the satellite in a neighbourhood of one of 4 equilibria stated in Theorem 7.1.1, thus also in the neighbourhood of the reference, if $I_x > I_y > I_z$.*

Remark 7.1.3 *The differential equations describing the satellite motion actuated according to Eq. (7.1) are uniformly continuous, therefore a small perturbation of the control law in a form of the attitude quaternion feedback provides a locally asymptotically stable control action.*

Remark 7.1.4 *If the velocity controller (7.1) is applied for a limited time interval during an orbit, then the solution trajectory of the satellite motion still converges to one of four equilibria in Theorem 7.1.1, since the total energy from Eq. (7.7) is constant if the control torque is zero, and is dissipated when the controller is active.*

This control strategy is very useful if the attitude control can only take place via telecommand from a ground station, and time of radio contact is limited. The controller is also beneficial for a satellite with an attitude determination algorithm based on a sun sensor, since the attitude information may not be available when the satellite is in the eclipse. In both cases the controller (7.1) is activated when the feedback signals are available and switched off otherwise. This control law is still stable.

It was proved that the satellite with the control law (7.1) is asymptotically stable around four equilibria (7.2). The objective of the next sections is to design a controller that makes

all equilibria but the reference unstable. The desired reference considered in the sequel is

$$\{({}^{c}\mathbf{\Omega}_{co},\ {}^{c}\mathbf{k}_{o},\ {}^{c}\mathbf{i}_{o}) : (\mathbf{0},\ {}^{o}\mathbf{k}_{o},\ {}^{o}\mathbf{i}_{o})\}. \tag{7.15}$$

7.2 Local Attitude Stability

The operational mission phase of the Ørsted satellite is such that the boom is upright, i.e. the boom tip is above the horizon. The attitude controller designed for this mission phase shall be stable towards the reference (7.15) for all initial attitude such that the boom tip is above the horizon. This is done by inserting perturbations of the attitude in the control law (7.1). This is feasible since the maximum of the potential energy E_{gyro} in Eq. (7.3) is three times smaller than the maximum potential energy due to the gravity gradient. Hence, a shift from the equilibria $\{({}^{c}\mathbf{\Omega}_{co},\ {}^{c}\mathbf{k}_{o},\ {}^{c}\mathbf{i}_{o}) : (\mathbf{0},\ \pm^{o}\mathbf{k}_{o},\ \Leftrightarrow^{o}\mathbf{i}_{o})\}$ to $(\mathbf{0},\ \pm^{o}\mathbf{k}_{o},\ {}^{o}\mathbf{i}_{o})$ requires less energy than a jump from $(\mathbf{0},\ \Leftrightarrow^{o}\mathbf{k}_{o},\ \pm^{o}\mathbf{i}_{o})$ to $(\mathbf{0},\ {}^{o}\mathbf{k}_{o},\ \pm^{o}\mathbf{i}_{o})$. A scrutiny of the necessary energy to be generated by a controller in order to change between the equilibria, is provided in the next section.

The three axis attitude stabilization can be accomplished when some attitude information is added into the velocity control law. A proposed control law is

$$^{c}\mathbf{m}(t) = h^{c}\mathbf{\Omega}_{co}(t) \times {}^{c}\mathbf{B}(t) \Leftrightarrow \epsilon \mathbf{q}(t) \times {}^{c}\mathbf{B}(t), \tag{7.16}$$

where h and ϵ are positive constants. The properties of the control law (7.16) will be analyzed using linear control theory.

In equation (7.16) a small perturbation of the vector part of the attitude quaternion is added comparing with the control law (7.1). For small ϵ the satellite is stable in the neighbourhood of the reference $\{({}^{c}\mathbf{\Omega}_{co},\ {}^{c}\mathbf{k}_{o},\ {}^{c}\mathbf{i}_{o}) : (\mathbf{0},\ {}^{o}\mathbf{k}_{o},\ {}^{o}\mathbf{i}_{o})\}$, since the differential equations describing motion of the satellite are well posed. At this point of the analysis the gain h has been fixed. The next step of the design is to compute the gain ϵ for a given h such that the system is still locally stable and the domain of local stability is extended.

The system is first linearized. The satellite motion is considered in a neighbourhood of the following reference: the angular velocity of the satellite rotation w.r.t. the Orbit CS is zero (${}^{c}\mathbf{\Omega}_{co} = \mathbf{0}$), and the attitude is such that the Control CS coincides with the Orbit CS (${}^{c}_{o}\mathbf{q} = [0\ 0\ 0\ 1]^{T}$), Section 2.6.

The linearized equations of motion (2.12) to (2.20) using Eq. (7.16) as control law are

$$\frac{d}{dt}\left[\begin{array}{c} \delta\mathbf{\Omega} \\ \delta\mathbf{q} \end{array}\right] = \mathbf{A}\left[\begin{array}{c} \delta\mathbf{\Omega} \\ \delta\mathbf{q} \end{array}\right] + \mathbf{B}(t)(h\delta\mathbf{\Omega} + \epsilon\delta\mathbf{q}), \tag{7.17}$$

where the system and control matrices, $\mathbf{A}$ and $\mathbf{B}(t)$, respectively, are given in Eq. (4.3).

Since the geomagnetic field is periodic, see Fig. 2.4, local stability of the satellite is analyzed with use of Floquet theory, Section 3.1.

Consider the following form of Eq. (7.17)

$$\frac{d\mathbf{x}}{dt} = \hat{\mathbf{A}}(\epsilon, t)\mathbf{x}, \tag{7.18}$$

where

$$\hat{\mathbf{A}}(\epsilon, t) = \mathbf{A} + \mathbf{B}(t)[h\mathbf{E}_{3\times 3} \; \epsilon\mathbf{E}_{3\times 3}],$$

$\mathbf{E}_{3\times 3}$ is the 3×3 identity matrix, h is considered to be a constant value, whereas ϵ is a parameter. Furthermore, $\hat{\mathbf{A}}(\epsilon, t) = \hat{\mathbf{A}}(\epsilon, t + T)$, for $T = \frac{2\pi}{\omega_o}$.

It was a result from the Floquet theory in Section 3.1 that the system (7.18) is asymptotically stable if all characteristic multipliers, i.e. the eigenvalues of the monodromy matrix $\Psi_{\hat{A}}(t_0, \epsilon)$ for a certain value of ϵ

$$det[\mathbf{I}\lambda \Leftrightarrow \Psi(t_0, \epsilon)] = 0 \tag{7.19}$$

satisfy the following inequality

$$|\lambda_i(\epsilon)| < 1, \; i = 1, ..., n. \tag{7.20}$$

Now, all ϵ are found for which the linearized satellite system (7.17), with a certain fixed value of the positive scalar h, is stable by plotting a locus for the characteristic multipliers as a function of ϵ. An example is shown in Fig. 7.2. The value of the velocity gain, h, was chosen equal $1 \cdot 10^8 \frac{Ams}{T}$. Then the locus of the characteristic multiplier, $\epsilon \in [0, \; 7 \cdot 10^5] \frac{Am^2}{T}$ was plotted. The gain $\tilde{\epsilon} = 5 \cdot 10^5 \frac{Am^2}{T}$ is the limit of stability. Hence, a certain $\hat{\epsilon}$ may be chosen for which the satellite motion is guaranteed to be asymptotically stable about the reference. Notice that $\hat{\epsilon}$ must satisfy the inequality $\hat{\epsilon} < \tilde{\epsilon}$. For $\epsilon = 0$ the controller (7.16) is equivalent to the velocity controller, which is also seen to be stable.

7.2.1   Simulation Results

A Monte Carlo simulation was made to investigate stability towards the reference (7.15). The initial state is random with the nominal condition as mean. The envelope for the Monte Carlo simulation includes all values of the attitude above the horizon, i.e. $^ck_{oz} > 0$ and $\Omega_{co} = \mathbf{0}$. The attitude controller implemented has velocity gain, $h = 1 \cdot 10^8 \frac{Ams}{T}$, and the quaternion gain, $\epsilon = 3 \cdot 10^5 \frac{Am^2}{T}$.

One example is the simulation in Fig. 7.3 which is started at the equilibrium $\{(^c\mathbf{\Omega}_{co}, \; ^c\mathbf{k}_o, \; ^c\mathbf{i}_o) : (\mathbf{0}, \; ^o\mathbf{k}_o, \; \Leftrightarrow^o\mathbf{i}_o)\}$. Already after one orbit the trajectory is within the margin of $10 \; deg$ from the reference. This is far better than required. Additional attitude information in the controller made the equilibrium $\{(\mathbf{0}, \; ^o\mathbf{k}_o, \; \Leftrightarrow^o \mathbf{i}_o)\}$ unstable,
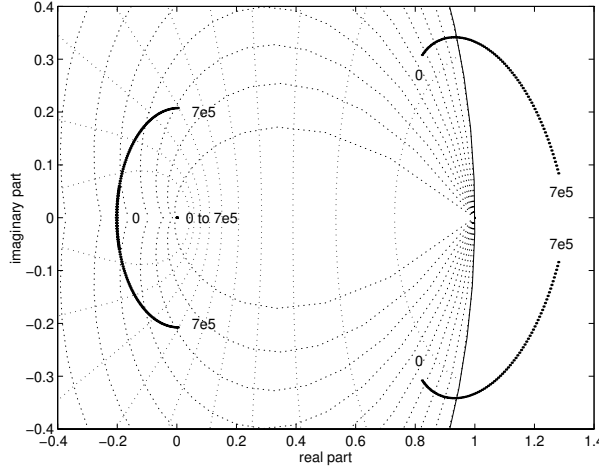
Figure 7.2: The locus for the characteristic multiplier $\lambda(\epsilon)$ for $\epsilon \in [0, 7 \cdot 10^5] \frac{Am^2}{T}$, $h = 1 \cdot 10^8 \frac{Ams}{T}$ using Eq. (7.16) as control law.

and thus extending the region of convergence to all initial values of the attitude such that the boom is above the horizon and the initial satellite angular velocity in the Orbit CS is zero.

7.3 Energy Dissipation Control

It was proved that the satellite with the control law (7.1) is asymptotically stable around four equilibria (7.2). The objective of this section is to design a globally stable controller that makes all other equilibria but the reference (7.15) unstable.

Two control principles are analysed in this section: an angular velocity feedback and a rate/attitude control. The first one is similar to that of Eq. (7.1), the latter resembles the feedback (7.16), except it is only activated in a defined area in state space around the reference point.

Consider first the following preliminary control concept.

Procedure 7.1

1. *Divide the state space into C_i, $i = 1, 2, 3, 4$ four regions of convergence to the equilibria (7.2) of the control law (7.1),*

2. *Let the angular velocity controller (7.1) (or alternatively rate/attitude controller (7.16)) be activated only in the region C_1, which is the subset of the state space*
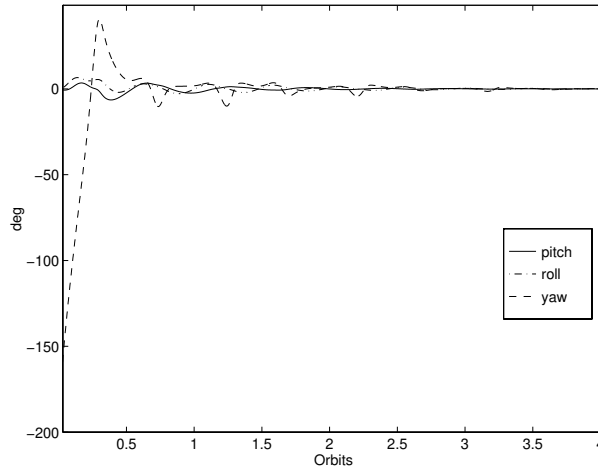
Figure 7.3: The satellite trajectory converges from the equilibrium $\{(^c\mathbf{\Omega}_{co},\ ^c\mathbf{k}_o,\ ^c\mathbf{i}_o)\ :\ (\mathbf{0},\ ^o\mathbf{k}_o,\ \Leftrightarrow^o\mathbf{i}_o)\}$ to the reference.

containing the reference (7.15).

If the trajectory is in the region C_1 the entire energy of the satellite is dissipated. Otherwise it is maintained at the same level. Therefore, it is anticipated that if the trajectory is once in the region C_1 the entire energy of the satellite angular motion will be decreased to zero. It will be shown in this section that this control procedure is stable to the reference.

The region of convergence about the reference (7.15) is determined from potential energy, since it comprises a measure of the distance from the actual state to an equilibrium.

Potential energy according to Section 2.4 consists of energy due to gravity gradient and energy originated from the revolution of the satellite about the Earth. In order to reach overall comprehension of the system behaviour these two types of potential energy are considered separately in Subsections 7.3.1 and 7.3.2. Total energy is investigated in Subsection 7.3.3. Last, but not least a control strategy for dissipation of the entire energy of a LEO satellite will be investigated in Subsection 7.3.4.

7.3.1 Potential Energy due to Gravity Gradient

Consider the following geometrical interpretation. Potential energy due to the gravity gradient, E_{gg}, varies from 0 to $\frac{3}{2}\omega_o^2(I_x \Leftrightarrow I_z)$. It is minimum when the z axis of the Control CS is parallel to the z axis of the Orbit CS. The maximum value is reached when the z axis of the Control CS is in the horizontal plane (perpendicular to the z axis of the Orbit CS). The baseline of this analysis is that E_{gg} is the only component of potential
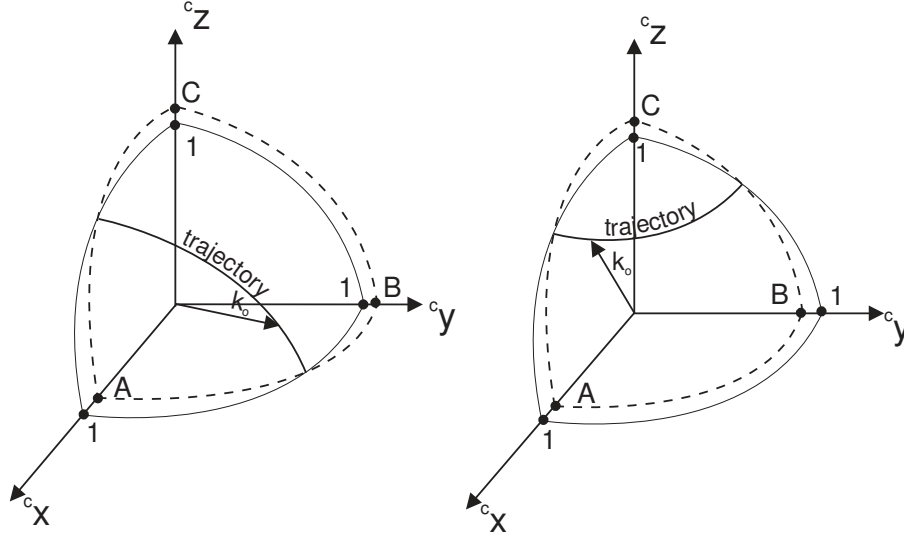
Figure 7.4: Points A, B, C are $\frac{1}{I_x}(\frac{2}{3}\frac{\bar{E}}{\omega_o^2} + I_z)$, $\frac{1}{I_y}(\frac{2}{3}\frac{\bar{E}}{\omega_o^2} + I_z)$, $\frac{1}{I_z}(\frac{2}{3}\frac{\bar{E}}{\omega_o^2} + I_z)$, respectively. The unit vector ${}^c\mathbf{k}_o$ evolves on the intersection of the sphere (7.23) and the ellipsoid (7.22). At the energy level $\tilde{E} \geq \frac{3}{2}\omega_o^2(I_y \Leftrightarrow I_z)$ the intersection ellipse is of the type illustrated in the l.h.s. drawing. The r.h.s. drawing illustrates the intersection ellipse at energy level $\tilde{E} \leq \frac{3}{2}\omega_o^2(I_y \Leftrightarrow I_z)$.

energy, which is relaxed in Subsection 7.3.3.

Consider a certain constant value of potential energy, $\tilde{E}$. From the expression for potential energy of the gravity gradient

$$\tilde{E} = \frac{3}{2}\omega_o^2({}^c\mathbf{k}_o^T\mathbf{I}^c\mathbf{k}_o \Leftrightarrow I_z), \qquad (7.21)$$

the unit vector ${}^c\mathbf{k}_o$ will satisfy two equations: an equation of an ellipsoid

$$^c\mathbf{k}_o\mathbf{I}^c\mathbf{k}_o = \frac{2\tilde{E}}{3\omega_o^2} + I_z, \qquad (7.22)$$

and an equation of a sphere

$$\|^c \mathbf{k}_o \| = 1. \qquad (7.23)$$

The unit vector ${}^c\mathbf{k}_o$ evolves on the intersection of the sphere with the ellipsoid Fig. 7.4. The Orbit CS's z axis in the Control CS may initially evolve on the intersection ellipse of the type depicted on the l.h.s. of Fig. 7.4. If the total energy of the satellite is dissipated

then the potential energy due to the gravity gradient is decreased. At the energy level $\tilde{E} \leq \frac{3}{2}\omega_o^2 (I_y \Leftrightarrow I_z)$ the intersection ellipse is of the type illustrated on the r.h.s. of Fig. 7.4. Notice that, if additionally kinetic and potential energy due to revolution of the satellite about the Earth are taken into account i.e.

$$\tilde{E} = E_{kin} + E_{gg} + E_{gyro} < \frac{3}{2}\omega_o^2(I_y \Leftrightarrow I_z),$$

then the z axis of the Orbit CS evolves always above the intersection ellipse on the r.h.s. of Fig. 7.4.

The projection of the unit vector ${}^c\mathbf{k}_o$ on the z axis of the Orbit CS, ${}^c k_{oz}$ provides the information whether the z axis of Control CS (the boom axis) is upright or upside-down. A proposed control law is to activate the controller (7.1) whenever ${}^c k_{oz} \geq 0$, then the satellite trajectory tends to one of two equilibria

$$\{({}^c\mathbf{\Omega}_{co},\ {}^c\mathbf{k}_o,\ {}^c\mathbf{i}_o) : (\mathbf{0},\ {}^o\mathbf{k}_o,\ \pm{}^c\mathbf{i}_o)\}, \tag{7.24}$$

both defining the attitude of the satellite with the boom axis upright.

This can be explained as follows. If the z axis of the Control CS is in the horizontal plane, perpendicular to $\mathbf{k}_o$, potential energy changes from $E_{gg}^y = \frac{3}{2}\omega_o^2(I_y \Leftrightarrow I_z)$, when the z axis of the Control CS coincides with the y axis of the Orbit CS, to $E_{gg}^x = \frac{3}{2}\omega_o^2(I_x \Leftrightarrow I_z)$, when the z axis of the Control CS is parallel to the x axis of the Orbit CS. If the total energy (in this subsection a sum of E_{kin} and E_{gg}) is above E_{gg}^x kinetic energy has a bias, due to which the satellite will tumble from the boom axis upside-down to upright. If the total energy is below E_{gg}^y, and the initial attitude is such that the z axis of the Control CS is upright, the solution trajectory will never cross the horizon, i.e. it will stay with the Control CS's z axis upright for ever.

There is still an unsolved issue for the energy level between E_{gg}^y and E_{gg}^x. The boom axis can stay upright or upside-down or even change between the attitude above and below the horizon. The difference $\Delta_{gg} = E_{gg}^x \Leftrightarrow E_{gg}^y$ is approximately 0 for $I_x \approx I_y$. Thus, the controller (7.1) activated whenever ${}^c k_{oz} \geq 0$ provides two locally stable equilibria (7.24) for the satellite with $I_x > I_y >> I_z$.

7.3.2 Energy due to Revolution of Satellite about Earth

Analogously, consider potential energy due to revolution of the satellite about the Earth. A constant value of this energy, $\hat{E}$ in the interval from 0 to the maximum value $E_{gyro}^z = \frac{1}{2}\omega_o^2(I_x \Leftrightarrow I_z)$, is investigated. The unit vector ${}^c\mathbf{i}_o$ evolves in Fig. 7.5 on the intersection of the sphere

$$\|{}^c\mathbf{i}_o\| = 1 \tag{7.25}$$
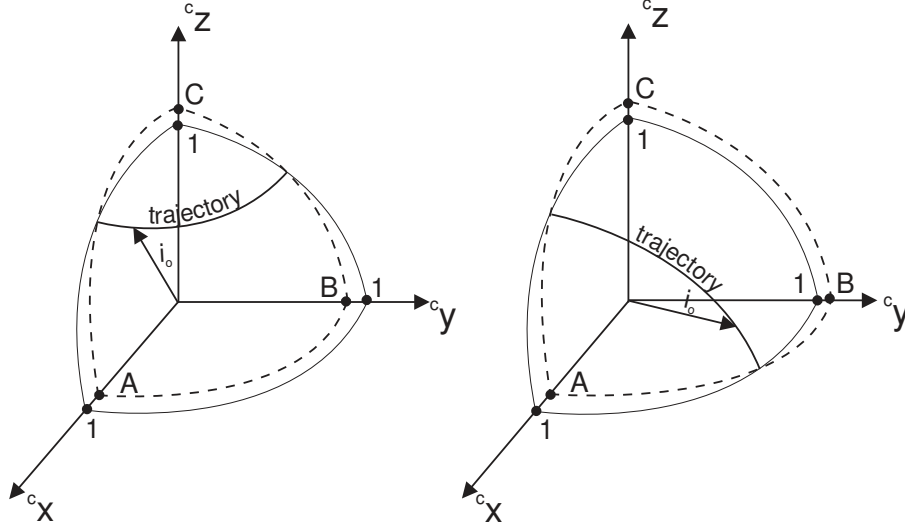
Figure 7.5: Points A, B, C are $\frac{1}{I_x}(I_x \Leftrightarrow 2\frac{\hat{E}}{\omega_o^2})$, $\frac{1}{I_y}(I_x \Leftrightarrow 2\frac{\hat{E}}{\omega_o^2})$, $\frac{1}{I_z}(I_x \Leftrightarrow 2\frac{\hat{E}}{\omega_o^2})$, respectively. The unit vector $^c\mathbf{i}_o$ evolves on the intersection of the sphere (7.25) and the ellipsoid (7.26). At the energy level $\hat{E} \geq \frac{1}{2}\omega_o^2(I_x \Leftrightarrow I_y)$ the intersection ellipse is of the type illustrated on the l.h.s. of the drawing. The drawing on r.h.s. illustrates the intersection ellipse at energy level $\hat{E} < \frac{1}{2}\omega_o^2(I_x \Leftrightarrow I_y)$.

with the ellipsoid

$$^c\mathbf{i}_o\mathbf{I}^c\mathbf{i}_o = I_x \Leftrightarrow \frac{2\hat{E}}{\omega_o^2}. \tag{7.26}$$

If potential energy is less than $E_{gyro}^y = \frac{1}{2}\omega_o^2(I_x \Leftrightarrow I_y)$, the x axis of the Orbit CS observed in the Control CS (or the unit vector $^c\mathbf{i}_o$) evolves on an ellipse illustrated on the l.h.s of Fig. 7.5. Otherwise, the motion of the unit vector $\mathbf{i}_o$ in the Control CS is on the ellipse on the r.h.s. of Fig. 7.5. If additionally kinetic and potential energy of the gravity gradient are taken into account i.e.

$$\tilde{E} = E_{kin} + E_{gg} + E_{gyro} < E_{gyro}^y$$

then the x axis of the Orbit CS evolves always above the intersection ellipse on the l.h.s. of Fig. 7.5.

7.3.3 Total Energy

If the total energy, E_{tot}, the sum of E_{gg}, E_{gyro} and E_{kin} is above the energy level $E_{gg}^x + E_{gyro}^z$ (the maximum potential energy required for the boom axis to cross the horizontal plane), then the kinetic energy has a nonzero bias, and the satellite will tumble, i.e. the boom axis will evolve between upright and upside-down attitude. Whereas, if the total energy is below E_{gg}^y (the minimum potential energy necessary to cross the horizontal plane), and the initial attitude is such that the boom axis is above the horizon, then it moves above the horizon for ever. The time propagation of the solution trajectory for the energy level between $E_{gg}^x + E_{gyro}^z$ and E_{gg}^y, where the energy gap Δ_{tot} is

$$\Delta_{tot} = E_{gg}^x + E_{gyro}^z \Leftrightarrow E_{gg}^y = 2\omega_o^2(I_x \Leftrightarrow I_z) \Leftrightarrow \frac{3}{2}\omega_o^2(I_y \Leftrightarrow I_z),$$
(7.27)

remains undetermined. The control algorithm proposed in the next subsection takes this gap into account.

7.3.4 Energy Dissipation Controller

The objective of this section is to formulate a control law making the reference asymptotically stable for initial kinetic energy above level $E_{gg}^x + E_{gyro}^z$. This control law can be used for a tumbling satellite and constitutes an intermediate solution towards a globally stable controller investigated in the next section.

The angular velocity feedback (7.1) activated for $^ck_{oz} > 0$ provides two locally stable equilibria (7.24). The reason for this is a lack of the attitude information in the control law. A recipe is to add a small perturbation of the attitude to the velocity control. This technique was already discussed in Section 7.2, and it was concluded that the attitude controller in Eq. (7.16) is asymptotically stable for all initial values of the attitude such that the boom axis is upright. Based on these results, a proposed control algorithm for dissipation of the entire energy, i.e. $E_{kin} + E_{gg} + E_{gyro}$, is

Procedure 7.2
- *Activate the rate/attitude controller in Eq. (7.16) when the satellite attitude is in C, where*

$$C = \{\mathbf{\Omega}_{co}, {}_o^c\mathbf{q} : {}^ck_{oz} > 0\}.$$
(7.28)

- *Otherwise send zero magnetic moment (${}^c\mathbf{m} = \mathbf{0}$).*

The essence of Procedure 7.2 is to make the satellite convergent towards the reference if the boom is above the horizon, and keep the total energy constant if the boom is below

it. Monte Carlo simulation tests show that the reference is asymptotically stable for the initial kinetic energy above $E_{gg}^x + E_{gyro}^z$, indeed. This control principle has performed very satisfactory in the simulation study, though there still exists an uncertainty. The solution trajectory of the satellite at the energy level between E_{gg}^y and $E_{gg}^x + E_{gyro}^z$ has not been found. A modified control law taking this uncertainty into account is

Procedure 7.3

- *If $E_{tot} > E_{gg}^x + E_{gyro}^z$ activate the angular velocity controller (7.1).*

- *Else wait until $^c k_{oz}$ changes the sign from negative to positive, then activate the rate/attitude control (7.16) for $^c k_{oz} > 0$.*

The first stage of Procedure 7.3 is to diminish the total energy using the angular velocity feedback (7.1) to the level $E_{gg}^x + E_{gyro}^z$, then wait with the attitude controller disactivated until the boom axis crosses the horizon plane from upside-down to upright. At this moment the rate/attitude controller (7.16) takes over. The controller needs only to dissipate a small amount of energy Δ_{tot} in order to keep the boom axis above the horizon for ever. Hence, the solution trajectory converges asymptotically to the reference.

The simulation study presented in the next subsection has shown that from a practical point of view both Procedures 7.2 and 7.3 can be implemented for control of a tumbling satellite to the desired reference $\{(^c\mathbf{\Omega}_{co}, {}^c\mathbf{k}_o, {}^c\mathbf{i}_0) : (\mathbf{0}, {}^o\mathbf{k}_o, {}^o\mathbf{i}_o)\}$.

The last but not least control issue is to turn the boom axis from the upside-down to upright attitude, which is investigated in Section 7.4.

7.3.5 Simulation Results

The controllers for energy dissipation were validated in a detailed simulation study. An example of a test is depicted in Figs. 7.6 to 7.9. The initial angular velocity in the example is $^c\mathbf{\Omega}_{co} = [0.005\,0.003 \Leftrightarrow 0.003]^T\,\frac{rad}{s}$, pitch, yaw and roll are $40\,deg$, $\Leftrightarrow 40\,deg$, and $80\,deg$, respectively. The velocity gain applied in the simulation study is $h = 1 \cdot 10^8\,\frac{Ams}{T}$. The velocity controller in Fig. 7.6 is active all the time, and the satellite trajectory converges to the equilibrium $\{(^c\mathbf{\Omega}_{co}, {}^c\mathbf{k}_o, {}^c\mathbf{i}_0) : (\mathbf{0}, \Leftrightarrow^o\mathbf{k}_o, \Leftrightarrow^o\mathbf{i}_o)\}$. The angular velocity controller in Fig. 7.7 is only active until the total energy is below $E_{gg}^x + E_{gyro}^z$. The satellite at this energy level is still tumbling. Performance of Procedures 7.2 and 7.3 is depicted in Figs. 7.8 and 7.9. The rate/attitude controller implemented in these procedures has velocity gain, $h = 1 \cdot 10^8 \frac{Ams}{T}$, and the quaternion gain, $\epsilon = 3 \cdot 10^5 \frac{Am^2}{T}$. These gains are equivalent to a proportional band in the angular velocity of $4.4 \cdot 10^{-3} \frac{rad}{s}$ and 1.48 in the attitude quaternion with a maximum control value of $20\,Am^2$ and an average amplitude of the geomagnetic field vector of $4.5 \cdot 10^{-5}\,T$. The rate/attitude controller in Fig. 7.8 is disactivated whenever $^c k_{oz} < 0$. In Fig. 7.9, the rate controller is applied first, then the the rate/attitude controller takes over. The satellite trajectory in
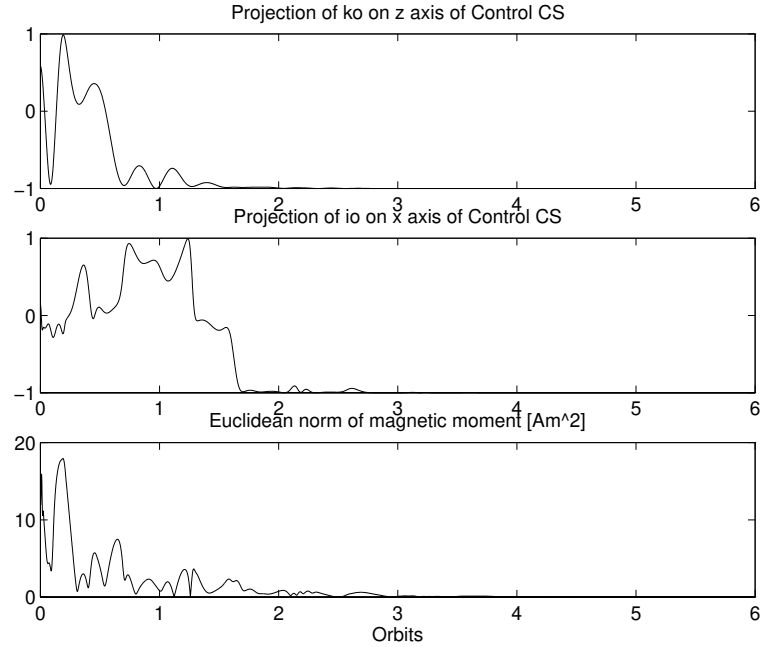
Figure 7.6: Simulation using the angular velocity controller. The controller is active all the time. ${}^{c}k_{oz}$ characterizes convergence of ${}^{c}\mathbf{k}_{o}$ towards ${}^{o}\mathbf{k}_{o}$, whereas ${}^{c}i_{ox}$ characterizes convergence of ${}^{c}\mathbf{i}_{o}$ to ${}^{c}\mathbf{i}_{o}$. The satellite trajectory converges towards the equilibrium $\{({}^{c}\boldsymbol{\Omega}_{co}, {}^{c}\mathbf{k}_{o}, {}^{c}\mathbf{i}_{0}) : (\mathbf{0}, \Leftrightarrow{}^{o}\mathbf{k}_{o}, \Leftrightarrow{}^{o}\mathbf{i}_{o})\}$, since ${}^{c}k_{oz}$ and ${}^{c}i_{ox}$ converge to $\Leftrightarrow$1.

both examples converges to the reference ${}^{c}k_{oz} = 1$ and ${}^{c}i_{ox} = 1$, which corresponds to $\{({}^{c}\boldsymbol{\Omega}_{co}, {}^{c}\mathbf{k}_{o}, {}^{c}\mathbf{i}_{0}) : (\mathbf{0}, {}^{o}\mathbf{k}_{o}, {}^{o}\mathbf{i}_{o})\}$.

7.4 Globally Stabilizing Controller

The control law in Procedure 7.3 was shown to be locally stable in the sense that if the boom axis is upside-down and the total energy is below $E_{gg}^{x} + E_{gyro}^{z}$ (more precisely below E_{gg}^{y}) there are no means to turn the boom axis upright. A globally stable controller, turning the boom axis from the upside-down to upright attitude, is the ultimate goal. The main obstacle is again the cross product with the geomagnetic field vector.
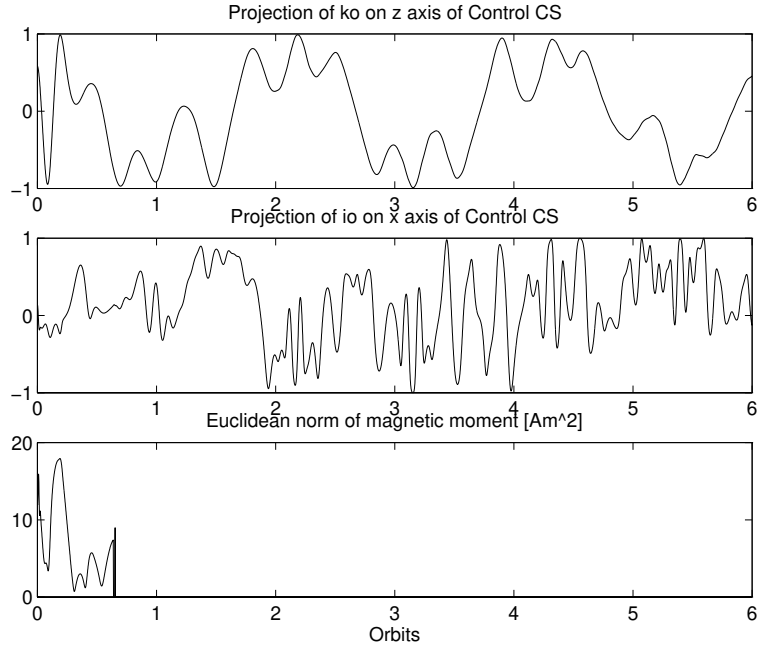
Figure 7.7: The velocity controller is active until $E_{tot} < E_{gg}^x + E_{gyro}^z$. The satellite at this energy level is still tumbling.

7.4.1   Idealized Quaternion Feedback

If it was possible to produce a control torque proportional to the quaternion error, a globally stable controller would result. This is shown in the following theorem.

Theorem 7.4.1 *The control law*

$$^c\mathbf{N}_{ctrl}(t) = (h\,{}^c\mathbf{\Omega}_{co}(t) \times {}^c\mathbf{B}(t)) \times {}^c\mathbf{B}(t) \Leftrightarrow \epsilon_o^c\mathbf{q}(t), \tag{7.29}$$

where h and ϵ are positive scalars, makes the system globally asymptotically stable at the reference $\{({}^c\mathbf{\Omega}_{co}, {}^c\mathbf{k}_o, {}^c\mathbf{i}_o) : (\mathbf{0}, {}^o\mathbf{k}_o, {}^o\mathbf{i}_o)\}$.

Note that the control law (7.29) is given in the form of the desired control torque, which is not producible by the magnetorquers, since the term $\epsilon_o^c\mathbf{q}(t)$ does not have to be perpendicular to the local geomagnetic field. The idea does give some useful hints, however.

Proof of Theorem 7.4.1   The Lyapunov candidate function resembles the total energy in Eq. (7.3) (Proof of Theorem 7.1.1), however an extra attitude quaternion term has been
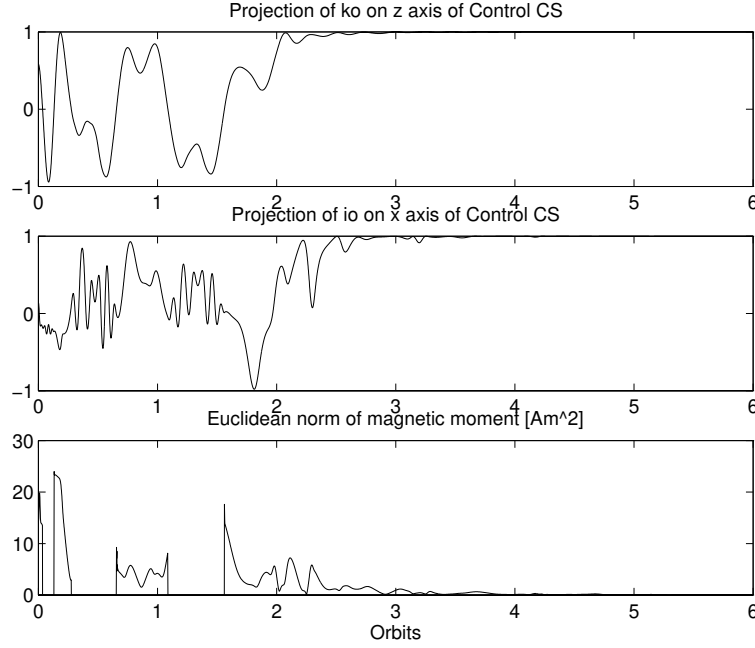
Figure 7.8: Performance of the attitude controller in Procedure 7.2. The rate/attitude controller is activated only in the region $^c k_{oz} > 0$. The satellite trajectory converges to the reference $^c k_{oz} = 1$ and $^c i_{ox} = 1$.

added

$$E_{tot} = \tfrac{1}{2}{}^c\mathbf{\Omega}_{co}^T\mathbf{I}^c\mathbf{\Omega}_{co} + \tfrac{3}{2}\omega_o^2({}^c\mathbf{k}_o^T\mathbf{I}^c\mathbf{k}_o \Leftrightarrow I_z)$$
$$+\tfrac{1}{2}\omega_o^2(I_x \Leftrightarrow {}^c\mathbf{i}_o^T\mathbf{I}^c\mathbf{i}_o) + \epsilon(q_1^2 + q_2^2 + q_3^2 + (1 \Leftrightarrow q_4)^2). \tag{7.30}$$

The attitude quaternion satisfies the constraint equation $q_1^2 + \cdots + q_4^2 = 1$, thus

$$E_{tot} = \frac{1}{2}{}^c\mathbf{\Omega}_{co}^T\mathbf{I}^c\mathbf{\Omega}_{co} + \frac{3}{2}\omega_o^2({}^c\mathbf{k}_o^T\mathbf{I}^c\mathbf{k}_o \Leftrightarrow I_z) + \frac{1}{2}\omega_o^2(I_x \Leftrightarrow {}^c\mathbf{i}_o^T\mathbf{I}^c\mathbf{i}_o) + 2\epsilon(1 \Leftrightarrow q_4). \tag{7.31}$$

The time derivative of Eq. (7.31) gives

$$\dot{E}_{tot} = {}^c\mathbf{\Omega}_{co}^T{}^c\mathbf{N}_{ctrl} + \epsilon{}^c\mathbf{\Omega}_{co}^T{}_o^c\mathbf{q}. \tag{7.32}$$

Applying the control law defined in Eq. (7.29), $\dot{E}_{tot}$ is

$$\dot{E}_{tot} = \Leftrightarrow h {}^c\mathbf{\Omega}_{co}^T\tilde{\mathbf{B}}^T\tilde{\mathbf{B}}^c\mathbf{\Omega}_{co}. \tag{7.33}$$
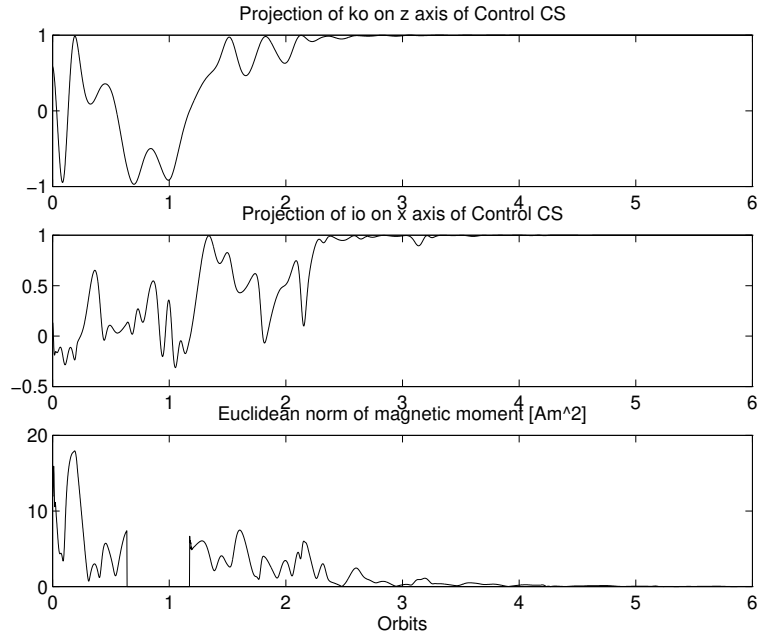
Figure 7.9: Performance of the attitude controller in Procedure 7.3. First, the rate controller is activated, then the the rate/attitude controller takes over. The satellite trajectory converges to the reference $^c k_{oz} = 1$ and $^c i_{ox} = 1$.

This complies with Eq. (7.9). Thus the satellite with control law (7.29) would be globally asymptotically stable at the reference $\{(^c\mathbf{\Omega}_{co}, \ ^c\mathbf{k}_o, \ ^c\mathbf{i}_o) : (\mathbf{0}, \ ^o\mathbf{k}_o, \ ^o\mathbf{i}_o)\}$ or in the quaternion notation $\{(^c\mathbf{\Omega}_{co}, \ _o^c\mathbf{q}) : (\mathbf{0}, [0\ 0\ 0\ 1]^T)\}$ if the desired control torque could be produced. ■

Achievable control with magnetorquers involves the cross product with the geomagnetic field, and it would be a very significant step forward if one could derive a global stabilizing control algorithm under this limitation. This is considered in the next section.

7.4.2   Quaternion Feedback with Magnetic Torquing

The attitude of the Ørsted satellite such that the boom is pointing towards the centre of the Earth may likely occur due to considerable influence of the aerodynamic torque. This undesired attitude is to be corrected by the attitude control system. It was illustrated in Section 7.2 that the linear attitude controller performs satisfactory for all initial value of attitude $^c\mathbf{k}_{oz} > 0$ (boom is upright). If the satellite is tumbling the nonlinear con-

troller (7.1) can be implemented, and the resultant attitude is either of the four equilibria $\{(^c\mathbf{\Omega}_{co},\ ^c\mathbf{k}_o,\ ^c\mathbf{i}_o)\ :\ (\mathbf{0},\ \pm^o\ \mathbf{k}_o,\ \pm^o\ \mathbf{i}_o)\}$. The last but not least attitude control problem is to turn the satellite from the upside-down attitude i.e. from the equilibria $\{(^c\mathbf{\Omega}_{co},\ ^c\mathbf{k}_o,\ ^c\mathbf{i}_o)\ :\ (\mathbf{0},\ \Leftrightarrow^o\ \mathbf{k}_o,\ \pm^o\ \mathbf{i}_o)\}$ to the upright attitude, $^c\mathbf{k}_{oz} > 0$.

First, the following control law is considered

$$^c\mathbf{m}(t) = h^c\mathbf{\Omega}_{co}(t) \times {}^c\mathbf{B}(t) + \epsilon(t)^c_o\mathbf{q}(t) \times {}^c\mathbf{B}(t), \tag{7.34}$$

where h is a positive constant and $\epsilon(t)$ is a piecewise continuous positive scalar function satisfying

$$\epsilon(t) = const > 0,\ t \in (kT_s, (k+1)T_s),\ k = 1, 2, ...$$
$$\epsilon(kT_s) > \epsilon((k+1)T_s) > 0, \tag{7.35}$$

where T_s is a positive constant. Recognize that the control law (7.34) has the time varying attitude gain $\epsilon(t)$ comparing with the control law (7.16).

Before the features of the control law (7.34) are given, the following theorem is presented.

Theorem 7.4.2 *Consider the control law (7.34) then the satellite, given by Eqs. (2.12) to (2.20), has 4 asymptotically stable local equilibria*

$$\{(^c\mathbf{\Omega}_{co},\ ^c\mathbf{k}_o,\ ^c\mathbf{i}_o)\ :\ (\mathbf{0},\ \pm^o\ \mathbf{k}_o,\ \pm^o\ \mathbf{i}_o)\}.$$

Proof of Theorem 7.4.2 For simplicity of notation the equations of satellite Eqs. (2.12) to (2.20) with controller (7.1) are represented by

$$\dot{\mathbf{x}}(t) = \mathbf{f}(\mathbf{x}(t), t), \tag{7.36}$$

and the equations of satellite motion with controller (7.34), for constant $\epsilon(t) = \epsilon(kT)$, are denoted as

$$\dot{\mathbf{x}}(t) = \mathbf{f}_k(\mathbf{x}(t), t). \tag{7.37}$$

Furthermore, the differential equation (7.36) for the initial condition $\mathbf{x}(t_0) = \mathbf{x}_0$ has the solution $\mathbf{x}(t, t_0, \mathbf{x}_0)$, and the differential equation (7.37) for the initial condition $\mathbf{x}(t_0) = \mathbf{x}_0$ has the solution $\mathbf{x}_k(t, t_0, \mathbf{x}_0)$.

The kinematic and dynamic differential equations are Lipschitz, and the following is true

$$\text{if } lim_{k\to\infty}\mathbf{f}_k(\mathbf{x}(t), t) = \mathbf{f}(\mathbf{x}(t), t) \text{ then}$$

$$lim_{k\to\infty}\mathbf{x}_k(t, t_0, \mathbf{x}_0) = \mathbf{x}(t, t_0, \mathbf{x}_0),$$

thus

$$\text{if } lim_{t\to\infty}\mathbf{x}(t, t_0, \mathbf{x}_0) = \mathbf{y}_f \text{ then}$$

$$lim_{t\to\infty}\mathbf{x}_k(t, t_0, \mathbf{x}_0) = \mathbf{y}_f.$$

This means, if $lim_{t\to\infty}\epsilon(t) = 0$, each trajectory of the satellite actuated by the control law (7.34) converges to one of the equilibria: $\{({}^c\mathbf{\Omega}_{co}, {}^c\mathbf{k}_o, {}^c\mathbf{i}_o) : (\mathbf{0}, \pm^o\mathbf{k}_o, \pm^o\mathbf{i}_o)\}$. ∎

The stability analysis demonstrated that the equilibrium $(\mathbf{0}, {}^o\mathbf{k}_o, {}^o\mathbf{i}_o)$ is locally stable if $\epsilon(t) = \hat{\epsilon} < \tilde{\epsilon}$, where $\tilde{\epsilon}$ is the limit of stability for the control law (7.16). On the other hand if $\epsilon(t) = \bar{\epsilon}$ is large enough so that the quaternion feedback is the most significant component on the r.h.s. of Eq. (2.12)

$$\mathbf{I}^c\dot{\mathbf{\Omega}}_{co} \approx \bar{\epsilon}(\mathbf{q} \times {}^c\mathbf{B}) \times {}^c\mathbf{B} \tag{7.38}$$

then the vectors $\mathbf{I}^c\mathbf{\Omega}_{co}$ and $(\mathbf{q} \times {}^c\mathbf{B}) \times {}^c\mathbf{B}$ become parallel, and

$$\mathbf{I}^c\mathbf{\Omega}_{co}^T((\mathbf{q}(t) \times {}^c\mathbf{B}) \times {}^c\mathbf{B}) > 0. \tag{7.39}$$

It was assumed in Eq. (7.39) that the vectors ${}^c\mathbf{B}$ and $\mathbf{q}$ are not parallel. This conjecture is viable, since the controller can be activated when the most favourable conditions in orbital motion for boom upside-down algorithm occur, see Fig. 7.10. It follows from Eq. (7.39) that

$${}^c\mathbf{\Omega}_{co}^T((\mathbf{q} \times {}^c\mathbf{B}) \times {}^c\mathbf{B}) > 0, \tag{7.40}$$

since $\mathbf{I}$ is positive definite.

If Eq. (7.39) is always satisfied, then the satellite is asymptotically stable about the reference $\{({}^c\mathbf{\Omega}_{co}, {}^c\mathbf{k}_o, {}^c\mathbf{i}_o) : (\mathbf{0}, {}^o\mathbf{k}_o, {}^o\mathbf{i}_o)\}$. The proof of this statement is similar to the proof of asymptotic stability of the control law (7.29). The Lyapunov candidate function is

$$\begin{aligned} E_{tot} &= \frac{1}{2}{}^c\mathbf{\Omega}_{co}^T\mathbf{I}^c\mathbf{\Omega}_{co} + \frac{3}{2}\omega_o^2({}^c\mathbf{k}_o^T\mathbf{I}^c\mathbf{k}_o \Leftrightarrow I_z) + \frac{1}{2}\omega_o^2(I_x \Leftrightarrow {}^c\mathbf{i}_o^T\mathbf{I}^c\mathbf{i}_o) \\ &+ \eta(q_1^2 + q_2^2 + q_3^2 + (1 \Leftrightarrow q_4)^2). \end{aligned} \tag{7.41}$$

The time derivative of the Lyapunov candidate function is

$$\dot{E}_{tot} = {}^c\mathbf{\Omega}_{co}^T {}^c\mathbf{N}_{ctrl} + \eta^c\mathbf{\Omega}_{co}^T {}_o^c\mathbf{q}. \tag{7.42}$$

Finally, $\dot{E}_{tot}$ is

$$\dot{E}_{tot} = \Leftrightarrow h^c\mathbf{\Omega}_{co}^T\tilde{\mathbf{B}}^T\tilde{\mathbf{B}}^c\mathbf{\Omega}_{co} \Leftrightarrow \bar{\epsilon}^c\mathbf{\Omega}_{co}^T\tilde{\mathbf{B}}^T\tilde{\mathbf{B}}^c\mathbf{q} + \eta^c\mathbf{\Omega}_{co}^T {}_o^c\mathbf{q}, \tag{7.43}$$

which is negative definite for sufficiently small value of η (or sufficiently large $\bar{\epsilon}$). Notice that Eq. (7.39) is satisfied only until the angular velocity term in Eq. (2.12) becomes
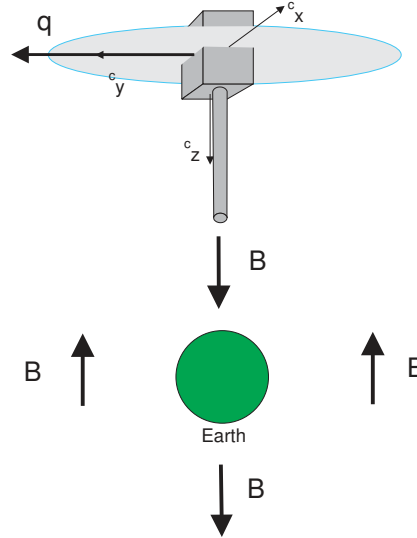
Figure 7.10: Boom upside-down algorithm is recommended to be activated in the regions of North or South Poles.

dominant. The objective of this investigation, however, is not to derive a complete globally stabilizing controller in one step, but rather to get a control law providing necessary acceleration to turn the satellite from the upside down to upright attitude.

It was assumed that the vectors $^c\mathbf{B}$ and $\mathbf{q}$ are not parallel. This implies that the boom upside-down algorithm must be triggered in the zones near the North or South Poles. As mentioned in Section 2.2 the vector part of the attitude quaternion, $\mathbf{q}$, determines the axis of rotation from the Orbit CS to the Control CS. If the boom is upside-down, then $\mathbf{q}$ is perpendicular to the z-axis of the Orbit CS (the zenith). The zenith though is parallel to the geomagnetic field vector over the poles, see Fig. 7.10.

From the analysis carried out so far it follows that for $\epsilon(t) = \bar{\epsilon}$ large enough the satellite trajectory is turned from the boom upside-down towards the boom upright attitude. For practical implementation $\bar{\epsilon}$ shall be chosen larger than

$$\frac{max(\| \mathbf{N}_{gg} \|)}{min(\| {}^o\mathbf{B} \|^2)} \approx 9 \cdot 10^5 \; \frac{Nm}{T}$$

such that the control torque is larger than the gravity gradient.

Concluding, if $\epsilon(t) = \hat{\epsilon}$ the system is asymptotically stable for all values of attitude such that the boom tip is above the horizon. If $\epsilon(t) = \bar{\epsilon}$ the satellite boom axis is turned from upside-down to upright. Furthermore, if $\epsilon(t)$ satisfies Eq. (7.35) then the satellite is locally asymptotically stable towards four equilibria $\{({}^c\mathbf{\Omega}_{co}, \; {}^c\mathbf{k}_o, \; {}^c\mathbf{i}_o)$:

$(\mathbf{0}, \ \pm^o \mathbf{k}_o, \ \pm^o \mathbf{i}_o)\}$. The following algorithm is now straightforward. If the boom tip is below the horizon, ${}^c k_{oz} \leq 0$, implement control law (7.34) with $\epsilon(t) = \bar{\epsilon}$. The satellite reaches a boom upright attitude, ${}^c k_{oz} > 0$, and $\epsilon(t)$ shall gradually decrease from $\bar{\epsilon}$ to $\hat{\epsilon}$. Nevertheless, due to the possibility of a large angular velocity the satellite may again end up to be upside-down. Now, if ${}^c k_{oz} \leq 0$ the magnetic moment, ${}^c \mathbf{m}$, is set to $\mathbf{0}$ until the boom is upright once again. Similarities between this approach and the Procedure 7.2 are striking.

Note that that this strategy rejects the equilibria $\{({}^c \mathbf{\Omega}_{co}, {}^c \mathbf{k}_o, {}^c \mathbf{i}_o) : (\mathbf{0}, \Leftrightarrow^o \mathbf{k}_o, \pm^o \mathbf{i}_o)\}$, since no control torque is generated when the boom tip is below the horizon. Furthermore, the equilibrium $(\mathbf{0}, \ ^o \mathbf{k}_o, \ \Leftrightarrow^o \mathbf{i}_o)$ is also unstable since $\epsilon(t)$ converges to a constant nonzero value $\hat{\epsilon}$. Finally, only one equilibrium $(\mathbf{0}, \ ^o \mathbf{k}_o, \ ^o \mathbf{i}_o)$ remains asymptotically stable, thus it is globally asymptotically stable.

7.4.3 Simulation Results

A simulation study has confirmed our hypothesis that the boom upside-down control algorithm provides globally asymptotically stable satellite motion. Simulation results are shown in Figs. 7.11 to 7.13. The initial conditions are such that the satellite has the upside-down attitude corresponding to the equilibrium $\{({}^c \mathbf{\Omega}_{co}, {}^c \mathbf{k}_o, {}^c \mathbf{i}_o) : (\mathbf{0}, \Leftrightarrow^o \mathbf{k}_o, {}^o \mathbf{i}_o)\}$. The velocity gain is $h = 1 \cdot 10^8 \frac{Ams}{T}$, and the quaternion gain is chosen $\hat{\epsilon} = 15 \cdot 10^5 \frac{Am^2}{T}$. The controller is quite convincing. It takes less than half an orbit to turn the satellite up, and it is stabilized to the operational region within 6 orbits. This is rather satisfactory considering that the available mechanical torque is less than $1.2 \cdot 10^{-3} \ Nm$, which is only three times more than the magnitude of the maximum gravity gradient torque for this satellite. A simulation for the same initial conditions as before but with a new attitude gain $\hat{\epsilon} = 27 \cdot 10^5 \frac{Am^2}{T}$ is depicted in Fig. 7.14. The acceleration imposed by the attitude controller is high enough to turn the boom upright, but the controller is not able to decelerate the motion when ${}^c k_{oz} > 0$, and the satellite turns upside-down again. The attitude controller is now be activated, only if ${}^c k_{oz} > 0$. This control action is globally asymptotically stable.

The controller for acquisition of the satellite attitude from the boom upside-down was developed in this section. It is, however, an advantage to design a boom upside-down controller applying the existing energy of the satellite motion, and in this way decreasing electrical energy utilized by the control system. This issue is addressed in the next section.
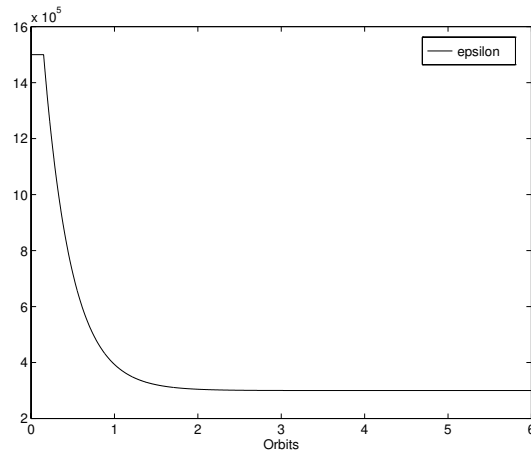
Figure 7.11: The velocity gain h is $1 \cdot 10^8 \frac{Ams}{T}$. The attitude gain is time varying and initially $\epsilon(t_0)$ is $15 \cdot 10^5 \frac{Am^2}{T}$. It converges to $\hat{\epsilon} = 3 \cdot 10^5 \frac{Am^2}{T}$.
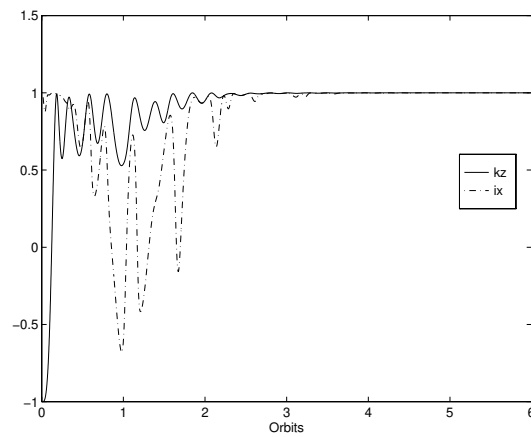
Figure 7.12: $^c k_{oz}$ characterizes convergence of $^c\mathbf{k}_o$ towards $^o\mathbf{k}_o$ (if $^c k_{oz} < 0$ satellite is upside-down), whereas $^c i_{ox}$ characterizes convergence of $^c\mathbf{i}_o$ towards $^o\mathbf{i}_o$
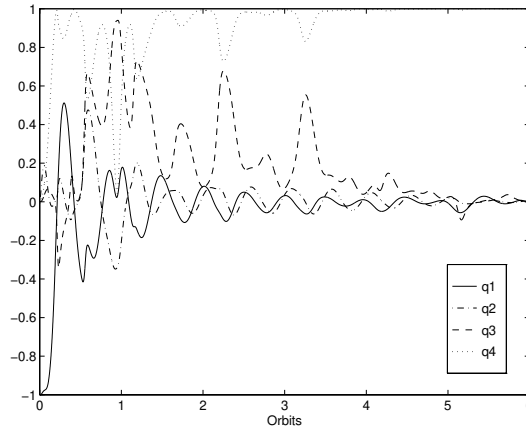
Figure 7.13: The attitude quaternion, ${}^c_o\mathbf{q}$ converges to $[0\ 0\ 0\ 1]^T$ from an upside-down attitude.
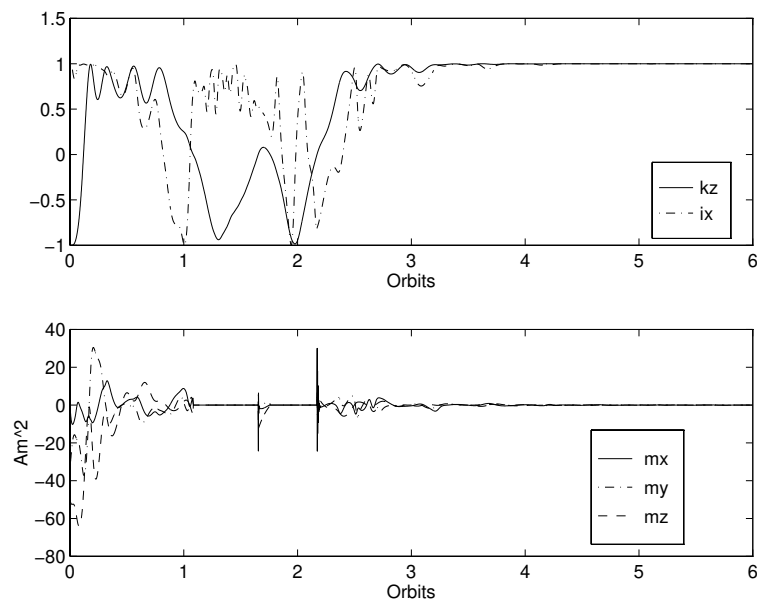
Figure 7.14: The velocity and attitude gains are $1 \cdot 10^8 \frac{Ams}{T}$ and $27 \cdot 10^5 \frac{Am^2}{T}$ respectively. The attitude controller is activated when ${}^c k_{oz} > 0$ (if ${}^c k_{oz} \leq 0$ then ${}^c\mathbf{m} = \mathbf{0}$).

7.5   Alternative Boom Upside-Down Control

An alternative boom upside-down algorithm is investigated in this section. A control concept is to apply a destabilizing controller when the gravity gradient boom is upside-down and a stabilizing when it is above the horizon.

The idea of an algorithm is to generate a mechanical torque in the direction of the minimum potential energy until the boom axis appears above the horizon, then to apply Procedures 7.2 or 7.3.

A proposed control algorithm is

Procedure 7.4
- *If the boom axis is upside-down (below the horizon) generate the magnetic moment according to Eq. (7.44) until $^c k_{oz} > 0$*

$$^c \mathbf{m} = g \, ^c \mathbf{i}_o \times {}^c \mathbf{B}, \tag{7.44}$$

  where g is a positive or negative constant, a design parameter, then

- *Use Procedure 7.2 or 7.3.*

There are two reasons to propose this algorithm as it will be explained below.

- A minimum effort controller is a controller which generates a control torque perpendicular to the local geomagnetic field. The unit vector $^c \mathbf{i}_o(t)$ is approximately perpendicular to $^c \mathbf{B}(t)$ for all t, since it is perpendicular to the orbit plane. The resultant control torque generated according to Eqs. (7.44) and (2.15) is parallel to $^c \mathbf{i}_o(t)$ and therefore perpendicular to the local geomagnetic field.

- The minimum potential energy necessary to turn the boom axis upright is the rotation about the pitch axis, which is at most

$$E_p = E_{gg}^y + E_{gyro}^y = \frac{2}{3}\omega_o^2(I_y \Leftrightarrow I_z) + \frac{1}{2}\omega_o^2(I_x \Leftrightarrow I_y). \tag{7.45}$$

  The potential energy necessary to turn the satellite about the roll axis is at most

$$E_r = E_{gg}^x + E_{gyro}^z = 2\omega_o^2(I_x \Leftrightarrow I_z). \tag{7.46}$$

  The meaning of the constants E_{gg}^x, E_{gg}^y, and E_{gyro}^z were explained in Section 7.3, whereas

$$E_{gyro}^y = \frac{1}{2}\omega_o^2(I_x \Leftrightarrow I_y).$$

Procedure 7.4 can be improved by utilization of the angular momentum due to the satellite revolution about the Earth, $\mathbf{h}_o$. The design parameter g is strictly positive, thus the angular momentum $\mathbf{h}_o$ acts in the same direction as the control torque, and the necessary effort to turn the satellite upright is decreased.
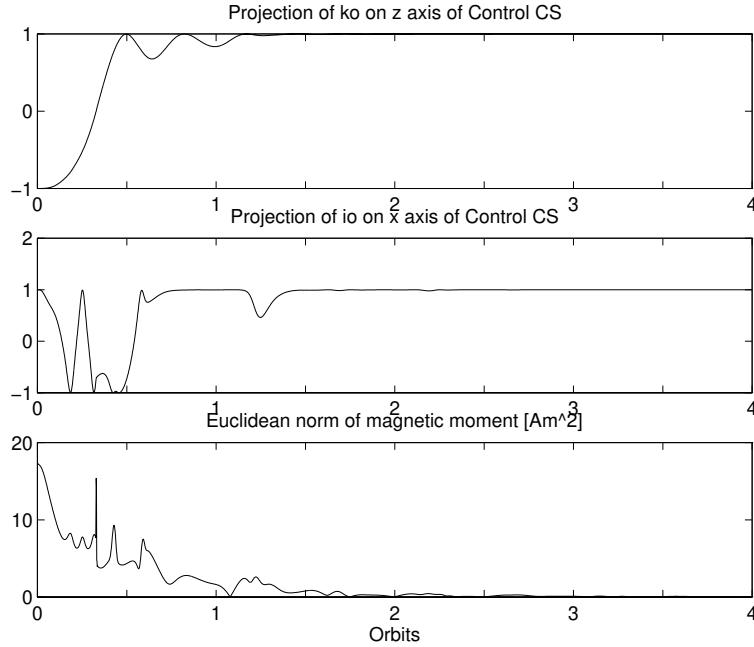
Figure 7.15: Performance of the attitude controller in Procedure 7.4. First, the destabilizing controller in Eq. (7.44) is activated, then after $\frac{1}{3}$ orbit the rate/attitude controller takes over. The satellite trajectory converges to the reference $^{c}k_{oz} = 1$ and $^{c}i_{ox} = 1$.

7.5.1   Simulation Results

An example of the simulation test carried out for Procedure 7.4 is depicted in Fig. 7.15. The gain $g = 5.2 \, 10^{5} \, \frac{Nm}{T^{2}}$ of the destabilizing controller is chosen empirically. The remaining control parameters coincide with those implemented in the test study described in Subsection 7.3.5. The initial attitude is again such that the boom axis is upside-down $\{(^{c}\mathbf{\Omega}_{co}, \, {}^{c}\mathbf{k}_{o}, \, {}^{c}\mathbf{i}_{o}) : (\mathbf{0}, \, \Leftrightarrow^{o}\mathbf{k}_{o}, \, {}^{o}\mathbf{i}_{o})\}$. First, the destabilizing controller in Eq. (7.44) is activated, then after $\frac{1}{3}$ orbit the boom is above the horizon, and the rate/attitude controller takes over. The satellite trajectory converges to the reference $^{c}k_{oz} = 1$, $^{c}i_{ox} = 1$, i.e. $\{(^{c}\mathbf{\Omega}_{co}, \, {}^{c}\mathbf{k}_{o}, \, {}^{c}\mathbf{i}_{o}) : (\mathbf{0}, \, {}^{o}\mathbf{k}_{o}, \, {}^{o}\mathbf{i}_{o})\}$.

The performance of this controller and the controller (7.34) is similar. Both algorithms are simple for on board implementation, therefore both are equally well suitable for a magnetic actuated satellite.

Controller type	Features
${}^c\mathbf{m}(t) = h\,{}^c\mathbf{\Omega}_{co}(t) \times {}^c\mathbf{B}(t)$	Locally stable about 4 equilibria $\{({}^c\mathbf{\Omega}_{co},\ {}^c\mathbf{k}_o,\ {}^c\mathbf{i}_o) : (\mathbf{0},\ \pm^o\mathbf{k}_o,\ \pm^o\mathbf{i}_o)\}$
${}^c\mathbf{m}(t) = h\,{}^c\mathbf{\Omega}_{co}(t) \times {}^c\mathbf{B}(t)$ $+\epsilon_o^c\mathbf{q}(t) \times {}^c\mathbf{B}(t)$	Locally stable about reference for all attitude such that ${}^ck_{oz} > 0$ and small ${}^c\mathbf{\Omega}_{co}$
${}^c\mathbf{m}(t) = h\,{}^c\mathbf{\Omega}_{co}(t) \times {}^c\mathbf{B}(t)$ $+\epsilon(t)_o^c\mathbf{q}(t) \times {}^c\mathbf{B}(t)$	Globally stable about reference; $\epsilon(t)$ decays from $\bar{\epsilon}$ to $\hat{\epsilon}$
${}^c\mathbf{m} = g\,{}^c\mathbf{i}_o \times {}^c\mathbf{B}$	Destabilizing controller used for turning boom axis upright

Table 7.1: A summary of the properties of the magnetic attitude control.

7.6 Summary of Magnetic Attitude Control

This chapter contributes to the development of proportional-derivative feedback control based only on magnetic torquing for low Earth orbit satellites. Both locally and globally stabilizing controllers were proposed, and a rigorous stability analysis was carried out. The velocity controller cross product with the local geomagnetic field provided four stable equilibria, one of which was the reference. A number of methods for perturbing the satellite motion from three undesired equilibria, such that the satellite is globally asymptotically stable to the reference, were presented. Simulation results showed the proficiency of the proposed controllers, even in the upside-down configuration, which is the worst case situation for a satellite.

A summary of the properties of the attitude control laws derived in this chapter is given in Table 7.1.

7.7 Mission Scenarios

This section provides attitude control algorithms for a number of the Ørsted mission scenarios. The features of the magnetic attitude control listed in the previous sections are combined giving globally stable control action. The similarities between the locally and globally stable controllers are striking. The only difference is the gain factor $\epsilon(t)$. This makes implementation exceptionally simple.

7.7.1 Nominal Operation

The boom tip is detected to be above the horizon, i.e. ${}^ck_{oz} > 0$. The control law (7.34) with constant value of $\epsilon(t) = \hat{\epsilon}$, $\hat{\epsilon} \leq \tilde{\epsilon}$ is implemented.

7.7.1.1　Tumbling Satellite

The satellite is detected to tumble, i.e. it rotates with the angular velocity above an operational limit, the following algorithm may be implemented:

- Activate the angular velocity controller (7.1).

- If the total energy is below $2\omega_o^2(I_x \Leftrightarrow I_z)$ and the boom axis is detected above the horizon activate the rate/attitude controller (7.16).

7.7.2　Boom is Upside-Down

A large disturbance torque impacts on the satellite body or temporary malfunction occurs on board. As the consequence the boom tip remains below the horizon.

- Activate the boom upside-down algorithm, Eq. (7.34), where $\epsilon(t) = \bar{\epsilon}$. Start the algorithm when the boom is over South or North Poles.

- If $^ck_{oz} > 0$ apply Eq. (7.34), where

$$\epsilon_{k+1} = L\epsilon_k, \ 0 < L < 1, \ \epsilon_0 = \bar{\epsilon}.$$

  The gain ϵ is updated every sampling time if $^ck_{oz} > 0$, and it is kept constant otherwise.

- If $^ck_{oz} \leq 0$ apply $^c\mathbf{m} = \mathbf{0}$.

Alternatively

- If the boom axis is upside-down (below the horizon) then generate the magnetic moment according to Eq. (7.44).

- If $E_{tot} > 2\omega_o^2(I_x \Leftrightarrow I_z)$ activate the rate controller (7.1).

- Else wait until $^ck_{oz}$ changes the sign from negative to positive and activate the rate/attitude control (7.16) for $^ck_{oz} > 0$.

Chapter 8

Ørsted Attitude Control

The objective of this chapter is to summarize and evaluate performance of the control algorithms chosen for implementation in the Ørsted attitude control system. The baseline for the design in the previous chapters was that the satellite was in a circular orbit and an influence of the aerodynamic drag was rejectable. In this chapter performance of the attitude control system is a subject of simulation test in the realistic environment.

Complete disturbance rejection is not feasible due to lack of controllability in the direction of the local geomagnetic field. As an example consider a disturbance torque acting in the direction of nadir during the satellite passage in the polar regions. The geomagnetic field is parallel to the disturbance torque resulting in large amplitude of yaw oscillations. The design criterion is to adjust the control parameters such that deviations of pitch, roll, yaw from the reference are within specified values (pitch $\pm 10 \ deg$, roll $\pm 10 \ deg$, yaw $\pm 20 \ deg$).

Two independent approaches: linear and nonlinear to the magnetic attitude control were presented in this thesis. The linear methods focused on periodic character of the system's parameters. The result was the family of energy optimal periodic controllers. The proposed control algorithm were, however, relatively complex, since it was necessary to solve the Riccati differential equation. The nonlinear part of the work gave a deep insight into physics of the rigid body motion. The finding of the nonlinear analysis was a number of globally and locally stable controllers. All of them had similar structure of PD regulator vector product with the local geomagnetic field vectors. These attitude controllers were chosen for further implementation in the Ørsted attitude control system, due to their simplicity, efficiency, and independence on exact knowledge of the system parameters as moments of inertia.

Dependent on the mission phase three separate attitude controllers are implemented:

- **Rate Detumbling Controller**
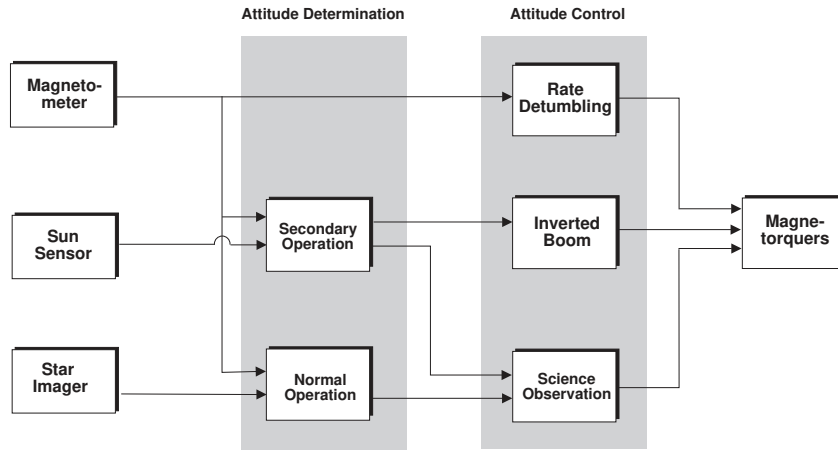
Figure 8.1: Architecture of the attitude control system consisting of the rate detumbling controller, the science observation controller and the continence operation controller for the inverted boom.

The rate detumbling controller is used just after release from the launch vehicle. Kinetic energy is dumped and the satellite is stabilized relative to the local geomagnetic field. The feedback signal is the rate of the local geomagnetic field.

- **Controller for Science Observation Phase**
  After boom deployment the satellite is three axis stabilized. Attitude is measured from the star imager or alternatively from the magnetometer and the sun sensor, see Bak (1994) and Bak (1996).

- **Contingency Operation for Inverted Boom**
  The objective of the controller is to acquire the satellite from the boom upside down. Attitude is obtained from the magnetometer and the sun sensor.

The structure of the control system is illustrated in Fig. 8.1 The algorithms are summarized and the performance is investigated in the next sections.

The baselines for the simulation study are given in Tables 8.1 and A.1. The aerodynamic drag torque implemented in the simulator, see Appendix A, corresponds to atmospheric density in April 1997.

Item	Description
Body size	H 680 x W 450 x D 340 mm
Boom	8 m Deployable
Mass	61.8 kg
Moments of inertia about principal axes:	
· boom deployed	X 181.78, Y 181.25, Z 1.28 kgm^2
· boom stowed	X 3.428, Y 2.904, Z 1.275 kgm^2
Maximum amplitude of magnetic moment	20 Am^2
Apogee	850 km
Perigee	450 km
Eccentricity	0.028599
Argument of Perigee	0
Inclination	96.1 deg
RAAN	105.2 deg
Nodal drift	0.77 deg/day
Epoch	3 April 1997 at 1200 UTC

8.1   Rate Detumbling Controller

8.1.1   Objectives

The objective of the rate detumbling controller is to generate a magnetic moment, such that the kinetic energy of the satellite is dissipated and it is turned in the negative direction of the local geomagnetic field vector. Hence, radio contact with the ground stations in Copenhagen and Aalborg is viable.

8.1.2   Control Law

The following control law is implemented

$$^c\mathbf{m} = -k^c\dot{\mathbf{B}} - \mathbf{m}_{const}, \tag{8.1}$$

where $\mathbf{m}_{const} = [0 \ 0 \ m_{const}]^T$.

The first summand contributes to kinetic energy dissipation, whereas the second is a bias term. The satellite acts like a compass needle which tends to align with the local geomagnetic field, while adequate angular velocity damping is retained. More details about the rate detumbling control can be found in Appendix B.
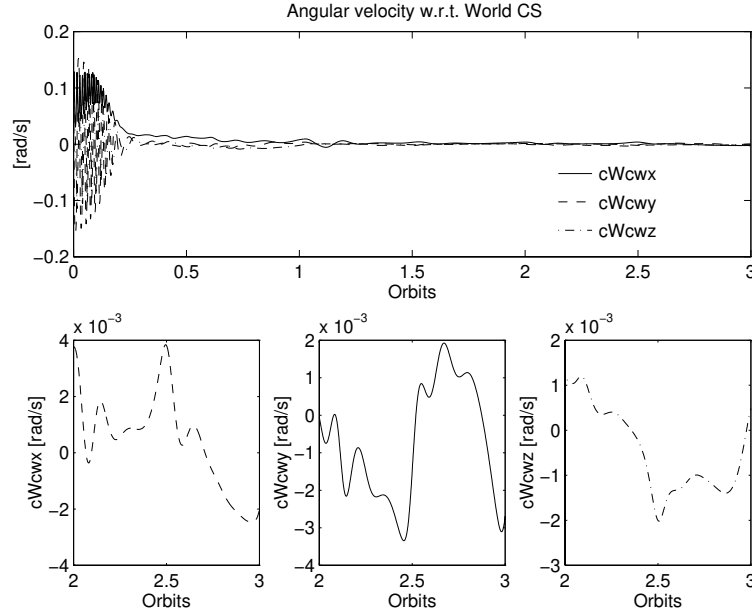
Figure 8.2: Rate detumbling simulation. The controller decreases initially high angular velocity $1.6 \cdot 10^{-1} \frac{rad}{s}$ to absolute value below $5 \cdot 10^{-3} \frac{rad}{s}$.

8.1.3   Control Coefficients

The control coefficients, that is the gain, k and the bias magnetic moment, m_{const} were found empirically. The best performance was obtained for $k = 5 \cdot 10^{6} \frac{Am^2 s}{T}$ and $m_{const} = 3 \ Am^2$.

8.1.4   Simulation Evaluation

The algorithm for the rate detumbling controller has been verified by a simulation study in realistic environment of the gravity gradient and the aerodynamic drag torques acting on the satellite body. Figures 8.2 to 8.4 show simulation results for the initial value of the satellite angular velocity $\mathbf{\Omega}_{cw}(t_0) = [0.10 \ 0.10 \ 0.09]^T \ rad/s$, which is above the upper limit of $2 \ rpm$ for the tumbling satellite after release from the launcher. The angular velocity w.r.t. the World CS depicted in Fig. 8.2 is decreased to absolute value below $5 \cdot 10^{-3} \frac{rad}{s}$. The second figure shows the time history of satellite attitude. The satellite tracks the inverse direction of the geomagnetic field. The inclination angle between the z principal axis and the local geomagnetic field is influenced by the increase of
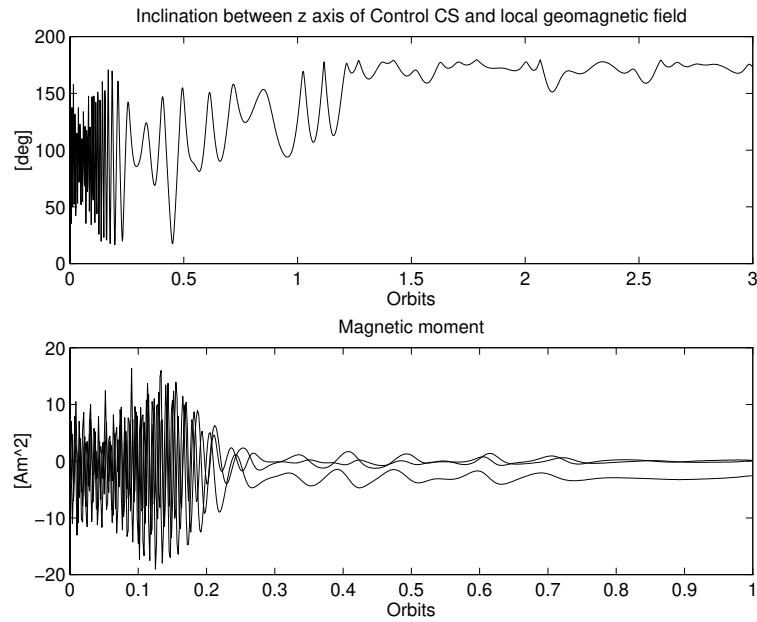
Figure 8.3: Rate detumbling simulation. Satellite tracks the inverse geomagnetic field. The inclination angle between the z principal axis and the local geomagnetic field is influenced by the increase of the geomagnetic field rate over equator at 1 , 1.5, 2, and 2.5 orbits.
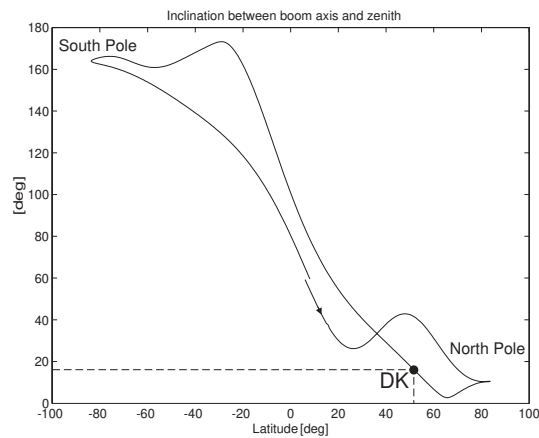

Figure 8.4: Rate detumbling simulation. The plot shows the steady state deviation of the boom axis from the zenith for one orbit. The deviation is below $20\ deg$ at $56\ deg$ North, which is the latitude of Denmark.

the geomagnetic field rate over equator. This phenomena is depicted by periodic peaks of the inclination angle, here at approximately 1, 1.5, 2, and 2.5 orbits. The last figure 8.4 shows the deviation of the boom axis from the zenith for one orbit. The deviation is below $20\ deg$ at $56\ deg$ North, which is the latitude of Denmark. Thus, the boom deployment for the satellite stabilized with use of the biased rate detumbling controller is feasible.

8.1.5   Pros and Cons

Advantages of the rate detumbling controller are:

- simple implementation,

- no three axis attitude information is necessary,

- deployment of the boom over Denmark is feasible,

- very rough knowledge of moments of inertia is required.

The main disadvantage is that the rate detumbling is not three axis stabilizing controller thereby alignment of the z axis of the Control CS with the z axis of the Orbit CS, the ideal situation for the boom deployment, is reached only within $\pm 20\ deg$ over Denmark. The three axis attitude control is possible using the sliding mode control approach described in Chapter 6, however the necessary attitude information is not available in this mission phase.

8.2   Science Observation Controller

8.2.1   Objectives

The aim of the science observation control is to provide three axis stabilization of the satellite after boom deployment. The controller corrects all initial values of the attitude with the boom upright to the reference. The reference is such that the boom axis is aligned with the zenith, and x axes of the Control and the Orbit CSs coincide. Furthermore, an optional yaw reference for the attitude controller is added.

8.2.2   Control Law

The general structure of the attitude controller for the science observation is as follows

$$^{c}\mathbf{m}(t) = (\mathbf{H}\,^{c}\boldsymbol{\Omega}_{cr}(t)) \times {}^{c}\mathbf{B}(t) \Leftrightarrow (\boldsymbol{\epsilon}\tilde{\mathbf{q}}(t)) \times {}^{c}\mathbf{B}(t), \tag{8.2}$$

where $^c\boldsymbol{\Omega}_{cr}$ is the angular velocity of the Control CS w.r.t. a Reference Coordinate System. The Reference CS is defined relatively to the Orbit CS by rotation about the z axis of an angle θ. $\tilde{\mathbf{q}}$ is the vector part of $^c_r\mathbf{q}$, i.e. a quaternion, representing the transformation from the Reference CS to the Control CS. $\mathbf{H}$ and ϵ are matrices of control coefficients.

The quaternion $^c_r\mathbf{q}$, see Appendix C, is given by

$$^c_r\mathbf{q} = \mathbf{Q}(^c_o\mathbf{q})^o_r\mathbf{q}, \tag{8.3}$$

where $\mathbf{Q}(\cdot)$ was defined in Section 2.2 and

$$^o_r\mathbf{q} = \begin{bmatrix} 0 & 0 & \Leftrightarrow\frac{1}{2}sin\ \theta & \frac{1}{2}cos\ \theta \end{bmatrix}^T, \tag{8.4}$$

finally, θ is the desired yaw reference.

The angular velocity $^c\boldsymbol{\Omega}_{cr}$ is calculated according to

$$^c\boldsymbol{\Omega}_{cr} = {}^c\boldsymbol{\Omega}_{cw} + \mathbf{A}(^c_r\mathbf{q})^r\boldsymbol{\Omega}_{rw}, \tag{8.5}$$

where $^r\boldsymbol{\Omega}_{rw} = \omega_o \begin{bmatrix} cos\ \theta & \Leftrightarrow sin\ \theta & 0 \end{bmatrix}^T$.

Note that the yaw reference 0 and $180\ deg$ comply with the stable equilibria discussed in Chapter 7.

8.2.3   Control Coefficients

A proper choice of control parameters is a crucial issue. The moments of inertia for the Ørsted satellite are approximately the same about the x and y principal axes, therefore zero yaw is no longer a stable equilibrium. Even small perturbations about the boom axis heavily disturbs yaw from the reference, since the moment of inertia about the z principal axis is nearly 200 times smaller than ones about other axes. Hence, the influence of the same torque acting in the direction of the boom axis is 200 times more severe than e.g. in the direction of the x principal axis.

The control parameters $\mathbf{H}$ and ϵ are computed using LQR/Floquet technique as described in Section 4.4, however the system and the control matrices are slightly modified in order to incorporate a new yaw reference if necessary, see Appendix C. The weight matrix $\mathbf{Q} = diag([18\ 900\ 18000\ 18\ 900\ 18000]^T)$ was applied for zero yaw reference. The weight matrix has large values of the components corresponding to yaw and its rate, $\mathbf{Q}(3,3)$, $\mathbf{Q}(6,6)$[1]. This helps to avoid large fluctuations of the rotation about the boom axis. Pitch and roll motion is marginally stable due to considerable influence of the gravity gradient torque, but roll and yaw are coupled through dynamics. Therefore, some additional punishment on roll and its rate ($\mathbf{Q}(2,2)$, $\mathbf{Q}(5,5)$) is imposed. The weight matrix $\mathbf{Q}$ provides the following control gain matrices for the nominal reference (complying

---

[1]Notice that for small angles pitch, roll, yaw complies with q_1, q_2, q_3 components of the attitude quaternion.
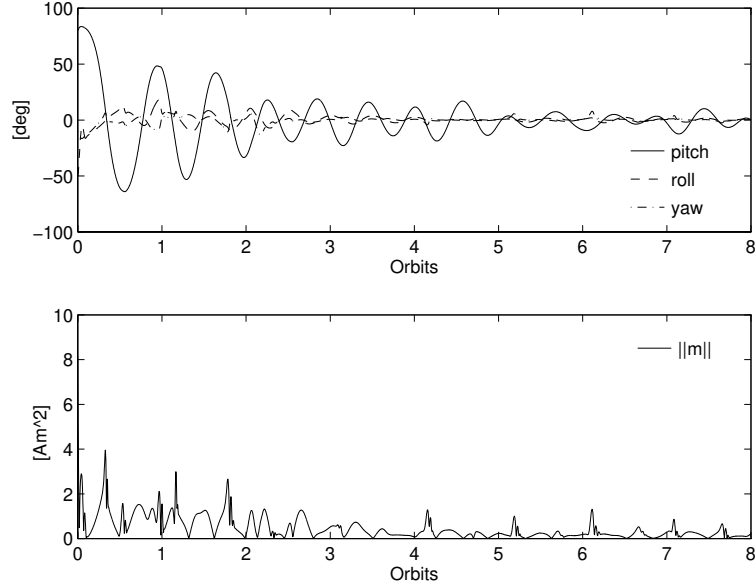
Figure 8.5: Simulation of the science observation controller. The plot shows time history of pitch, roll, yaw for the Ørsted satellite influence by the aerodynamic drag torque. The initial attitude is extreme, pitch $80 \ deg$, roll $\Leftrightarrow 50 \ deg$, and yaw $\Leftrightarrow 10$. The initial angular velocity is $\mathbf{\Omega}_{co}(t_0) = \mathbf{0}$. The steady state deviation is below $10 \ deg$ in all directions. The lower plot depicts the Euclidean norm of the magnetic moment, which is much below the limit of $20 \ Am^2$.

with the Orbit CS)

$$\mathbf{H} = \begin{bmatrix} 0.3537 & \Leftrightarrow 0.0290 & 0.0014 \\ \Leftrightarrow 0.0392 & 1.4333 & \Leftrightarrow 0.0348 \\ \Leftrightarrow 0.0306 & 0.0508 & 0.8463 \end{bmatrix} \cdot 10^{-1} \frac{A \ m^2 \ s}{T \ rad},$$

$$\mathbf{\epsilon} = \begin{bmatrix} 0.0088 & 0.0459 & 0.0541 \\ \Leftrightarrow 0.0671 & 0.2000 & 0.0902 \\ \Leftrightarrow 0.1283 & \Leftrightarrow 0.1168 & 2.6837 \end{bmatrix} \cdot 10^{-3} \frac{A \ m^2}{T}.$$

Recognize also that pitch feedback has pure derivative character, since $\epsilon(1,1) \approx 0$.

8.2.4   Simulation Evaluation

The controller was evaluated for a large envelope of initial conditions. An examples of the extreme initial attitude when the boom is only slightly above the horizontal plane
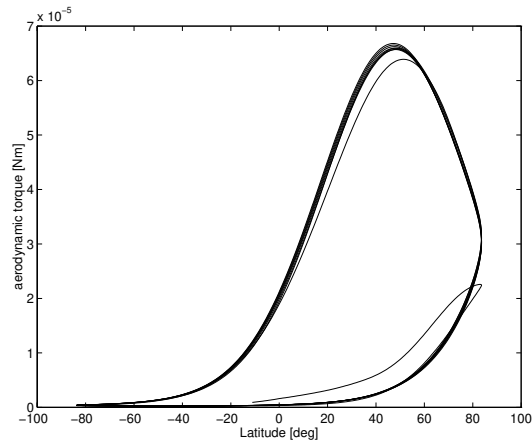
Figure 8.6: Plot of the aerodynamic drag torque against latitude corresponding to the attitude as in Fig. 8.5. The amplitude of the aerodynamic torque is maximum at perigee (latitude 45 deg North).
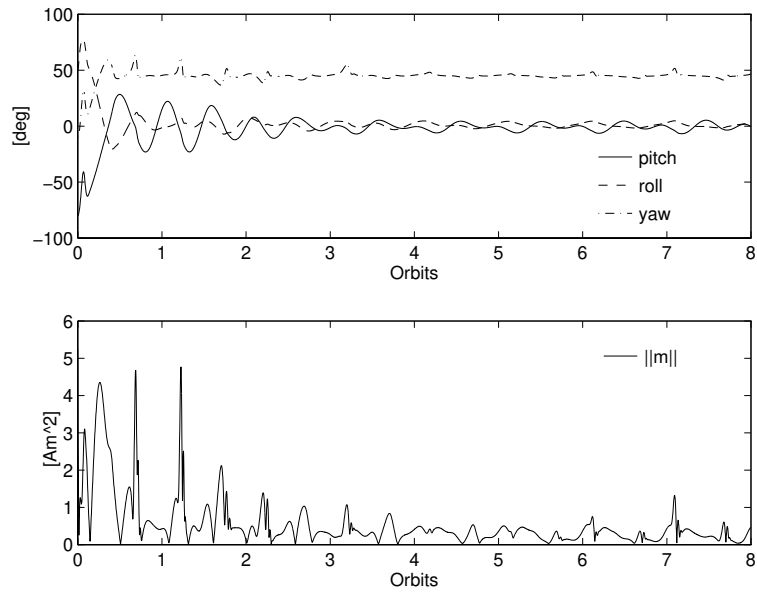
Figure 8.7: The figure shows time history of the Ørsted satellite attitude. The yaw reference is set to $\theta = 45$ deg. The initial attitude is pitch $\Leftrightarrow$80 deg, roll $\Leftrightarrow$50 deg, and yaw $\Leftrightarrow$10 deg. The initial angular velocity is $\mathbf{\Omega}_{co}(t_0) = \mathbf{0}$.
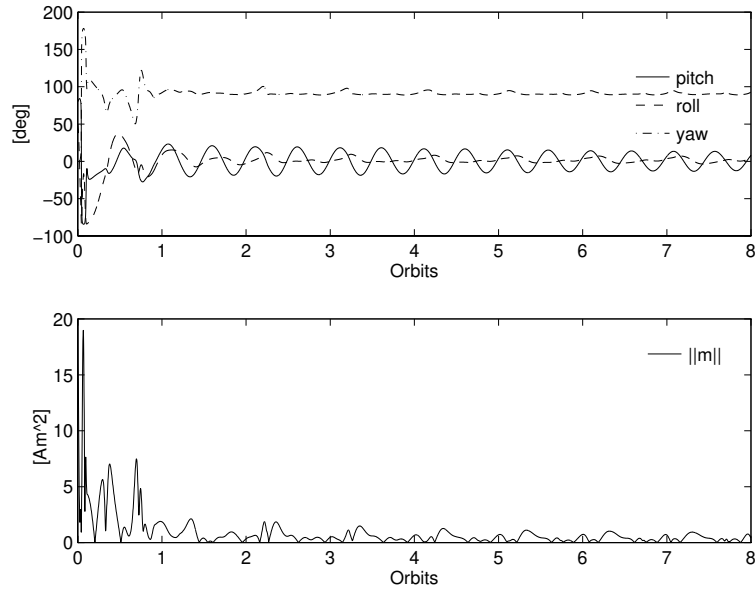
Figure 8.8: The figure shows time history of the Ørsted satellite attitude. The yaw reference is set to $\theta = 90\ deg$. The initial attitude is pitch $\Leftrightarrow$80 deg, roll 50 deg, and yaw $\Leftrightarrow$10 deg. The initial angular velocity $\mathbf{\Omega}_{co}(t_0) = \mathbf{0}$.

is given in Fig. 8.5. The motion is heavily influenced by the aerodynamic drag torque plotted in Fig. 8.6. This causes in the steady state motion of pitch, roll, and yaw just below 10 deg. Performance of the science observation controller for 45 deg and 90 deg yaw reference is depicted in Figs. 8.7 and 8.8.

Steady state behaviour of the controller is evaluated in Figs. 8.9 to 8.11. Fig. 8.9 shows steady state motion of the satellite during 8 orbits. Deviation of pitch, roll, and yaw from the nominal reference are plotted as functions of latitude. Particularly good performance is reached in equatorial regions (latitudes near 0 deg). The largest deviation of the Euler angles is observed near the North Pole (latitude 90 deg), due to prominent influence of the aerodynamic drag torque encountered at latitude 45 deg North and lack of yaw controllability in the polar regions.

Much attention was devoted to empirical sensitivity analysis of the controller towards uncertainties of the moments of inertia. Fig. 8.10 depicts steady state performance of the science observation controller for the moment of inertia about the y principal axis being 10 percent smaller than anticipated for the controller design. The difference between I_x and I_y is enlarged. Thus, the reference is now the stable equilibrium and much better performance of yaw is attained. Fig. 8.11 presents steady state performance of the con-
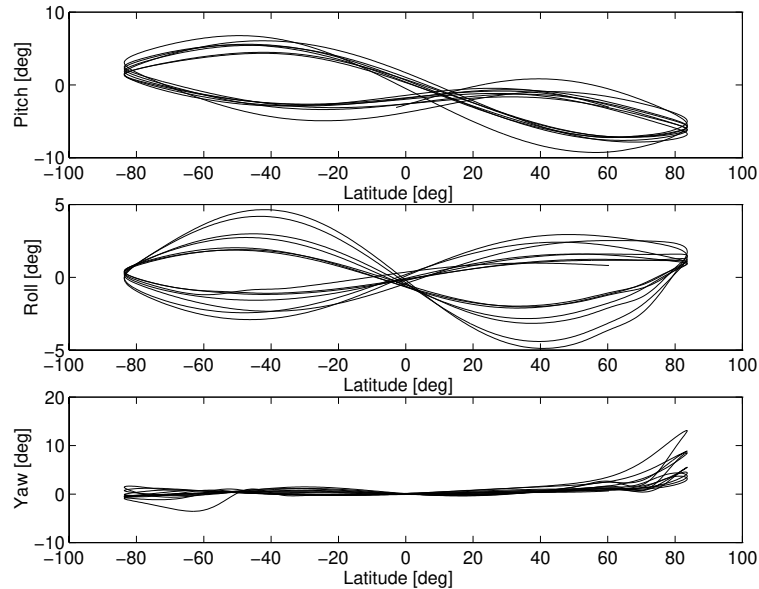
Figure 8.9: The figure shows steady state performance of the science observation controller during 8 orbits. Deviation of pitch, roll, and yaw are plotted as functions of latitude. Well performance is reached in equatorial regions, latitudes near $0\ deg$. The largest deviation of the attitude angles is observed near the North Pole (latitude $90\ deg$), due to prominent influence of the aerodynamic drag torque at latitude $45\ deg$ North and lack of yaw controllability in the polar regions.

troller when the moment of inertia I_y is 10 percent larger than assumed for the controller design. The difference between I_x and I_y is negative, therefore the reference is not an equilibrium and the amplitude of yaw fluctuation is increased.

8.2.5 Pros and Cons

Advantages of the science observation controller are:

- the controller is robust to uncertainties of the moments of inertia,

- it is stable for very wide envelope of initial attitudes,

- it is power efficient,

- it is easy to implement.

Figure 8.10: The figure shows steady state performance of the science observation controller for the moment of inertia about the y principal axis, I_y is 10% smaller than anticipated for the controller design. The difference between I_x and I_y is enlarged. Now, the reference is the stable equilibrium and much better performance of yaw is attained.

The drawback of the controller is that high pointing accuracy is not viable for a satellite subject to large influence of the aerodynamic drag torque in elliptic orbit. This is due to the magnetic torquing is lacking controllability in the direction of the local geomagnetic field.

8.3   Contingency Operation for Inverted Boom

8.3.1   Objectives

The inverted boom controller is activated when the satellite boom is detected to be upside-down. The objective of the controller is to turn the boom upright, and then coarsely stabilize the satellite in three axes. Afterwards, the science observation controller takes over.
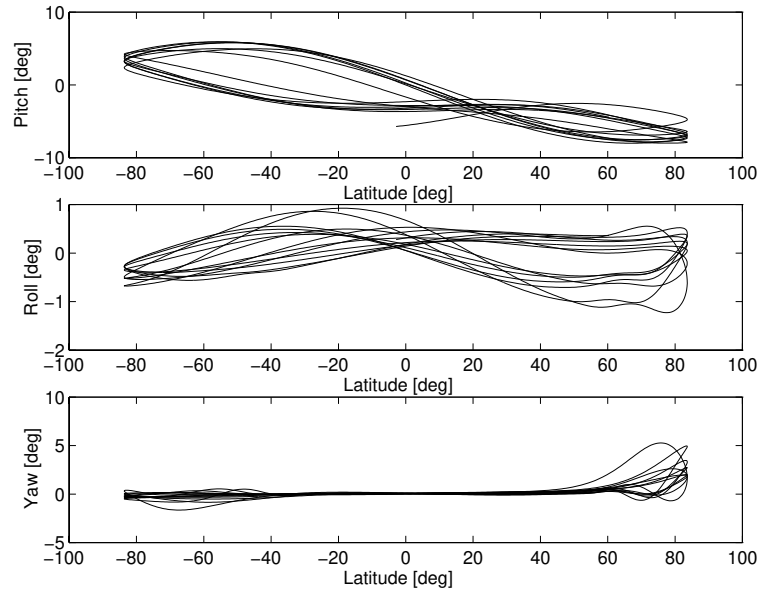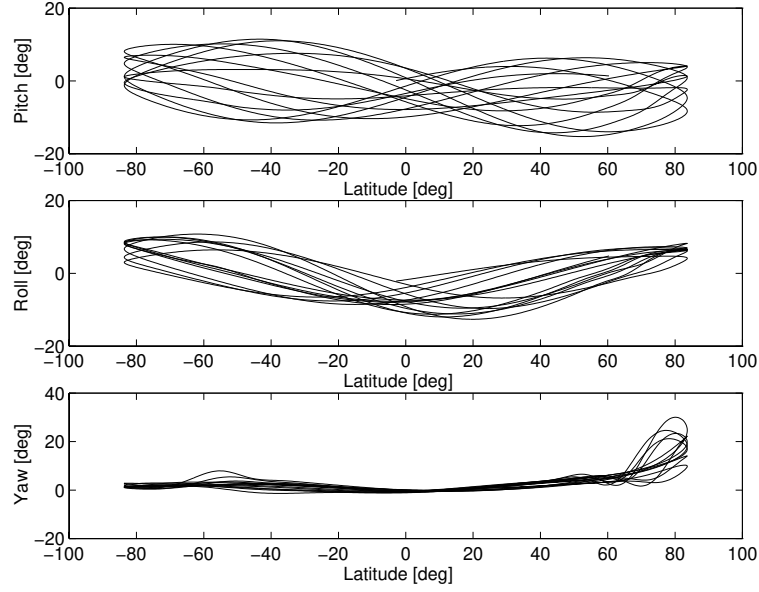
Figure 8.11: The figure shows steady state performance of the science observation controller when moment of inertia I_y is 10% larger than anticipated for the controller design. The difference between I_x and I_y is negative, therefore the reference is not an equilibrium and the performance of yaw is deteriorated.

8.3.2 Control Law

The following control law is implemented

$$
{}^c\mathbf{m}(t) = \begin{cases} \mathbf{H}{}^c\mathbf{\Omega}_{co}(t) \times {}^c\mathbf{B}(t) + \boldsymbol{\epsilon}(t){}^c_o\mathbf{q}(t) \times {}^c\mathbf{B}(t) & \text{if } {}^ck_{oz} > 0, \\ \mathbf{0} & \text{otherwise.} \end{cases} \tag{8.6}
$$

where $\mathbf{H}$ is a matrix of control parameters, whereas $\boldsymbol{\epsilon}$ is a piecewise continuous matrix function

$$
\boldsymbol{\epsilon} = \boldsymbol{\epsilon}_k + \boldsymbol{\epsilon}_c, \tag{8.7}
$$

where $\boldsymbol{\epsilon}_k$ is updated in every sampling cycle according to

$$
\boldsymbol{\epsilon}_k = \begin{cases} L\boldsymbol{\epsilon}_{k-1} & \text{if } {}^ck_{oz} > 0, \\ \boldsymbol{\epsilon}_{k-1} & \text{otherwise,} \end{cases}
$$

$\boldsymbol{\epsilon}_c$ is another matrix of control parameters, and $0 < L < 1$.
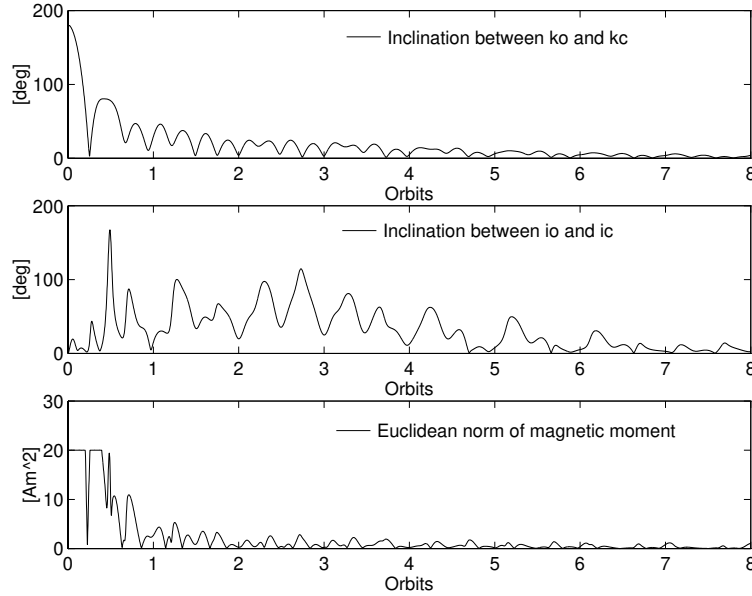
Figure 8.12: Simulation of the inverted boom controller. The first plot shows time history of the inclination angle between the z axis of Control CS and the z axis of Orbit CS. The second plot depicts the inclination between the x axes of the Control and Orbit CSs. Finally, the third one illustrates the magnetic moment used for attitude control. Initial attitude is pitch $180\ deg$, roll and yaw are zeros. The initial angular velocity is $\mathbf{\Omega}_{co}(t_0) = \mathbf{0}$. It takes quarter of an orbit to turn the satellite boom from upside-down to upright.

8.3.3 Control Coefficients

The velocity gain was chosen empirically $\mathbf{H} = 1 \cdot 10\ \mathbf{E}_{3\times3} \frac{Ams}{T}$. Initial value of the quaternion gain $\epsilon_k(t_o)$ must be large enough to turn the satellite boom from upside-down to upright attitude, $\epsilon_k = 9 \cdot 10^5\ \mathbf{E}_{3\times3} \frac{Am^2}{T}$. Furthermore, the forgetting factor $L = 0.995$, and $\epsilon_c = 3 \cdot 10^5\ \mathbf{E}_{3\times3} \frac{Am^2}{T}$.

8.3.4 Simulation Evaluation

The inverted boom controller was evaluated for a large number of initial conditions, both for the satellite boom pointing ideally toward the Earth centre and just below the horizontal plane. The result of simulation study is summarized in Figs. 8.12 to 8.15. The simulation for the initial conditions of pitch $180\ deg$, roll 0, yaw 0, and the angular ve-
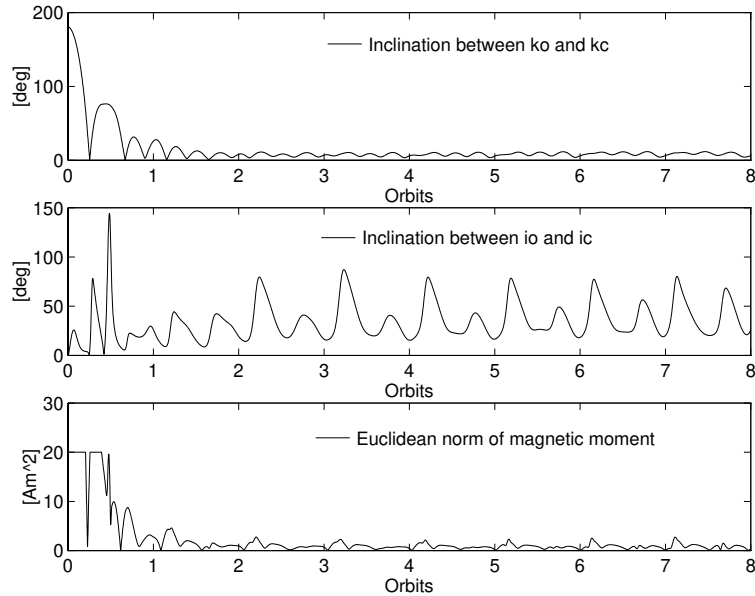
Figure 8.13: Simulation of the inverted boom controller with the initial conditions corresponding to ones in Fig. 8.12. The moment of inertia about the y principal axis is increased by 10 percent. The time necessary to turn the boom upright is approximately the same as in Fig. 8.12, however, the steady state performance of the inverted boom controller is now degraded.

locity $\mathbf{\Omega}_{co}(t_0) = \mathbf{0}$ is depicted in Fig. 8.12. The first plot shows time history of the inclination angle between the z axis of Control CS and the z axis of Orbit CS. The second plot depicts the inclination between the x axes of the Control and Orbit CSs. Finally, the third one illustrates the magnetic moment used for attitude control. It takes quarter of an orbit to turn the satellite boom from upside-down to upright.

Uncertainty of moments of inertia has very little influence on the controller performance. The moment of inertia about the y principal axis is increased by 10 percent in Fig. 8.13. The time necessary to turn the boom upright is roughly the same as in Fig. 8.12, however, the steady state performance of the inverted boom controller is now degraded.

The energy necessary to turn the satellite from upside-down to upright is minimal when rotation takes place about the x principal axis. This case is depicted in Fig. 8.14. Initial attitude is roll $180\,deg$, pitch and yaw are zeros, the initial angular velocity is $\mathbf{\Omega}_{co}(t_0) = \mathbf{0}$. The controller makes the satellite to rotate about the x principal axis, hence the energy necessary to turn the satellite boom from upside-down to upright is minimal. The control system generates too much kinetic energy, and the boom rotates upright, then upside-
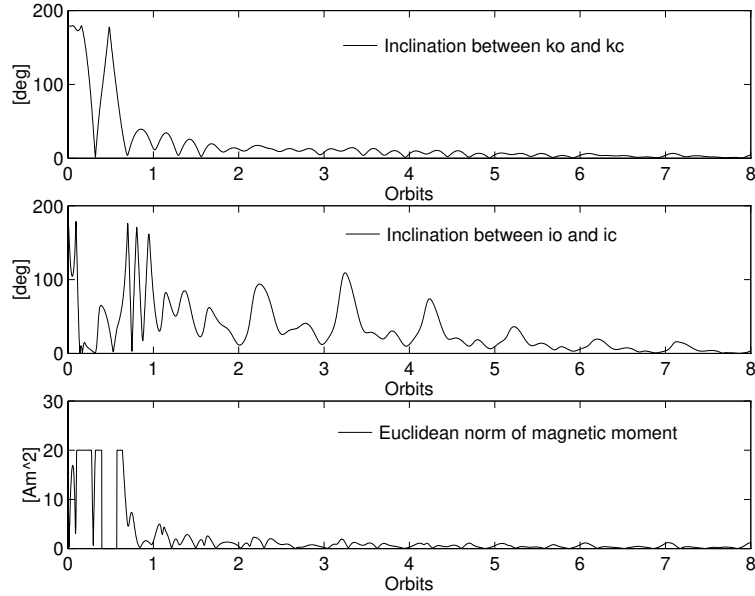
Figure 8.14: Inverted boom controller simulation. Initial attitude is roll $180\ deg$, pitch and yaw are zeros. The initial angular velocity is $\boldsymbol{\Omega}_{co}(t_0) = \mathbf{0}$. The controller makes the satellite to rotate about the x principal axis, hence energy necessary to turn the satellite boom from upside-down to upright is minimal. The controller generates to much energy, such that the boom rotates upright and then upside-down once again. The controller is disactivated when ${}^c k_{oz} \leq 0$ and waits until the boom is above the horizon. As soon as ${}^c k_{oz} > 0$, it is switched on and the remaining portion of energy is dissipated.

down once again. The controller is disactivated when ${}^c k_{oz} \leq 0$ and waits until the boom is above the horizon. As soon as ${}^c k_{oz} > 0$, it is switched on and the remaining portion of energy is dissipated.

Simulation for the initial attitude such that the boom is just below the horizon plane is shown in Fig. 8.15 (the initial values of the attitude and the angular velocity: pitch $100\ deg$, roll $30\ deg$, yaw $40\ deg$ and ${}^c\boldsymbol{\Omega}_{co}(t_0) = \mathbf{0}$). Acceleration imposed by the attitude controller is large. The satellite starts to tumble slightly, however, after one orbit the attitude is acquired and the solution trajectory converges to the reference.

8.3.5 Pros and Cons

The boom inverted controller is easy to implement, its structure is essentially the same as one for the science observation controller, except that a varying attitude gain matrix
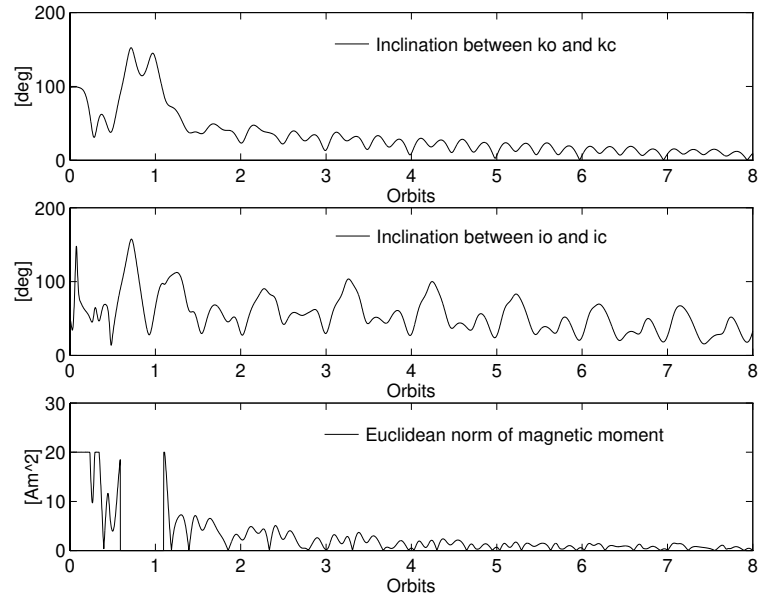
Figure 8.15: The inverted boom controller is activated for the following initial values of the attitude and angular velocity: pitch $100\ deg$, roll $30\ deg$, yaw $40\ deg$ and $^c\mathbf{\Omega}_{co}(t_0) = \mathbf{0}$ (the boom is just below the horizon). The acceleration imposed by the attitude controller causes the satellite to tumble immediately, and after one orbit the attitude is acquired and the solution trajectory converges to the reference.

is applied. The controller performance is independent on exact knowledge of moments of inertia.

Chapter 9

Conclusions and Recommendations

9.1 Conclusions

The main results of the work are summarized in this chapter. The primary purpose of the research was to develop control laws for three axis stabilization of a magnetic actuated satellite. Chapters 2 to 8 discussed the following

- Model of a low Earth orbit satellite was presented in terms of the quaternion attitude parameterization. Potential and kinetic energy was established. Model of motion was linearized using multiplicative nature of quaternion calculus.

- Introduction to periodic linear system was provided, where central part was devoted to the periodic differential Riccati equation. A number of control algorithms were elaborated including the infinite horizon, finite horizon and constant gain optimal controllers.

- Introduction to stability theory of nonlinear periodic systems was given.

- Sliding mode controller for a satellite actuated by a set of magnetic coils was established. A sliding manifold was designed, and a coninuous sliding condition was developed. The controller was tested in simulation test study.

- Both locally and globally stabilizing controllers based on energy dissipation techniques were proposed, and a rigorous stability analysis was carried out. Simulation results showed the proficiency of the new controller in the upside-down configuration, the worst case situation for the satellite.

- The attitude controllers implemented for the Ørsted satellite were tested in the realistic space environment simulator. Simulation was based on high fidelity models of the satellite dynamics and environmental disturbances.

The overall performance of the attitude controllers given in this thesis indicated applicability of the magnetic actuation on low Earth near polar orbit satellites, which pointing requirements are not very high. The magnetorquing was found especially useful on circular orbit for which influence of the aerodynamic drag is marginal.

9.2 Recommendations

The following topics are not covered in this work but it is believed that future investigation could be beneficial.

- Design of the magnetic attitude control based on robust techniques needs to be investigated. This issue is not trivial, due to the system is time varying and lacking controllability in the direction of the local geomagnetic field vector. Some theoretical work based on the frequency shaping method has already been initiated, e.g. Zhang *et al.* (1996).

- It seems promising to design an attitude controller based on fuzzy logic and the energetic approach covered in Chapter 7. An anticipated control structure is proportional derivative vector product with the local geomagnetic field vector. The control parameters are dependent on the attitude, and are determined by a fuzzy logic technique.

- Performance of the attitude control system can be increased by adding a reaction wheel in the direction of the x principal axis. Now, rejection of external disturbances is viable since the aerodynamic drag and the torque due to ellipticity of an orbit act predominantly on pitch. It is expected that the methods described in this thesis are still applicable with some necessary modifications.

Bibliography

Anderson, B.D.O. and J.B. Moore (1989). *Optimal Control. Linear Quadratic Methods*. Prentice-Hall.

Bak, T. (1994). Attitude Determination Methods. Technical report. Ørsted/TN-151.

Bak, T. (1996). Onboard Attitude Determination for a Small Satellite. In proc.: *3rd ESA International Conference on Spacecraft Guidance, Navigation and Control Systems, ESTEC, Noordwijk, The Netherlands*.

Bak, T., R. Wisniewski and M. Blanke (1996). Autonomous Attitude Determination and Control System for the Ørsted satellite. In proc.: *IEEE Aerospace Applications Conference*.

Bittanti, S., (Ed.) (1991). *The Riccati Equation*. Springer Verlag.

Byrnes, Ch. I. and A. Isidori (1991). On the Attitude Stabilization of Rigid Spacecraft. *Automatica* **27**(1), 87–95.

Cappellari, J.O. (1976). *Mathematical Theory of the Goddard Trajectory Determination System*. GSFC NASA , Greenbelt, Maryland.

Cavallo, A., G. De Maria, F. Ferrara and P. Nistri (1993). A Sliding Manifold Approach to Satellite Attitude Control. In proc.: *12th World Congress IFAC, Sidney*.

DeNicolao, G. (1994). Cyclomonotonicity, Riccati Equations and Periodic Receding Horizon Control. *Automatica* **30**(9), 1375–1388.

Hahn, W. (1967). *Stability of motion*. Springer-Verlag.

Hoots, F. R. and R.L. Roehrich (1980). Models for Propagation of NORAD Elements Sets. *Spacetrack Report*.

Isidori, A. (1994). *Nonlinear Control Systems*. Springer.

Krasovskii, N.N (1963). *Problems of the Theory of Stability of Motion (Russian)*. English translation, Stanford Univ. Press.

Kwakernaak, H. and R. Sivan (1972). *Linear Optimal Control Systems*. Wiley.

Kwon, W.H. and A.E. Pearson (1977). A Modified Quadratic Cost Problem and Feedback Stabilization of Linear Systems. *IEEE Transactions on Automatic Control* **22**(5), 838–846.

Martel, F., K.P. Parimal and M. Psiaki (1988). Active Magnetic Control System for Gravity Gradient Stabilized Spacecraft. In proc.: *Annual AIAA/Utah State University Conference on Small Satellites*.

Matwiejew, N.M. (1982). *Metody calkowania rownan rozniczkowych zwyczajnych*. Panstwowe wydawnictwo naukowe.

Mohler, R.R. (1991). *Nonlinear Systems*. Vol. Dynamics and Control. Prentice Hall.

Morton, H.S. (1993). Hamiltonian and Lagrangian Formulations of Rigid-Body Rotational Dynamics Based on the Euler Parameters. *The Journal of the Astronautical Sciemces* **41**(4), 569–591.

Musser, K.L. and L.E. Ward (1989). Autonomous Spacecraft Attitude Control Using Magnetic Torquing Only. In proc.: *Flight Mechanics Estimation Theory Symposium, NASA*.

Popov, V. M. (1973). *Hyperstability of Control Systems*. Springer-Verlag, New York.

Psiaki, M.L., F. Martel and P.K. Pal (1990). Three-axis Attitude Determination via Kalman Filtering of Magnetometer Data. *Journal of Guidance, Control and Dynamics*.

Rudin, W. (1987). *Real and Complex Analysis*. McGraw-Hill.

Slotine, J. E. and W. Li (1991). *Applied Nonlinear Control*. Prentice-Hall.

Utkin, V.I. (1992). *Sliding Modes in Control Optimization*. Springer-Verlag.

Vidyasagar, M. (1993). *Nonlinear Systems Analysis*. Prentice Hall.

Wen, J. Ting-Yung and K. Kreutz-Delgado (1991). The Attitude Control Problem. *IEEE Transactions on Automatic Control*.

Wertz, J.R. (1990). *Spacecraft Attitude Determination and Control*. Kluwer Academic Publishers.

Wisniewski, R. (1994*a*). Attitude Control Methods. Technical Report Ørsted Project TN-232. Aalborg University.

Wisniewski, R. (1994*b*). Nonlinear Control for Satellite Detumbling Based on Magnetic Torquing. In proc.: *Joint Services Data Exchange for Guidance, Navigation, and Control, Arizona*.

Wisniewski, R. (1995*a*). Influence of Aerodynamic Torque on Ørsted Satellite Motion. Technical Report TN-251. Aalborg University.

Wisniewski, R. (1995*b*). Three-axis Attitude Control - Linear Time-Varying Approach. In proc.: *10th IFAC Workshop on Control Applications of Optimization, Haifa, Israel*.

Wisniewski, R. (1997). Optimal Three-Axis Satellite Attitude Control with Use of Magnetic Torquing. Submitted to: *AIAA Guidance, Navigation, and Control Conference, New Orleans*.

Wisniewski, R. and M. Blanke (1996*a*). Attitude Control for Magnetic Actuated Satellite. In proc.: *Control of Nonlinear Systems Theory and Applications. EURACO Workshop*. Algarve. Portugal.

Wisniewski, R. and M. Blanke (1996*b*). Three-axis Satellite Atitude Control Based on Magnetic Torquing. Submitted to: *Automatica*.

Wisniewski, R. and M. Blanke (1996*c*). Three-axis Satellite Attitude Control Based on Magnetic Torquing. In proc.: *13th IFAC World Congress, San Francisco, California*.

Yon-Pin, Ch. and L. Shih-Che (1993). Sliding Mode Controller Design for Spacecraft Attitude Tracking Maneuvers. *IEEE Transactions on Aerospace and Electronic Systems* **29**(4), 1328–1332.

Zhang, C., J. Zhang and K. Futura (1996). Performance Analysis of Periodically Time Varying Controllers. In proc.: *13th IFAC World Congress, San Francisco, California*.

Appendix A

Orbit and Atmospheric Density Models

Simulation is based on high fidelity models of satellite dynamics and environmental disturbances. The focus in this appendix is on the models of the aerodynamic drag torque, orbit propagation, and geomagnetic field model.

A.1 Modeling of Satellite Geometry

An approximation of the satellite structure by a collection of simple geometrical figures has been assumed. The aerodynamic force on each element according to Wertz (1990) is determined by integrating the following equation

$$df_{aero} = \Leftrightarrow \frac{1}{2} C_D \rho v^2 (\hat{\mathbf{n}} \cdot \hat{\mathbf{v}}) dA, \tag{A.1}$$

where dA is the surface element, $\mathbf{n}$ is an outward normal to the surface, $\hat{\mathbf{v}}$ is the unit vector in the direction of translational velocity v, C_D is the drag coefficient, and ρ is the atmospheric density.

The total aerodynamic torque in Wisniewski (1995a) is the vector sum of the torques acting on individual parts of the satellite

$$\mathbf{N}_{aero} = \sum_{i=1}^{k} \mathbf{r}_i \times \mathbf{F}_i, \tag{A.2}$$

where $\mathbf{r}_i$ is the vector from the spacecraft centre of mass to the centre of pressure of the
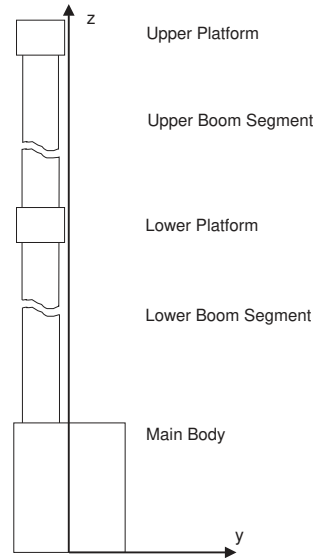
Figure A.1: Satellite structure decomposed into simple geometrical figures

ith element as in Figure A.1. The individual parts of the Ørsted satellite assembly are given in Table A.1.

A.2   Atmospheric Density Model

The NASA/GSFC Jacchia-Roberts Cappellari (1976) thermospheric density model is an empirical model of the neutral thermosphere and lower exosphere (86 to 2000 km). The atmospheric density modelled by Jacchia-Roberts is dependent on:

- solar activity,

- geodetic latitude,

- longitude,

- universal time,

- magnetic activity,

- semiannual, semidiurnal, terdiurnal, and diurnal variations.

Table A.1: Model of Ørsted satellite geometry

Part	Shape	Dimension [m]	CoP [m]
Main body	cuboid	height: 0.182	0.35
		length: 0.125	
		width: 0.34	
Lower boom segment	cylinder	diam.: 0.024	3.40
		length: 5.385	
Lower platform	cylinder	diam.: 0.195	6.25
		length: 0.34	
Upper boom segment	cylinder	diam.: 0.018	7.37
		length: 1.884	
Upper platform	cylinder	diam.: 0.182	8.37
		length: 0.125	

A.3   Orbit Propagation Model

The Norad SGP-4 orbital model Hoots and Roehrich (1980) is assumed. SGP-4 is an analytical model for prediction of satellite position and velocity for LEO satellites. The model incorporates perturbations due to:

- Atmospheric drag (based on a static, non rotating, spherically symmetric atmosphere described by a power density function),

- Fourth-order zonal geopotential harmonics (J2, J3, and J4),

- Spin-orbit resonance effects for synchronous and semi-synchronous orbits,

- Solar and lunar gravitational effects to first order.

A.4   Geomagnetic Field Model

The 10th order IGRF (International Geomagnetic Reference Field) spherical harmonic model is implemented Wertz (1990). The Earth's magnetic field is represented as the gradient of a scalar potential function given by a series of a spherical harmonics multiplied by empirically determined Gaussian coefficients.

Appendix B

Rate Detumbling Controller

The objectives of the rate detumbling control is to decrease kinetic energy and to turn the satellite in the direction of the local geomagnetic field. The controller utilizes only measurements of the geomagnetic field vector. The baseline for the design is that the influence of the gravity gradient and aerodynamic drag torque are negligible. The gravity gradient torque is small since the principal moments of inertia are of the same order of magnitude, furthermore the active area of the satellite in the boom stowed configuration is small, thus the influence of the aerodynamic torque is insignificant. The work presented in this appendix is based on Wisniewski (1994a).

A proposed control law is

$$
{}^{c}\mathbf{m} = \ominus k\, {}^{c}\dot{\mathbf{B}} \ominus \mathbf{m}_{const},
\tag{B.1}
$$

where $\mathbf{m}_{const} = [0\ 0\ m_{const}]^{T}$, then the control torque is given by

$$
{}^{c}\mathbf{N}_{ctrl} = (\ominus k\, {}^{c}\dot{\mathbf{B}} \ominus \mathbf{m}_{const}) \times {}^{c}\mathbf{B}.
\tag{B.2}
$$

Information about the satellite rotation in an inertial coordinate system can be extracted from the rate of the local geomagnetic field

$$
{}^{c}\dot{\mathbf{B}} = {}^{c}\mathbf{B} \times {}^{c}\boldsymbol{\Omega}_{cw} + {}^{c}_{w}\mathbf{A}\, {}^{w}\dot{\mathbf{B}} \approx {}^{c}\mathbf{B} \times {}^{c}\boldsymbol{\Omega}_{cw}.
\tag{B.3}
$$

This assumption is valid for the rate of the geomagnetic field in the regions near the North and the South Poles, since ${}^{w}\dot{\mathbf{B}}$ is smallest, however near the Equator the rate of geomagnetic field reaches its maximum value

$$
||{}^{w}\dot{\mathbf{B}}|| \approx 3.8 ||{}^{w}\mathbf{B}|| \omega_{o}
\tag{B.4}
$$

Recall that the boom deployment is to be executed from the Danish ground stations, and therefore the objective is to derive control law which is as accurate as possible near the North Pole or more precisely over Denmark.

The Lyapunov direct method covered in Chapter 5 is used in this analysis to design control law for despinning the satellite from an arbitrary initial tumbling. It is proved that kinetic energy of the satellite rotation is dissipated.

The Lyapunov function represents energy in a physical system, here the sum of kinetic energy and potential energy. The kinetic energy is $\frac{1}{2}{}^c\mathbf{\Omega}_{cw}^T\mathbf{I}^c\mathbf{\Omega}_{cw}$, whereas the potential energy can be represented as $|\mathbf{m}_{const}|\,|{}^c\mathbf{B}|+\mathbf{m}_{const}^T{}^c\mathbf{B}$, which is proportional to the inclination angle between the z axis of the Control CS and the local geomagnetic field vector. Finally, the entire energy of the satellite motion and a Lyapunov candidate function is

$$E = \frac{1}{2}{}^c\mathbf{\Omega}_{cw}^T\mathbf{I}^c\mathbf{\Omega}_{cw} + |\mathbf{m}_{const}|\,|{}^c\mathbf{B}| + \mathbf{m}_{const}^T{}^c\mathbf{B}. \tag{B.5}$$

Applying the dynamics in Eq. (2.12) and neglecting $\mathbf{N}_{gg}$ the derivative of the Lyapunov function is

$$\dot{E}_k \approx {}^c\mathbf{\Omega}_{cw}^T{}^c\mathbf{N}_{ctrl} + \mathbf{m}_{const}^T{}^c\dot{\mathbf{B}}, \tag{B.6}$$

since the magnitude of the geomagnetic field vector in the polar regions is approximately constant.

Using Eq. (B.3) the time derivative of the satellite energy is

$$\dot{E}_k = \Leftrightarrow k^c\dot{\mathbf{B}}^T{}^c\dot{\mathbf{B}} \Leftrightarrow \mathbf{m}_{const}^T{}^c\dot{\mathbf{B}} + \mathbf{m}_{const}^T{}^c\dot{\mathbf{B}} = \Leftrightarrow k^c\dot{\mathbf{B}}^T{}^c\dot{\mathbf{B}}, \tag{B.7}$$

which is negative semidefinite. This corresponds to Eq. (7.9) in Section 7.1, hence it is concluded that the energy (B.5) is dissipated, indeed.

The approximate analysis of the rate detumbling control law was provided. The anticipated results are such that kinetic energy is dissipated and the satellite well tracks the geomagnetic field in the polar regions. Some deviations from the desired performance are expected over the equator, compare this with simulation results given in Section 8.1.

Appendix C

Yaw Reference

The moments of inertia about the x and y principal axes are approximately equal, therefore an arbitrary yaw reference in the Ørsted attitude control system could be implemented. Now, the objective of the controller is to turn the satellite such that the Control CS coincides with a Reference Coordinate System. The Reference CS is defined relatively to the Orbit CS as rotation about the z axis of the desired yaw reference θ.

C.1   Reference Coordinate System and Its Rate

The orientation of the Reference CS w.r.t. the Orbit CS is given by a quaternion $_o^r\mathbf{q}$. A unit quaternion according to Section 2.2 is given by the axis of rotation with the unit vector $\mathbf{e}$ and the angle of rotation ϕ. For rotation about the z principal axis, $\mathbf{e}$ has only the third component different from zero, furthermore the angle ϕ corresponds to the desired yaw reference θ

$$_o^r\mathbf{q} = \begin{bmatrix} 0 & 0 & sin\,\dfrac{\theta}{2} & cos\,\dfrac{\theta}{2} \end{bmatrix}^T. \tag{C.1}$$

Now, the rotation of the Control CS in the Reference CS is

$$_r^c\mathbf{q} = \mathbf{Q}(_o^c\mathbf{q})_r^o\mathbf{q}, \tag{C.2}$$

where $\mathbf{Q}(\cdot)$ was defined in Section 2.2, and $_r^o\mathbf{q} = [0\ 0\ \Leftrightarrow sin\,\frac{\theta}{2}\ cos\,\frac{\theta}{2}]^T$ is the inverse of $_o^r\mathbf{q}$.

The reference for the angular velocity is $^c\mathbf{\Omega}_{cr} = \mathbf{0}$. Having the satellite angular velocity w.r.t. the World CS, $^c\mathbf{\Omega}_{cr}$ is calculated

$$^c\mathbf{\Omega}_{cr} = {}^c\mathbf{\Omega}_{cw} + \mathbf{A}(_r^c\mathbf{q})^r\mathbf{\Omega}_{rw}, \tag{C.3}$$

where ${}^r\mathbf{\Omega}_{rw}$ is the angular velocity of the Reference CS w.r.t. the World CS, which is

$$
{}^r\mathbf{\Omega}_{rw} = \mathbf{A}\left({}^r_o\mathbf{q}\right){}^o\mathbf{\Omega}_{rw} = \mathbf{A}\left({}^r_o\mathbf{q}\right){}^o\mathbf{\Omega}_{ow} = \omega_o \begin{bmatrix} cos\,\theta & \Leftrightarrow sin\,\theta & 0 \end{bmatrix}^T .
$$
(C.4)

The findings of the linear attitude control methods developed in Chapters 3 and 4 are directly applicable, however, a new linearization about the reference quaternion ${}^o_r\mathbf{q}$ and angular velocity ${}^r\mathbf{\Omega}_{rw}$ is needed.

The linearization method is the same as in Section 2.6. The linearization of the angular velocity is based on the first order extension of the Taylor series, whereas the multiplicative linearization of the attitude quaternion ${}^c_r\mathbf{q}$ is applied, and a small perturbation of the attitude quaternion is

$$
{}^c_r\mathbf{q} \approx \begin{bmatrix} \delta\mathbf{q} \\ 1 \end{bmatrix} .
$$
(C.5)

C.2 Linearized Dynamics

The equation of dynamics is divided into the cross coupling, the contribution of the gravity gradient torque and the part due to control torque

$$
\frac{d}{dt}\delta\mathbf{\Omega} = \delta(\text{Cross Coupling}) + \mathbf{I}^{-1}\delta(\text{Gravity Gradient Torque}) + \mathbf{I}^{-1}\delta(\text{Control Torque}).
$$
(C.6)

C.2.1 Linearization of Cross Coupling

$$
\text{Cross Coupling} = \begin{bmatrix} \sigma_x{}^c\omega_{cwy}{}^c\omega_{cwz} \\ \sigma_y{}^c\omega_{cwz}{}^c\omega_{cwx} \\ \sigma_z{}^c\omega_{cwx}{}^c\omega_{cwy} \end{bmatrix} \approx \begin{bmatrix} \Leftrightarrow\sigma_x\omega_o\delta\omega_z sin\,\theta \\ \sigma_y\omega_o\delta\omega_z cos\,\theta \\ \sigma_z\omega_o\left(\delta\omega_y cos\,\theta \Leftrightarrow \delta\omega_x sin\,\theta\right) \end{bmatrix} ,
$$
(C.7)

where

$$
\sigma_x = \frac{I_y \Leftrightarrow I_z}{I_x}, \ \ \sigma_y = \frac{I_z \Leftrightarrow I_x}{I_y}, \ \ \sigma_z = \frac{I_x \Leftrightarrow I_y}{I_z}.
$$
(C.8)

C.2.2 Linearization of Gravity Gradient Torque

$$
\text{Gravity Gradient Torque} \approx 3\omega_o^2 \begin{bmatrix} \Leftrightarrow 2\delta q_2 \\ 2\delta q_1 \\ 1 \end{bmatrix} \times \begin{bmatrix} \Leftrightarrow 2I_x\delta q_2 \\ 2I_y\delta q_1 \\ I_z \end{bmatrix} \approx 6\omega_o^2 \begin{bmatrix} (I_z \Leftrightarrow I_y)\delta q_1 \\ (I_z \Leftrightarrow I_x)\delta q_2 \\ 0. \end{bmatrix}
$$
(C.9)

C.2.3 Linearization of Control Torque

$$\text{Control Torque} = {}^c\mathbf{m} \times \mathbf{A}\left({}^c_r\mathbf{q}\right){}^r\mathbf{B} \approx {}^c\mathbf{m} \times {}^r\mathbf{B} \Leftrightarrow 2{}^c\mathbf{m} \times (\delta\mathbf{q} \times {}^r\mathbf{B}) \approx {}^c\mathbf{m} \times {}^r\mathbf{B}, \tag{C.10}$$

where ${}^r\mathbf{B} = \mathbf{A}\left({}^r_o\mathbf{q}\right){}^o\mathbf{B}$ is the local geomagnetic field vector resolved in the Reference CS.

C.3 Linearized Kinematics

C.3.1 Linearized Kinematic Equation

$$\frac{d}{dt}\mathbf{q} = \frac{1}{2}{}^c\mathbf{\Omega}_{cr}q_4 \Leftrightarrow \frac{1}{2}{}^c\mathbf{\Omega}_{cr} \times \mathbf{q} \approx \frac{1}{2}{}^c\mathbf{\Omega}_{cr}. \tag{C.11}$$

Now, according to Eq. C.4 the linearized kinematics is

$$
\begin{aligned}
\frac{d}{dt}\boldsymbol{\delta}\mathbf{q} &= \frac{1}{2}\boldsymbol{\delta}\mathbf{\Omega} \Leftrightarrow \frac{1}{2}\left[\omega_o cos\,\theta \quad \Leftrightarrow\omega_o sin\,\theta \quad 0\right]^T \Leftrightarrow \boldsymbol{\delta}\mathbf{q} \times \left[\omega_o cos\,\theta \quad \omega_o sin\,\theta \quad 0\right]^T \\
&= \frac{1}{2}\begin{bmatrix} \delta\omega_x \Leftrightarrow \omega_o cos\,\theta + 2\omega_o\delta q_3 sin\,\theta \\ \delta\omega_y + \omega_o sin\,\theta + 2\omega_o\delta q_3 cos\,\theta \\ \delta\omega_z \Leftrightarrow 2\omega_o\delta q_2 cos\theta \Leftrightarrow 2\omega_o q_1 sin\,\theta \end{bmatrix}.
\end{aligned}
\tag{C.12}
$$

C.4 Linearized Equation of Satellite Motion

The matrix form of the linearized satellite motion is

$$\frac{d}{dt}\begin{bmatrix} \boldsymbol{\delta}\mathbf{\Omega} \\ \boldsymbol{\delta}\mathbf{q} \end{bmatrix} = \mathbf{A}\begin{bmatrix} \boldsymbol{\delta}\mathbf{\Omega} \\ \boldsymbol{\delta}\mathbf{q} \end{bmatrix} + \mathbf{B}(t){}^c\tilde{\mathbf{m}}, \tag{C.13}$$

where

$$\mathbf{A} = \begin{bmatrix} 0 & 0 & \Leftrightarrow\omega_o\sigma_x sin\,\theta & \Leftrightarrow 2k\sigma_x & 0 & 0 \\ 0 & 0 & \omega_o\sigma_y cos\,\theta & 0 & 2k\sigma_y & 0 \\ \Leftrightarrow\omega_o\sigma_z sin\,\theta & \omega_o\sigma_z cos\,\theta & 0 & 0 & 0 & 0 \\ \frac{1}{2} & 0 & 0 & 0 & 0 & \omega_o sin\,\theta \\ 0 & \frac{1}{2} & 0 & 0 & 0 & \omega_o cos\,\theta \\ 0 & 0 & \frac{1}{2} & \Leftrightarrow\omega_o sin\,\theta & \Leftrightarrow\omega_o cos\,\theta & 0 \end{bmatrix},$$

$$\mathbf{B}(t) = \begin{bmatrix} \mathbf{I}^{-1} \begin{bmatrix} 0 & \Leftrightarrow^r B_z(t) & {}^r B_y(t) \\ {}^r B_z(t) & 0 & \Leftrightarrow^r B_x(t) \\ \Leftrightarrow^r B_y(t) & {}^r B_x(t) & 0 \end{bmatrix} \\ \begin{bmatrix} 0 & 0 & 0 \\ 0 & 0 & 0 \\ 0 & 0 & 0 \end{bmatrix} \end{bmatrix} .$$